Fall 2016

CT image registration-based lung mechanics In COPD

Sandeep Bodduluri
University of Iowa

CT IMAGE REGISTRATION-BASED LUNG MECHANICS IN COPD

by

Sandeep Bodduluri

A thesis submitted in partial fulfillment
of the requirements for the Doctor of Philosophy
degree in Biomedical Engineering in the
Graduate College of
The University of Iowa

December 2016

Thesis Supervisor: Professor Joseph M. Reinhardt

Graduate College
The University of Iowa
Iowa City, Iowa

CERTIFICATE OF APPROVAL

PH.D. THESIS

This is to certify that the Ph.D. thesis of

Sandeep Bodduluri

has been approved by the Examining Committee for
the thesis requirement for the Doctor of Philosophy degree
in Biomedical Engineering at the December 2016 graduation.

Thesis Committee: _____
Joseph M. Reinhardt, Thesis Supervisor

_____
Eric A. Hoffman

_____
John D. Newell Jr.

_____
Jessica C. Sieren

_____
David W. Kaczka

_____
Surya P. Bhatt

To Mom, Dad, and Vijaya

Failure is simply the opportunity to begin again, this time more intelligently. There is no disgrace in honest failure; there is disgrace in fearing to fail

Henry Ford

ACKNOWLEDGEMENTS

I would like to extend my heartfelt gratitude to my advisor Prof. Reinhardt for giving me the grand opportunity to undertake this research work. I am deeply indebted to him for his belief and patience towards me throughout my M.S. and Ph.D. education. The discussions, encouragement and constant feedback from Prof. Reinhardt made me a better researcher and taught me how to efficiently address a research hypothesis. He has always been very supportive to explore different ideas for which am highly thankful for. I am most thankful for his time spent on revising our manuscripts and showing me a proper way to articulate my thoughts. I am also very grateful to Prof. Hoffman and Dr. Newell for their constant support and feedback throughout this research. I really appreciate their invaluable advice and grateful for providing me the access to necessary imaging data.

I am deeply indebted to Dr. Surya Bhatt whose collaboration and thoughts led the research towards new advances and applications. This research work would not have reached the position it is today without his support and inputs. I got invaluable feedback from him on clinical aspects of the work and how to address the research towards better clinical applications. I am always grateful for his guidance, thought-provoking conversations and encouragement. I also would like to thank Prof. Christensen, Dr. Kai ding, Dr. Kunlin Cao, Dr. Ryan Amelon, and Dr. Kaifang Du for their support and help with the image registration. I would like to thank my lab mate Sarah Gerard who spent lot of time listening to my crazy ideas and gave me a great deal of feedback. I also would like to thank KP Abhilash for his support and friendship. He has always been the first peer critique of my work and helped me a great deal in professional and personal life.

Finally, I am extremely fortunate to have Vijaya as my partner in crime. I never could have finished this journey on my own. She has been my greatest motivation during my tough times and a solid reminder during my lazy times. Thanks to my mom and dad for everything and being the best. My special thanks to Dr. Gopi and Dr. Sai Ramadugu for their constant support and friendship. I am also extremely thankful and fortunate to have the best bunch of friends (Chaitanya, Rahil, Raghu, Vivek, Sampada, Parin, Radhika, Namita, Ankur, and Monica) who made this journey memorable and fun. Also, special thanks to AID Iowa group for keeping me grounded and closer to the roots.

ABSTRACT

Chronic obstructive pulmonary disease (COPD) is a growing health concern associated with high morbidity and mortality, and is currently the third-ranked cause of death in the United States. COPD is characterized by airflow limitation that is not fully reversible and includes chronic bronchitis, functional small airway disease, and emphysema. The interrelationship between emphysema and airway disease in COPD makes it a highly complex and heterogeneous disorder. Appropriate diagnosis of COPD is vital to administer targeted therapy strategies that can improve patient's quality of life and reduce the frequency of COPD associated exacerbations. Although spirometry or pulmonary function tests are currently the gold standard for the diagnosis and staging of the disease, their lack of reproducibility and minimal information on regional characterization of the lung tissue destruction makes it hard to rely on to phenotype COPD population and predict disease progression. Quantification of COPD, as done by computed tomography (CT) methods has seen significant advancements, helping us understand the complex pathophysiology of this disease. The prospective and established techniques that are derived from CT imaging such as densitometry, texture, airway, and pulmonary vasculature-based analyses have been successful in regional characterization of emphysema related lung tissue destruction and airway disease related morphological changes in COPD patients. Although, these measures enriched our diagnostic and treating capability of COPD, they lack information on patient specific alterations in lung mechanics and regional parenchymal stresses. This valuable information can be achieved through the use of image registration protocols. Our main goal of this research work is to examine and evaluate the role of lung mechanical measures derived from CT image registration techniques in COPD diagnosis, phenotyping, and progression.

PUBLIC ABSTRACT

Chronic obstructive pulmonary disease (COPD) is the third leading cause of death in the United States. COPD is a characterized by progressive airflow limitation and is associated with increasing mortality and morbidity. COPD is often used as an umbrella term for multiple disease components: tissue destruction due to emphysema, airway remodeling and narrowing due to small and large airway disease. The complex admixture of individual disease components in COPD makes it a highly heterogeneous disorder. The current gold standard of COPD diagnosis is by quantifying airflow obstruction using spirometry. However, spirometry is a global measure and is not helpful in assessing the contribution of emphysema and airway disease separately in COPD patients. Computed tomography (CT) is increasingly being used to characterize and quantify the lung tissue of COPD patients. The vast majority of CT image-based research of COPD is based on the density and the texture analysis of either inspiratory or expiratory CT images, thus providing the regional characterization of the disease. In this thesis, we used the information derived from both inspiratory and expiratory CT to capture mechanical properties of lung tissue in COPD patients. We further explored the role of the CT-derived lung mechanics in COPD presence and severity, and disease progression.

TABLE OF CONTENTS

LIST OF TABLES

TABLE

LIST OF FIGURES

FIGURE

CHAPTER 1

INTRODUCTION

1.1 Respiratory Anatomy and Physiology

The respiratory system is vital to the human body and is responsible for the delivery of oxygen and removal of carbon dioxide to and from the blood stream. As most of the cells in our body lie too far from the lungs to have inhaled oxygen reach them directly, oxygen is instead carried by the blood stream which comes in contact with the inhaled air in the respiratory system. The exchange of gases takes place at the alveoli where oxygen diffuses into the blood stream and carbon dioxide diffuses out of the blood stream during inhalation and exhalation. Although the primary function of the respiratory system is the gas exchange, other functions include filtering and temperature maintenance of the inhaled air, sound production through vocal chords in the larynx, and control of body pH levels. Anatomically, the respiratory system can be separated into upper and lower respiratory tract. The upper respiratory tract comprises of nasal cavity, pharynx, and larynx whereas the lower respiratory tract comprises of trachea, bronchial tree, terminal bronchioles, and alveoli.

Functionally, the organs that are not involved in the gas exchange in the respiratory anatomy are described as conducting zone (nasal cavity to bronchioles). The role of conducting zone is to deliver the inhaled air into the deep regions of the lung. The structures including trachea, bronchi, and bronchioles are often called the airway tree since the trachea splits into right and left bronchi and the airways further subdivide, forming tree-like structure. The bronchial division, or generation, is usually described by a number indicating the current division from the trachea. The cross-sectional trachea diameter in the normal

human adult is roughly 1.3-2.5 cm in the coronal plane while females have slightly smaller diameters, 1.0-2.1 cm [1]. The trachea divides into the main bronchi at the carina and the right bronchus is wider and shorter than the left bronchi. This is often the reason to believe that inhaled noxious particles have higher chances of deposition in the right bronchus than the left bronchus [2]. The right bronchus is further subdivided into three lobes: the right upper, right middle, and right lower lobes, while the left bronchus divides into the left upper and left lower lobes. The lobar bronchi further divide into segmental bronchi, which serves as bronchopulmonary segments of each lobe. The bronchi keep dividing into much smaller segments up to 24 generations from the main trachea. The passage way that starts from the trachea and continues until the terminal bronchioles is called the conducting airways. This area contributes to the anatomic dead space, which takes up approximately 150 mL in volume.

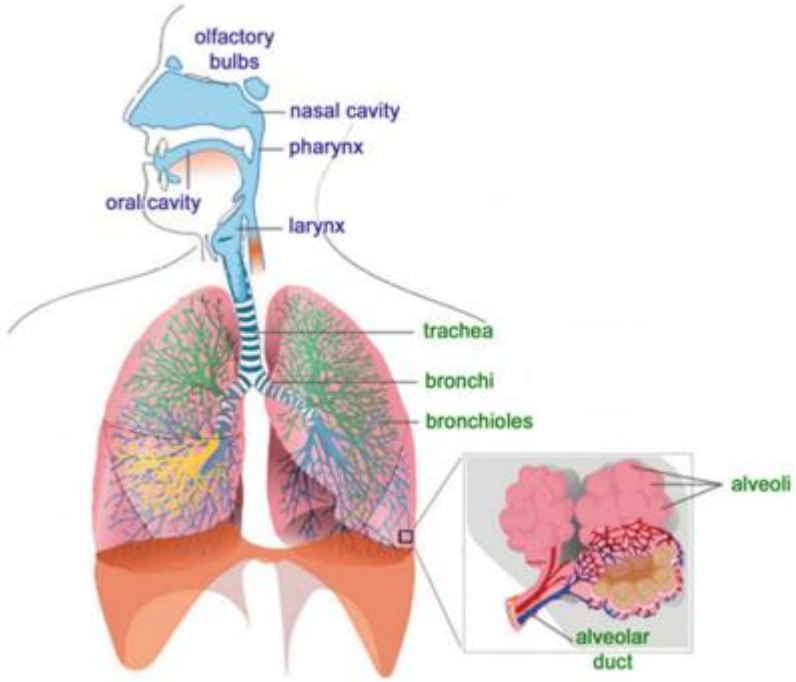

Figure 1.1: Schematic of the human respiratory system, reprint from [3]

The regions from the alveolar duct to alveoli are responsible for gas exchange, and are referred as the respiratory zone. The terminal bronchioles divided into respiratory bronchioles where fewer alveolar structures present at the walls. The respiratory bronchioles further divide into alveolar ducts which are completed filled with alveoli. This region is called the acinar region. The acinar region is responsible for the functional lung tissue or parenchyma. This region takes up most part of the lung, approximately 3 liters in volume. The entire acinar region is surrounded by a rich network of blood capillaries. It is estimated that each adult lung has about 300 million alveoli, with a total surface area for gas exchange of 70-80 m^2. Gas exchange at alveolar surface that separates the alveoli from the blood capillaries. There are approximately 300 million of alveoli and each is smaller than a grain of salt. The gas exchange occurs through diffusion. The partial pressure of oxygen in the inhaled air at the alveoli is greater than the partial pressure of blood oxygen allowing for the exchange.

Inspiration is carried out by the diaphragm contraction which can descend up to 10 cm on forced breathing. The contraction of diaphragm pulls the anterior end of each rib enlarging the volume of the thorax. As a result, the intrathoracic pressure and intrapulmonary pressure decreases relative to the external atmospheric pressure. The pressure gradient initiates the movement of inhaled air from higher pressure regions to the lower pressure regions. During expiration, which is mostly a passive process, the lung and chest wall return to its original shape and position due to their elastic recoil. This increases the pressure inside the lung and releases the air from the lungs. In normal quiet breathing, the elastic recoil of the lungs and chest wall is needed to return the thorax to its original state where intercostal muscles in the thorax take part in forced expiration. A pressure-

volume curve measured during breathing describes the mechanical properties of the lungs and its ability to stretch. The change in lung volume as a result of change in the pressure is referred to as lung compliance. A high lung compliance means the lung can be easily distended where as a low lung compliance means that the lung is 'stiff'. The measurement of lung volumes at different time points is vital to our understanding of pulmonary pathophysiology. A spirometer or pulmonary function test is used to measure lung volumes which generates a spirogram, as shown in Figure 1.2.

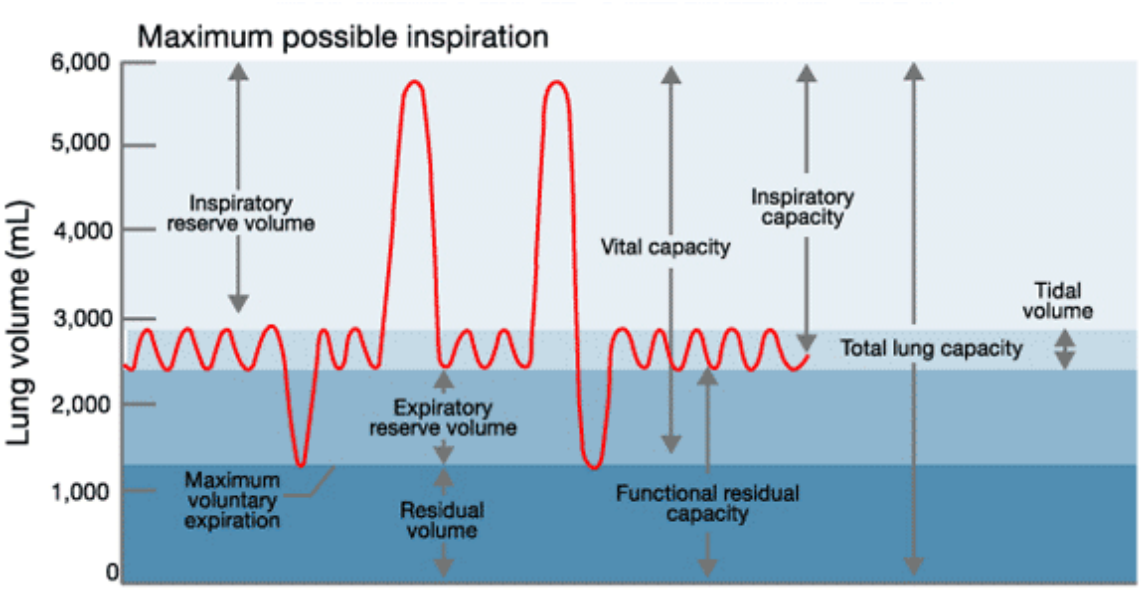

Figure 1.2: Static lung volumes and capacity tracing measured by a spirometer, from [6]

Although there are numerous diseases that affect the lung, they are broadly described as either obstructive or restrictive lung disease. Obstructive lung diseases diminish a person's ability to completely expel air from the lung resulting in air getting trapped inside after each breath. The common obstructive lung diseases are chronic obstructive pulmonary disease (COPD), asthma, bronchiectasis, and cystic fibrosis. On the other hand, persons with restrictive lung disease face a hard time expanding the lungs to their maximum capacity during inspiration due to stiffness of chest walls and/or damage to

the muscles involved in breathing. The most common restrictive diseases are interstitial lung disease, sarcoidosis, pulmonary fibrosis, and silicosis.

1.2. Chronic Obstructive Pulmonary Disease (COPD)

Chronic obstructive pulmonary disease (COPD) is currently the third-ranked cause of death in the United States behind cancer and heart disease [7, 8]. Although it is largely preventable, the morbidity and mortality associated with COPD is ever increasing [9]. Our limited understanding of the underlying pathophysiology and minimal access to targeted therapies for COPD has made prevention difficult. COPD is largely undiagnosed and often misdiagnosed as asthma. COPD, as defined by Global Initiative for Chronic Obstructive Lung Disease (GOLD) [8], is:

"A common preventable and treatable disease, is characterized by persistent airflow limitation that is usually progressive and associated with an enhanced chronic inflammatory response in the airways and the lung to noxious particles or gases."

Although tobacco smoking is a major risk factor for COPD, other factors such as environmental pollution, occupational exposure to noxious gases, and genetic factors also known to cause COPD. The pathological consequences of COPD induce a series of structural and physiological changes which eventually impact the patient's quality of life and health status. COPD is an obstructive lung disease where the affected lung tissue loses its ability to expel air from the lung, resulting in air trapping in the lungs. This difficulty in emptying air out of the lungs lead to shortness of breath (dyspnea) and reduced exercise capacity in COPD patients. Other major symptoms include chronic cough and sputum

production. COPD is often an umbrella term for three major disease components: emphysema, large airway disease, and/or functional small airway disease. COPD is also increasingly associated with other comorbidities such as pneumonia, hypertension, and cardiovascular disease.

Emphysema is characterized by thinning and hyperinflation of the alveoli. The alveolar structures that are damaged by emphysema loses their elastic recoil and trap air at the end of each breath. Over time, the muscles involved in breathing are forced to adjust for trapped air in the lungs, which in turn compromises their ability to function. The lungs become more difficult to ventilate resulting in increased effort to breathe and reduced exercise capacity. Large airway disease or chronic bronchitis is a condition of increased mucus production in the airways. This causes morphological changes to the airways (narrowing or remodeling). The main site of airflow obstruction occurs in the small airways generally defined as those that are less than 2 mm in diameter. The loss of lung elastic recoil, inflammation, and airway remodeling contributes to the airflow limitation at the small airways causing hyperinflation at rest and dynamic hyperinflation during exercise.

The clinical diagnosis of COPD is considered for the patients who has dyspnea, chronic cough or sputum production, and a history of exposure to any risk factors of the disease. Spirometry is the current gold standard to diagnose COPD. If the ratio of forced expiratory volume in one second (FEV1) to the forced vital capacity (FVC) is less than 0.7, the diagnosis of COPD is confirmed. The rate of decline in FEV1 is steeper in smokers than nonsmokers. However, this ratio is known to underestimate the disease in younger patients and overestimation in older patients. Older subjects tend to have a decline in their lung function as a result of their age and physical capability. For many years, COPD was

categorized into four severity stages (I-IV), based on the GOLD guidelines [8, 11, 12]. However, the complex interplay between emphysema and airway disease in COPD patients makes the spirometry-based phenotyping less useful. Since then, the GOLD classification system of COPD has gone through several iterations,. The updated classification also looks at the validated patient's questionnaires such as the COPD assessment test (CAT), the clinical COPD questionnaire (CCQ), and/or the modified British Medical Research Council (mMRC), in addition to the frequency of exacerbations. An exacerbation in COPD patient is characterized by a worsening of the patient's respiratory symptoms leading to a change in medication. The frequency of exacerbations and hospitalization is associated with poor prognosis. In the wake of new additions to the current GOLD classification system, it is still challenging to separate emphysema from airway disease component in COPD patients solely based on pulmonary function tests and quality of life questionnaires. Although, there has been considerable research done in elevating the usefulness of spirometry in COPD diagnosis, the use of imaging modalities has become main stream to identify COPD presence, severity, and progression.

1.3. CT Imaging in COPD

Multi-detector computed tomography imaging in COPD has seen significant advancements in the past decade helping the clinicians to better phenotype and characterize pathology [13]. In 1895, William Roentgen was the first person to discover X-rays [14] and found that the inner details of the body could be made visible non-invasively using this imaging technique. Almost half a century later in 1972, Godfrey Hounsfield invented computed tomography (CT), where a volumetric object was reconstructed from a series of axial scans [15]. Conventional X-ray radiography passed rays through the body and

projected a three-dimensional object onto a two-dimensional plane. In this process, there is a clear overlap of the structures and very limited depth information. On the other hand, CT measures the attenuation of X-rays within the tissue into thin sections and a three-dimensional (3D) can be reconstructed from a series of scans. In the first-generation CT scanner, a pencil-like single beam X-source and the detector are moved in linear steps, and also rotated at regular intervals to obtain the slices at different angular orientations. In the second-generation, thin fan beam of X-rays were produced that improved the image quality by reducing the motion effects. In third and fourth-generation scanners, rotational motion of X-ray tube and detector arrays were introduced. Modern CT scanner now-a-days cover a large volume of tissue in a relatively short time. Image acquisition is done by employing multiple detector rings to scan several slices through the body during each rotation. These scanners are referred as spiral CT or helical CT or multi-slice CT scanners. Hundreds of images can be acquired in a single study with spiral CT technique. Image reconstruction after image acquisition has also seen significant advancements. The primary reconstruction algorithm used in CT scanners is filtered back projection. Radon first introduced the foundation for the reconstruction methods in 1917. In simple back projection, each X-ray that pass through the body is separated into equally spaced element and each element is contributed equally to the final attenuation values that is derived from different angular orientations. Filtered back projection is a convolution method that uses a one-dimensional integral equation for the image reconstruction. A sharpening filter is convolved with the X-ray attenuation data prior to back projections to counter the blurring effects. The main advantage of this method is that image reconstruction can be done simultaneously while X-ray transmission data is collected.

In chronic obstructive pulmonary disease (COPD), CT imaging has revolutionized the diagnosis by allowing the quantification of pathological changes that are associated with airflow obstruction in the patients. CT imaging of the thorax lets us visualize the lung structure and parenchyma non-invasively. The measurement of the individual contribution of the emphysema and the airway disease components in COPD is not possible yet, however, several research groups used quantitative CT with a considerable success in phenotyping COPD population [18-20]. Most of phenotyping related to COPD population is either the determination of emphysema predominant or airway predominant disease, and is based on the morphological appearance of the lung tissue associated with structural changes and airflow limitation. The basis of quantification in CT is largely reliant on the intensity or Hounsfield Units (HU) values that constitutes the CT image. The HU values are proportional to the degree of x-ray attenuation and represents the density of the lung tissue. The HU value for the lung parenchyma ranges from -1000 HU (air) to approximately 50 HU (blood). Air present in the lung appears dark and blood vessels appear bright in a typical lung CT scan, as shown in Figure 1.3. This information is valuable for the quantification of COPD related manifestations to the lung parenchyma.

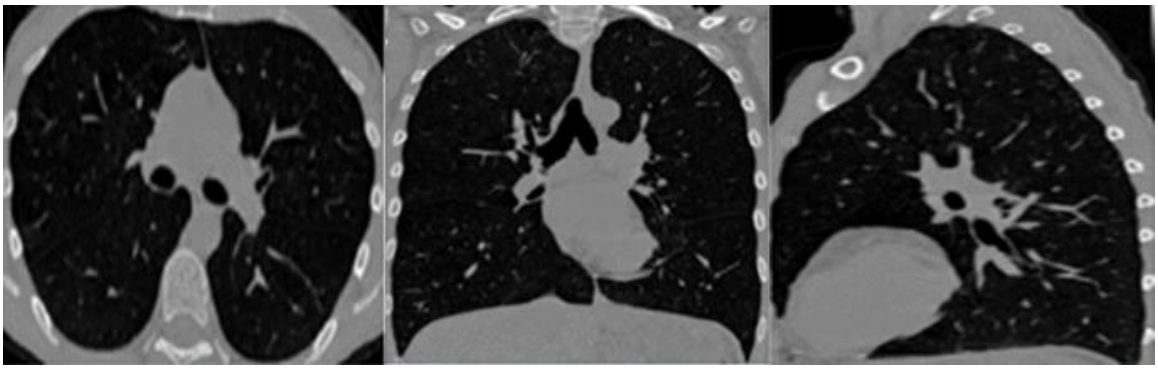

Figure 1.3: Typical axial, coronal, and sagittal views from the pulmonary CT scan

Pulmonary emphysema involves damage to alveolar walls due to permanent enlargement of airspaces that are distal to the terminal bronchioles [22]. The parenchyma that is affected by emphysema loses its elastic recoil causing small airway collapse during expiration. This further increases the amount of air trapped inside the lungs. There are three subtypes of emphysema relative to the involvement of pulmonary acinus. Centriacinar emphysema predominantly appears in upper lobes and is associated with inflammation at the centers of pulmonary acinus [13]. Panacinar emphysema occurs uniformly throughout the acinar structures and is more common in lung bases. Distal acinar emphysema is primarily involved with the destruction near the alveolar ducts and sacs. The early detection of emphysema in mild COPD patients is challenging as it has been shown that it takes 30% of lung parenchymal destruction in order to see the changes in the spirometry diagnosis. Prior to CT, emphysema assessment required post-mortem specimens, therefore limiting the available data to analyze and understand the pathology. Emphysema is usually defined from the inspiration CT scan, whereas a similar technique can be used on the expiration scan to extract the percentage of air trapping in COPD patients. The most commonly used cutoff for the quantification of air trapping is -856 HU. The extent of emphysema is generally assessed by measuring the percentage of CT intensity values that are closer to air (-1000 HU). This method is often referred as CT densitometry technique. Hayhurst et al. [23] initially used the frequency distribution of HU values to distinguish patients with and without emphysema. Later, Muller et al. extended this analysis and introduced the concept of "density mask" that highlights voxels that are below a fixed threshold [24]. A fixed threshold of -910 HU was initially used to estimate emphysema extent. Emphysema severity is defined as the relative percentage of voxels that are less than -910 HU, these

regions are called low attenuation areas (LAA). Coxson et al. used percentile cut off method on the frequency distribution curve to accurately estimate the emphysema extent [25]. Gevenois et al. later reported the use of -950 HU as a cutoff as it yielded strongest correlations with emphysema at microscopic and macroscopic levels [26]. However, the smaller size of emphysema lesions in mild COPD patients makes it challenging to diagnose the disease. Mishima and Coxson et al. used fractal analysis to find a relationship between the lesion size and its correlations with clinical outcomes in COPD patients [20, 27]. The latter study by Coxson et al. showed that the patients with larger emphysematous lesions had better outcomes after lung volume reduction surgery. A similar outcomes has shown by Flaherty et al. that the emphysema in the upper lobes as a best predictor of increased FEV1 after surgery. The National Emphysema Treatment Trail (NETT) confirmed these associations that patients with upper-lobe emphysema showed better outcomes after the lung volume reduction surgery. As the use of CT in emphysema quantification seen significant advancements in the clinical front, its dependency on the single cutoff made it less reproducible. Boedeker et al. showed that the CT reconstruction algorithm alone can make a difference of up to 15% in the emphysema quantification using the threshold technique after carefully controlling the patient's lung volume. There are multiple other factors which might influence the measurement of emphysema on CT, such as respiratory status of the patient, CT acquisition protocol, slice thickness, and patient's lung volume at the time of scanning.

Pulmonary CT scans are also being increasing used to quantify airway disease in COPD patients. Wall area percent (WA %), defined as 100 times the airway wall area divided by total airway cross-sectional area, is used to estimate the morphological changes

in the airways in smokers. Hasegawa et al. showed strong correlations between distal airway wall thickness and lung function measurements. The expiratory-inspiratory CT attenuation ratio is also a popular method to estimate the degree of airflow obstruction in COPD patients [28, 29]. Several studies showed the percent low attenuation regions in the expiration CT image correlated better with the airflow limitation than the measurements from the inspiration CT images [30-32]. Matsuoka et al. [33] used the HU values in the range of -860 HU and -950 HU and showed there is significant correlation with airflow obstruction and change in low attenuation areas, especially in the presence of mild to moderate emphysema. However, the same study reported that there is no significant correlation in moderate to severe emphysema patients [33].

CT density-based measures of COPD showed sensitivity in recognizing COPD presence and severity, however its dependence on single threshold and its limitations in detecting the early disease led to studies exploring other computer-aided diagnostic (CAD) approaches in COPD. A majority of CT-based quantification work in COPD is expected to serve as a "second opinion" to the clinician in confirming the diagnosis. One way to characterize the lung tissue in CT images is by analyzing tissue texture patterns [35-37]. In other words, texture analysis looks at spatial relationship between CT density values that are consistent with particular pathology across patients. This relationship provides more relevant information on the heterogeneity and morphology of emphysema lesions. A CAD system learns such patterns based on clinical ground truth/label and can be further used to label an entirely new image, if such patterns are present. Uppaluri et al. used the CT-based texture measures to classify emphysematous lesions in COPD patients [35-37]. The authors derived a list of texture measures from the individual patches in the CT image based on

five first-order statistics: mean, median, skewness, kurtosis, and standard deviation. This 2D method, called as adaptive multiple feature method (AMFM), showed good sensitivity in discriminating normal from COPD patients. However, the AMFM method did not have a significant correlation with the pulmonary function measurements. Later, Xu et al. extended this approach to 3D tissue patches and was able to distinguish the normal appearing lung in non-smokers and smokers [38]. Several others extended this use of texture analysis and also evaluated the effectiveness of new measures such as gray-level co-occurrence matrices (GLCM), gray-level run-length matrices (RLM), local binary patterns (LBP), and Gaussian filter bank (GFB) [35-41]. Ginsburg et al. used GLCM and RLM based texture measures to discriminate normal lung tissue from centrilobular nodularity and lesions [42]. Ojala et al. proposed the use of 2D LBPs to define lung tissue texture and showed promising results in the classification [43]. Later, Sorensen et al. used LBPs and GFB feature sets to classifying emphysematous tissue at several stages of COPD [44]. They have successfully used a machine learning approach to train the computer a set of patterns based on the ground truth availability and tested the classifier on an entirely new dataset. Nishio et al. tested the effectiveness of LBP based texture measures that are derived from a low-dose CT image dataset in classification of emphysema subtypes [45]. Recently Teresa et al. used embedded principal component analysis (PCA) and achieved 77% accuracy in discriminating emphysema subtypes [46]. Lately, there is also a lot of interest generating towards using convolutional neural networks to classify emphysema subtypes [47-49]. The advantage of using convolutional neural networks is that, the classifier can learn the measures automatically instead of using hand-crafted measures, as mentioned in the above studies.

1.4. CT Image Registration

Although CT density and texture-based measures showed good sensitivities in characterizing lung parenchyma affected by COPD components, these measures do not provide any insights on mechanical properties of the lung tissue, which can be achieved through CT image registration techniques. The changes in pulmonary tissue mechanics in accordance to tissue destruction in COPD patients provides valuable information on lung elasticity and its ability to expel air from the lungs. Since many of the currently undergoing multi-center studies involving COPD research include CT image acquisition protocol of at least two volumes (full inspiration and full expiration/residual volume) [51-53], a proper extraction of useful information from the two images is highly desired. The first step in this process is to bring the two CT images taken at different levels of inspiration into the same coordinate system, allowing for voxel-by-voxel comparisons. This process is known as image registration or image matching. Image registration is frequently used in medical image processing to align images across modalities, to compare pre- and post-intervention changes, targeted radiotherapy applications, and segmentation tasks.

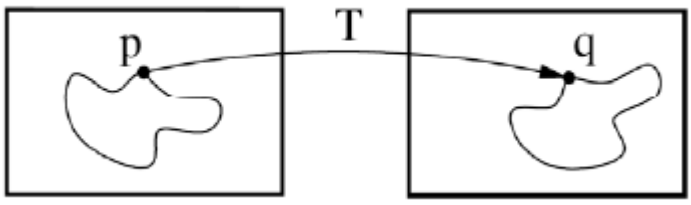

Figure 1.4: Image registration is the task of finding a spatial transformation mapping of one image (p) to another (q), adapted from Ibanez et al. [54]

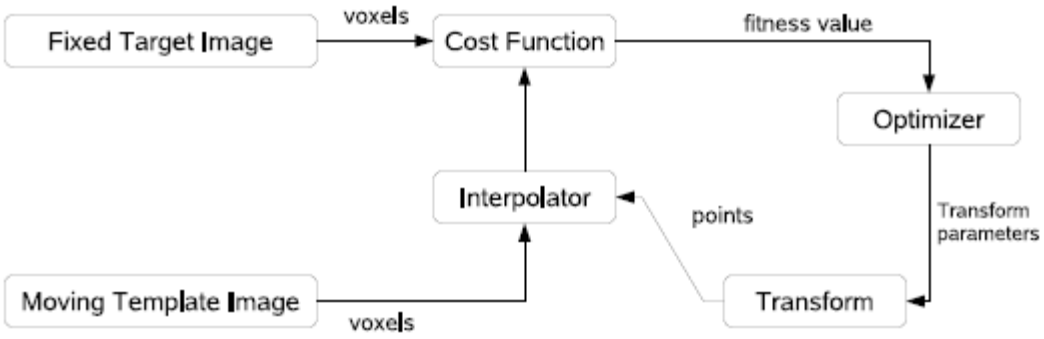

Figure 1.5: The framework of registration includes basic components as two input images (fixed and moving image), a transform, a cost function, an interpolator and an optimizer, adapted from Ibanez et al. [54]

Image registration is a task of finding spatial relationship between two images. In medical image registration, it is a process of deforming the moving image pixels or voxels to biologically corresponding points in the fixed image. A typical image registration framework is shown in Figure 1.4. The major components in the framework include similarity measure, transformation metric, and optimizer. The user has to define a moving image and fixed image, where the moving image is the image that will be spatially transformed in to the same coordinate system as the fixed image. The transformation metric represents the spatial mapping of points and establishes a correspondence for every pixel in the fixed image to a position in the moving image. A similarity measure is a cost function that measures the accuracy of the matching between two images and provides a quantitative criterion to the optimizer. Essentially, registration process can be seen as an optimization problem where a cost function C is minimized with respect to the transformation metric T.

The similarity measure is a key component of the image registration process. It measures the degree of similarity between the moving and fixed image and relays this information to the optimizer in the process. The mean sum-of-squared differences (SSD) is a commonly used metric. SSD computes the pixel-wise intensity differences at each iteration of the process and is heavily based on the assumption that the intensities shall remain same between the corresponding points of the images. However, this assumption is not true in the case of a lung image registration protocol, as the intensity or tissue densities do change due to the changes in airflow between inspiration and expiration. However, the measures such as normalized cross-correlation (NC) and mutual information (MI) metrics are insensitive to the CT density changes and are increasingly being used in lung image registration protocols. The lung tissue undergoes mechanical changes between breathing cycles that are highly heterogeneous in nature with the involvement of airways and blood vessels. The local expansion and contraction of the lung tissue varies and depends on the gravitational forces, body orientation, airway branching patterns, and underlying morphological changes caused by pulmonary disorders. To capture this non-rigid deformation of the lung tissue, a non-linear transformation function and a robust similarity measure that is insensitive to density changes is needed for the registration process. Lung image registration methods are mainly categorized into two types based on the similarity information used in the process: intensity-based and feature-based methods. Intensity-based methods make use of natural contrast present between pulmonary structures to find the voxel-by-voxel correspondence between the moving and fixed image. Manually annotated landmarks that can be based on airway bifurcations and vessel tree structures are the most common intensity-based registration methods. A number of registration

algorithms have been proposed for lung CT images. Ourselin et al. used block matching in the registration process [55]. Han et al. proposed the use of 3D SIFT descriptors and mutual information metrics to develop a hybrid feature-based registration method [56]. Recently, Garbunova et al. developed a modified SSD measures by using lung volume and weight information to preserve the lung mass between the two volumes [57]. In this work, we have used the similarity measure proposed in [58, 59], which preserves the lung tissue volume and has demonstrated superior registration accuracy.

The similarity measure from [58, 59] accounts for the lung CT intensity variations during the respiratory cycle, known as sum of squared tissue volume difference (SSTVD) [41, 58, 59]. The main objective of this measure is to provide a quantification criterion for the spatial match that has minimal local intensity variations. In lung CT images, the image voxel values are a function of tissue and air content. We can estimate the regional tissue volume and air volume from the HU values in the image. It is assumed that HU_{air} is equal to -1000 and HU_{tissue} is equal to 0, then the tissue volume (V) in a voxel at position **X** is estimated as

$$V(\mathbf{X}) = v(\mathbf{X})\frac{HU(\mathbf{X}) - HU_{air}}{HU_{tissue} - HU_{air}} = v(\mathbf{X})\,\beta\big(I(\mathbf{X})\big) \tag{1.1}$$

where v(x) is the volume of voxel x. Similarly, the air volume V' in a voxel can be estimated as

$$V'(\mathbf{X}) = v(\mathbf{X})\frac{HU_{tissue} - HU(\mathbf{X})}{HU_{tissue} - HU_{air}} = v(\mathbf{X}) \propto \big(I(\mathbf{X})\big) \tag{1.2}$$

Where the sum of $\propto (I(X))$ and $\beta(I(X))$ is equal to 1 and HU_{tissue} and HU_{air} is assumed as 0 and -1000. Then

$$\propto (X) = \frac{-HU(X)}{1000}, \beta(X) = \frac{HU(X) + 1000}{1000}$$

Let $I_1(\mathbf{X})$ and $I_2(\mathbf{X})$ be the intensity values, $v_1(\mathbf{X})$ and $v_2(\mathbf{X})$ be the voxel volumes, and $V_1(\mathbf{X})$ and $V_2(\mathbf{X})$ be the tissue volume in the voxel of images I_1 and I_2 respectively. Then the SSTVD is defined as [60, 61]

$$C_{SSTVD} = \int_{\Omega} \left[V_2(\mathbf{X}) - V_1(\boldsymbol{h}(\mathbf{X}))\right]^2 dx$$

$$C_{SSTVD} = \int_{\Omega} \left[V_2(\mathbf{X})\beta(I_2(\mathbf{X})) - V_1\left(\boldsymbol{h}(\mathbf{X})\beta\left(I_1(\boldsymbol{h}(\mathbf{X}))\right)\right)\right]^2 dx \quad (1.3)$$

The final step of the registration framework is choosing the optimization method that finds the best transformation matrix for the provided input images. In our work, we have used a limited-memory, quasi-Newton minimization methods with bounds (L-BFGS-B) algorithm that is often used in high dimensional problems. A spatial multiresolution approach is employed to tackle the memory-intensive task of registering two 3-dimensional CT images. The idea is such that the registration is initially performed at a coarse scale with fewer pixels in the images and the resulting transformation is used in the next finer scale. This approach is carried until the finest scale. The B-spline transformation grid spacing is also refined from large to small with the spatial resolution. The use of the multiresolution approach was shown to improve speed, accuracy, and robustness in obtaining the final transformation matrix.

1.5. CT Registration-based Lung Mechanics

Local lung tissue expansion and contraction measures can be estimated using image registration of pulmonary CT images taken at different levels of inflation. Reinhardt et al. used the Jacobian determinant of the transformation field to quantify the local volume changes in pulmonary CT images [59]. However, as the lung tissue is non-homogenous, the local volume change estimation is not enough to map the overall mechanical properties of lung tissue. The regional deformation is also depends on the orientation preference and its magnitude. In the next sections, we explain the measures that represents the mechanical properties of lung tissue, which can be derived from lung CT image registration methods.

1.5.1. Local Volume Change (Jacobian determinant)

This feature measures the local volume change under deformation from the inspiration to expiration registration procedure. The Jacobian determinant is a measurement to estimate the point wise volume expansion and contraction during the deformation [58, 61]. In a 3D space, Let $h(x) = [h_1(x), h_2(x), h_3(x)]^T$ be the vector transformation and $u(x) = [u_1(x), u_2(x), u_3(x)]^T$ represents the deformation fields. The relationship between $h(x)$ and $u(x)$ is shown as $h(x) = x + u(x)$. The Jacobian of transformation J (h(x)) at $x = (x_1, x_2, x_3)^T$ is defined as

$$J(h(x)) = \begin{vmatrix} 1 + \frac{\partial u_1(x)}{\partial x_1} & \frac{\partial u_2(x)}{\partial x_1} & \frac{\partial u_3(x)}{\partial x_1} \\ \frac{\partial u_1(x)}{\partial x_2} & 1 + \frac{\partial u_2(x)}{\partial x_2} & \frac{\partial u_3(x)}{\partial x_2} \\ \frac{\partial u_1(x)}{\partial x_3} & \frac{\partial u_2(x)}{\partial x_3} & 1 + \frac{\partial u_3(x)}{\partial x_3} \end{vmatrix} \quad (1.4)$$

where J > 0, preserve orientation; J > 1, local expansion; J = 1, no deformation; 0 < J < 1, local contraction; J = 0, non-injective; J < 0, reverse orientation.

The Jacobian at a given point gives important information about the transformation h near that point [62, 63]. If the Jacobian value is zero at x, then the transformation h is not invertible. If the Jacobian value is negative, then transformation reverses orientation. A positive Jacobian preserves the orientation.

1.5.2. Strain Analysis

Deformation patterns are characterized by the regional distribution of a strain or stretch tensor by the displacement fields from the registration process. A displacement gradient tensor u can be calculated as the partial differentiation of the displacement vector with respect to the material coordinates.

$$\nabla u = \begin{vmatrix} \frac{\partial u_x}{\partial x} & \frac{\partial u_x}{\partial y} & \frac{\partial u_x}{\partial z} \\ \frac{\partial u_y}{\partial x} & \frac{\partial u_y}{\partial y} & \frac{\partial u_y}{\partial z} \\ \frac{\partial u_z}{\partial x} & \frac{\partial u_z}{\partial y} & \frac{\partial u_z}{\partial z} \end{vmatrix} \quad (1.5)$$

By applying strain tensor on the deformation gradient, the distribution of stress in the lung can be calculated. Linear strain along $x, y\ and\ z$ axes are defined as

$$\varepsilon_x = \frac{\partial u_x}{\partial_x}, \varepsilon_y = \frac{\partial u_y}{\partial_y}, \varepsilon_z = \frac{\partial u_z}{\partial_z} \quad (1.6)$$

where $u = [u_x, u_{y,} u_z]^T$ is the 3D displacement field. The concept of the strain is used to evaluate how much a given displacement differs locally from a rigid body displacement [64]. The strain tensors are represented as orthogonal eigenvectors by single value decomposition method. The maximum eigenvalue for each tensor is called maximum

principle strain. Strain analysis gives valuable information about the directionalities in local tissue deformation.

1.5.3. Anisotropic Deformation Index

Orientation preference also plays a role in the lung deformation in addition to the volume change [65]. Some regions may undergo no volume change with significant deformation and vice versa due to the compensation effects of lung elasticity. Anisotropic deformation index calculates the ratio of length in the direction of maximal extension to the length in the direction of minimal extension. This index is calculated by decomposing the deformation gradient tensor in to stretch and rotational component.

$$F = \begin{vmatrix} 1 + \frac{\partial u_1(x)}{\partial x_1} & \frac{\partial u_2(x)}{\partial x_1} & \frac{\partial u_3(x)}{\partial x_1} \\ \frac{\partial u_1(x)}{\partial x_2} & 1 + \frac{\partial u_2(x)}{\partial x_2} & \frac{\partial u_3(x)}{\partial x_2} \\ \frac{\partial u_1(x)}{\partial x_3} & \frac{\partial u_2(x)}{\partial x_3} & 1 + \frac{\partial u_3(x)}{\partial x_3} \end{vmatrix} = RU \qquad (1.7)$$

where R is the rotational tensor and U is the stretch tensor. The Cauchy-green deformation tensor is defined as

$$C = FF^T = R^T U^T RU = U^T U \qquad (1.8)$$

To obtain the stretch information from U, C is decomposed using Eigen decomposition. After taking the square root of eigenvalues of C, we get the eigenvalues of U which are principal stretches. The ratio of maximum eigenvalue over the minimum gives the regional stretch information, which represents anisotropic deformation index [66]. The value of ADI is always greater than or equal to one. If the value is close to one, it means there is an isotropic expansion and if the value is big, it represents anisotropic deformation.

1.6. Application of Mechanical Analysis to COPD and Significance of Our Work

CT image density and texture-based analyses have been shown to be successful in the quantification of individual components, such as emphysema and air trapping in COPD patients. However, none of these methods provide information of lung mechanics and ability of lung parenchyma between breathing cycle, which is vital in any pulmonary disorders. With the availability of inspiration and expiration CT image for every patient in the ongoing COPD related clinical trials, there is a clear interest in extracting biomarkers by using the information from both the images to interpret the disease better. Several authors have used voxel-by-voxel registered maps to capture the change in CT attenuation values and extracted ventilation maps, phenotypical characteristics in the population and separated emphysema from small airway disease component [57, 67-70]. Recently, Galban et al. used image registration to distinguish non-emphysematous lung tissue from emphysematous lung tissue, using a method known as the parametric response mapping (PRM) technique [67]. This technique is based on the assumption that the common voxels that are less than -950 HU in the inspiration image and -856 HU in the expiration image constitute to emphysematous tissue, whereas the voxels that became less than -856 HU are solely related to functional small airway diseases (fSAD). The voxel-by-voxel comparison is only possible when inspiration and expiration are brought to the same coordinate system. The authors have used non-rigid image registration technique to achieve this. Later, Bhatt et al. used the PRM technique and showed the functional small airway disease (fSAD) component is associated with FEV_1 decline in COPD patients after 5-year follow up [71]. Similarly, Murphy et al. used image registration and showed that the information extracted

from the paired inspiratory and expiratory CT images provided better classification of the GOLD severity stages of COPD [70].

Gorbunova et al. subtracted the registered baseline image from the follow up CT image of COPD patients to quantify and monitor COPD disease progression [57, 68]. The authors have quantified the local destruction of lung tissue between baseline and follow up in COPD population. Choi et al. used mass-preserving image registration to extract lung functional measures and showed significant differences between normal and severe asthma patients [72]. Petersen et al. used CT image registration protocols to capture the longitudinal changes in the airways of COPD patients [73]. Each centerline point of the airway was matched to the nearest centerline point in the image at the future time point using the registration process. The authors have showed that there is change in mean airway density (MAD) between time points and MAD is negatively correlated with the change in predicted FEV_1 measure. Ederle et al. did similar analysis to evaluate the relationship between central airway dimensions and lung density in pulmonary CT images [74]. The authors found strong correlations between mean lung density and cross-sectional area of the trachea. Recently, Kim et al. used an in-house developed non-rigid registration technique to study the density change between inspiration and expiration CT of COPD patients [75]. The authors have showed that, in COPD patients, there is significant air trapping in the lung even though it is labeled as "normal" according to densitometry analysis. Matsuoka et al. paired the expiration CT to the inspiration CT image and showed the voxels between -500 and -950 HU are sensitive to spirometry measures of airflow obstruction in COPD patients [76]. Nishio et al. used a deformable registration technique

to evaluate the sole effect of air trapping component on the airflow limitation in COPD patients [77].

The above mentioned studies show that the measures that are derived based on CT image registration provide significant information in understanding and phenotyping COPD population. In this thesis, we evaluate the effectiveness of CT image registration-based lung mechanical measures in COPD diagnosis, severity and progression. We hypothesize that lung tissue mechanics in COPD patients were affected by the underlying disease components and quantification of these changes might be useful in identifying COPD presence and severity, phenotyping COPD population and also in monitoring and predicting disease progression. The use of lung mechanical measures that capture the local tissue expansion and contraction ability in COPD patient diagnosis is a significant contribution to the current research in COPD. Our measures and combined evaluations of quantitative CT measures related to COPD diagnosis may help interpret the disease better.

1.7. Organization of the Thesis

This thesis is divided into six chapters. The rest of the thesis is organized as follows. Chapter 2 presents our results on the effectiveness of registration-based lung mechanical measures in confirming COPD presence and severity. We have trained a classifier to predict COPD severity stages based on CT-based density, texture and lung mechanical measures and evaluated individual feature subset capability on a new test data set. Chapter 2 is based on the following publication:

Sandeep Bodduluri, John D. Newell, Eric A. Hoffman, and Joseph M. Reinhardt. "Registration-based lung mechanical analysis of chronic obstructive pulmonary disease (COPD) using a supervised machine learning framework." Academic Radiology (2013).

Chapter 3 presents the relationship between the derived CT-based lung mechanical measures and clinical outcomes in COPD patients. We create multiple prediction models that are adjusted for COPD patient demographic to evaluate the significance of lung mechanics in predicting clinical outcomes in COPD patients. Chapter 3 is based on the following article (manuscript in review):

Sandeep Bodduluri, Surya P Bhatt, Eric A. Hoffman, John D. Newell Jr., Carlos H. Martinez, Mark T. Dransfield, Meilan K. Han, and Joseph M. Reinhardt, for the COPDGene Investigators. Biomechanical CT Metrics Are Associated With Patient Outcomes in COPD. Thorax (accepted)

Chapter 4 presents the role of CT-based lung mechanical measures in diagnosis of COPD. We have used a subset of COPD patients that had a discordance between pulmonary function test diagnoses and CT density-based diagnosis, tested the role of lung mechanics in confirming the diagnoses. Chapter 4 is based on the following publication:

Surya P. Bhatt., Sandeep Bodduluri, John D. Newell, Eric A. Hoffman, Jessica C. Sieren, Meilan K. Han, Mark T. Dransfield, Joseph M. Reinhardt, and COPDGene Investigators. "CT-derived biomechanical metrics improve agreement between spirometry and emphysema." Academic Radiology (2016).

Chapter 5 presents our results related to the role of the normal lung tissue mechanics in predicting COPD progression. We use the mechanical characteristics of "normal looking" lung tissue based on CT-density and evaluate its importance in predicting FEV_1 decline in COPD patients. Chapter 5 is based on the following article (manuscript in preparation):

Sandeep Bodduluri, Surya P Bhatt, Eric A. Hoffman, John D. Newell Jr., Mark T. Dransfield, and Joseph M. Reinhardt, for the COPDGene Investigators. CT-based biomechanical measures of normal lung tissue and their role in disease progression. (in preparation).

Chapter 6 includes discussion and future directions of our work.

CHAPTER 2

IDENTIFICATION OF COPD PRESENCE AND SEVERITY USING CT REGISTRATION-BASED LUNG MECHANICS

2.1. Introduction

Chronic obstructive pulmonary disease (COPD), a growing health concern, is the fourth leading cause of death in the world [78]. COPD is primarily due to irreversible airflow obstruction caused by small airways disease and emphysema. Small airways disease causes structural changes within the lung with loss of airways, airway wall thickening and luminal narrowing. Emphysema leads to destruction of alveolar walls with decreasing lung elastic recoil, loss of blood vessels, airways and loss of extracellular matrix attachment to airway walls. While chronic smokers constitute the highest COPD susceptible population in the United States, worldwide people that are exposed to indoor air pollution using biomass for heating and cooking as well as other environmental lung irritants form another major group of COPD patients [10, 79]. Current diagnosis for COPD assessment is done by spirometry or pulmonary function testing (PFT), which is based on global lung volumes. The Global Initiative for Chronic Obstructive Lung Disease (GOLD) defines four severity stages (GOLD1-4) of COPD based on PFT measurements which lump all of the individual phenotypes associated with COPD into a single measure of gas flow at the mouth because PFT parameters ignore regional heterogeneity of the disease and the underlying disease components and disease etiology. Critical to the development of novel, targeted treatments for COPD is the identification of individual phenotypes which have historically been lumped together under the fairly non-descript title, "COPD."

Computed tomography (CT), has emerged as a tool for quantitatively characterizing parenchymal destruction and small airways involvement. CT allows regional assessment of the disease component and the CT derived measurements have been shown to correlate well with the pathology of the disease [18-20, 44, 50, 76]. CT is commonly used to measure the extent of emphysema in the lungs and can be more sensitive than spirometry in quantitating disease progression. Emphysema is quantified using CT densitometry techniques, which for example can calculate the percentage of voxels falling below a given Hounsfield Unit (HU) threshold in the inspiration image [25]. Expiratory CT has also been shown to be useful in calculating the extent of air trapping using CT densitometry techniques [13, 32, 33]. However, density measurements are influenced by CT reconstruction algorithm or other technical parameters and are dependent on the single threshold value [80]. CT image texture also plays an important role in characterizing lung tissue and its pathologies. Uppaluri et al. proposed the 2D adaptive multiple feature method (AMFM), which captures textural patterns on the CT image. This method has shown good sensitivity in characterizing lung tissue [35-37]. Later, an extension of this method to 3D by Xu et al. further showed good sensitivity in discriminating smoker and nonsmoker subjects [38]. Sorensen et al. proposed a multi-scale Gaussian filter bank approach to define the texture on the CT images and has shown better discrimination of COPD and normal subjects with good correlations to the lung function measurements [44, 50]. Although density and texture based features serve to map lung destruction and remodeling, these measures do not provide insights into the mechanism of disease onset or disease progression. Mishima et al. have suggested that once emphysema has been initiated with the appearance of small, regionalized tissue destruction, disease progression occurs, in part,

because of mechanical factors serving to cause small holes to converge rather than new, isolated small holes emerging [20]. It is important that new imaging-based metrics provide maps of parenchymal mechanics to allow for an improved understanding of subject-specific alterations in lung mechanics and regional parenchymal stresses.

Mechanical analysis on a regional level can be done from CT images by image registration of a pair of scans at different inflation levels. Regional ventilation measurements from the registration of inspiration and expiratory CT have been shown useful to determine pulmonary function in COPD subjects [70]. Previously, we have developed methods to estimate regional lung tissue expansion and contraction using image registration and biomechanical analysis, and have shown these measures compare well with the other indices of lung function [59]. In this study it has been our hypothesis that these regional lung tissue estimates from the image registration will provide valuable information on lung function changes in COPD subjects. We propose a biomechanical feature set comprising three registration based metrics of lung function to describe COPD presence and severity. We also hypothesize the combination of density, texture and biomechanical features can be used to evaluate the severity of COPD more accurately than the individual usage of the feature sets, thus leading to more descriptive measures of the disease. We have used a machine learning framework to evaluate the performance of the obtained biomechanical feature set and compared it to the density and texture based feature sets. Correlations with the PFT parameters and health status metrics were also reported.

2.2. Materials and Methods

2.2.1. Dataset

A database of 162 subjects with varying distribution of COPD severity and nonsmoker subjects without COPD were used in this study. All the subjects were approved by the institutional review boards and provided written consent for participation in the study. The distribution of the subjects was: 27 nonsmokers, 30 GOLD 0, 29 GOLD1, 29 GOLD2, 28 GOLD3, and 19 GOLD4. These subjects were selected from the Iowa Cohort of the COPDGene study. The COPDGene Study is a multi-institutional research focused on COPD and other smoking related pulmonary diseases [reference ISBN 1541-2563 (Electronic). All the patients in this study completed spirometry, health related quality of life questionnaires and CT scanning of the lungs at full inspiration and expiration.

2.2.2. Data Collection

The COPDGene protocol included the collection of demographic information, smoking history, using self-administered questionnaires. Health related quality of life is estimated using St. George's respiratory questionnaire (SGRQ), which comprises four categories (symptoms, activity, impact and total score) with scores in each category ranging from 0 to 100. The higher the score the more severe the disease. Spirometry was performed following the American Thoracic Society guidelines. The metrics reported include forced expiratory volume in 1 second (FEV_1), which is the volume of gas forcibly exhaled during the first second of the expiration maneuver, and forced vital capacity (FVC), which is the total volume of gas forcibly exhaled after a full inspiration. The demographic information and PFT measures are shown in Table 1.

2.2.3. CT Image Acquisition

CT scans were acquired at the University of Iowa with either a 64 or 128 multidetector CT scanner (Somatom Sensation 64 or Somatom Definition FLASH; Siemens Medical Solutions, Erlangen, Germany) following the COPDGene protocol. Images were acquired with the patient in the supine position during a single breath hold at full inspiration (total lung capacity (TLC)) and a single breath hold at normal expiration (functional residual capacity (FRC)). The scans followed an imaging protocol with a peak tube voltage of 120 kV; tube current time product of 200 mAs for TLC scans and 50 mAs for FRC scans; gantry rotation time of 0.5s; and pitch a pitch of 1. The images were reconstructed at B31f kernel with a slice thickness of 0.75 mm and a reconstruction interval of 0.5 mm respectively, study protocol specifications for Siemens CT scanners [51].

2.2.4. Image Preprocessing

CT inspiratory and expiratory images were downloaded, down sampled to reduce memory requirements, and stored in 16-bit Analyze (Mayo Clinic, Rochester, MN) format. CT images were first segmented to extract lung structures. Segmentation was carried out using a region growing technique where the given image is segmented into regions based on the discontinuities in the gray level and by the selection of initial seed points in the region. The flow of steps from the image preprocessing to machine learning experiments are shown in figure 1.

2.2.5. Image Registration

The inspiratory and expiratory CT images were registered for each subject. A lung mass preserving registration method was used to capture the large volume changes between these two images (9). This method uses a similarity metric called the sum of squared tissue

volume difference (SSTVD), which estimates the local tissue and air fraction by minimizing local tissue mass difference [58, 59]. This method has been shown effective in lung image registration protocols [59]. Displacement field information corresponding to the tissue deformation patterns in the lung from inspiration to expiration was extracted from the registration process.

2.2.6. Feature Calculation

In this study, we formed three sets of features from CT images: density based feature set, texture based feature set, and biomechanical feature set. 62 features were calculated from the inspiration and expiration images of a single subject. A summary of the features calculated is shown in figure 1.

The density based feature set consists of two measures representing the extent of emphysema and air trapping in a subject. These measures were estimated using the threshold technique computing the percent of voxels below a certain threshold in CT images. Emphysema extent is expressed as the percentage of voxels below -950HU in the inspiration image. Air trapping extent is expressed as the percentage of voxels below -856HU in the expiration image.

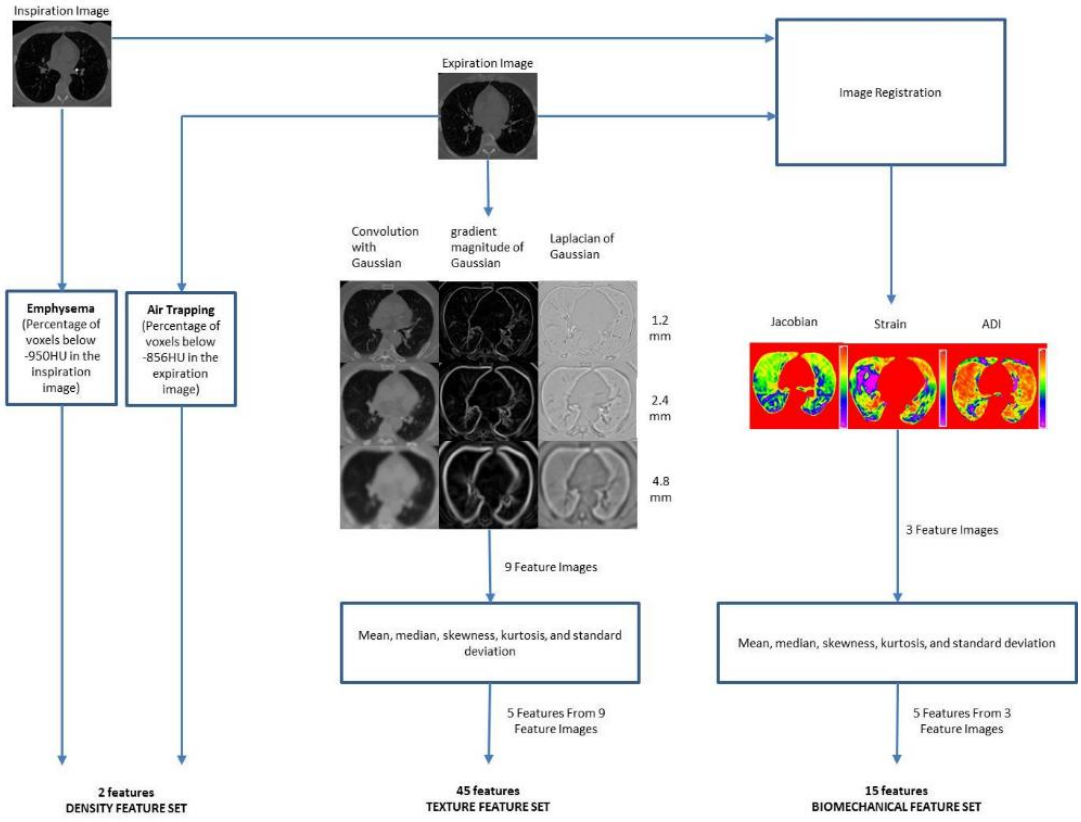

Figure 2.1: Flow chart explaining the steps involved from image acquisition to classification experiments

In order to capture the textural patterns, a set of 45 features was computed using three local image descriptors at three different scales. The local descriptors are based on the Gaussian function and its derivatives. The three local descriptors are: 1) convolution with Gaussian, which smooth the image and reduces the noise; 2) gradient magnitude of the Gaussian, which emphasizes edges and region boundaries; and 3) Laplacian of Gaussian, which computes second derivative of the image to highlight the regions of rapid intensity changes. These three filters were calculated at three different scales: 1.2 mm, 2.4 mm and 4.8 mm (18). Three filters at three scales were applied to the expiration images in the dataset giving rise to nine filtered versions of the image. For each of the filtered images,

the mean, median, skewness, kurtosis, and standard deviation was computed for voxels in the lung region, thus producing a total of 45 features as a texture-based feature set. Examples of the nine filtered images of a GOLD1 and GOLD4 subjects' expiration image are shown in figure 2.

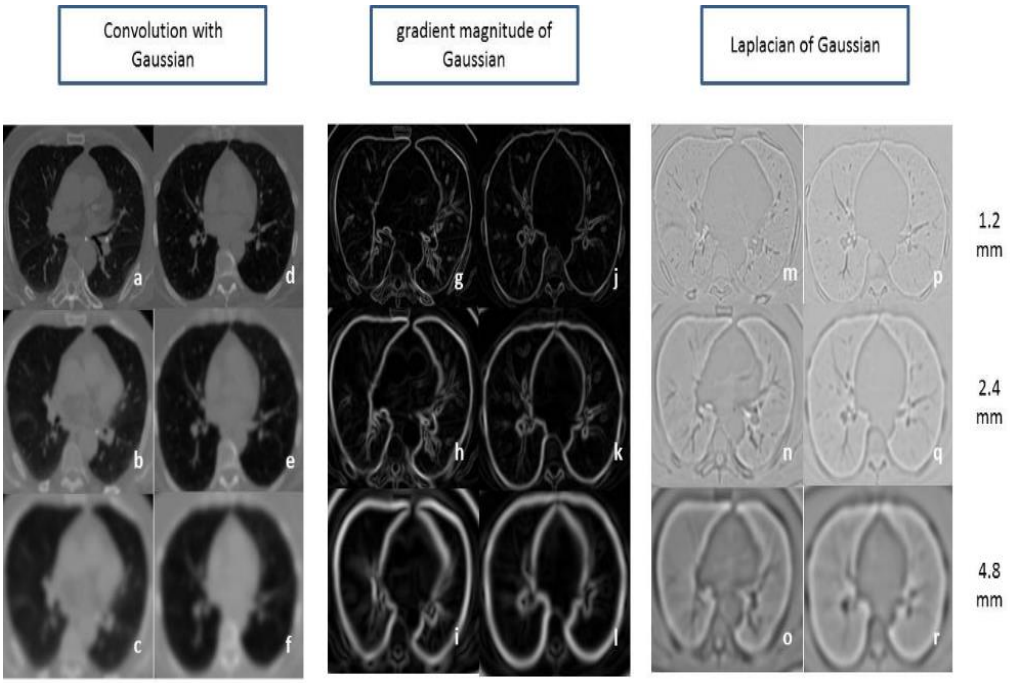

Figure 2.2.: Axial slices of a GOLD1 and GOLD4 COPD subject. a, d) Convolution with Gaussian at 1.2mm standard deviation b, e) Convolution with Gaussian at 2.4mm standard deviation c, f) Convolution with Gaussian at 4.8mm standard deviation g, j) Gradient magnitude of Gaussian at 1.2mm standard deviation h, k) Gradient magnitude of Gaussian at 2.4mm standard deviation i, l) Gradient magnitude of Gaussian at 4.8mm standard deviation m, p) Laplacian of Gaussian at 1.2mm standard deviation n, q) Laplacian of at 2.4mm standard deviation o, r) Laplacian of Gaussian at 4.8mm standard deviation

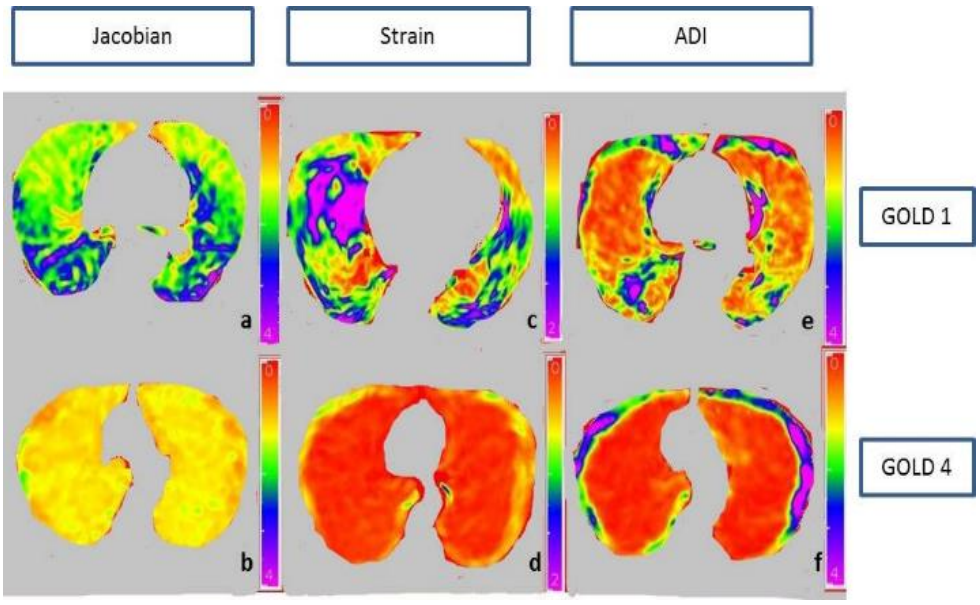

Figure 2.3.: Axial slices of a mild COPD (GOLD1) and severe COPD (GOLD4) subject. a) Jacobian map of GOLD1 subject b) Jacobian map of GOLD4 subject c) Strain map of GOLD1 subject d) Strain map of GOLD4 subject e) Anisotropic deformation index map of GOLD1 subject f) Anisotropic deformation of GOLD4 subject

The mechanical feature set is comprised of features calculated from the image registration of inspiration scan to the expiration scan. Mechanical analysis on a regional level is done by finding out the local tissue deformation pattern from the correspondence of each voxel between inspiration and expiration image. Three measures were calculated in this feature set: Jacobian, strain information and anisotropic deformation index (ADI). The Jacobian or Jacobian determinant measures the local volume change under deformation from the inspiration to the expiration. The Jacobian determinant is a measurement to estimate the point wise volume expansion and contraction during the deformation (9, 24). If the Jacobian value is one at a given voxel, then there is no deformation happened. If the value is greater than 1, it represents local expansion. If the

value is less than 1, it represents local contraction. The concept of the strain is used to evaluate how much a given displacement differs locally from the inspiration to the expiration (31). Maximum principle strain is computed using displacement fields from the registration process to represent strain information. Anisotropic deformation index provides the orientation preference of the lung deformation. It calculates the ratio of length in the direction of maximal extension to the length in the direction of minimal extension (3). We have calculated five first order statistical features: mean, median, skewness, kurtosis and standard deviation for each of three feature images. A total of 15 features were computed to form the lung biomechanical feature set. The three biomechanical feature images: Jacobian, strain and ADI of a GOLD1 and GOLD4 subject are shown in figure 3.

2.2.7. Feature Selection and Classification

Optimal features were selected out of 62 features using a linear forward feature selection technique. This technique is a modified version of the sequential forward selection technique (32, 33). In the linear forward selection, the user will be able to limit the number of features that are considered in each step which in turn reduces the run time and the number of evaluations. With the selection of optimal set of features from each set, we have performed two classification experiments using the k nearest neighbor learning algorithm (KNN) (34). This algorithm is a non-parametric approach based directly on distances computed between the test and training data points. For any given test data point, KNN searches its nearest neighbors formed by the training sets. The classifier returns the selected number of neighbors, k, which are closest in the distance. The decision is made based on the majority vote of its neighbors, with the test point assigned to the group most common among its nearest neighbors, shown in figure 5.

2.2.8. Statistical Analysis

Statistical experiments were performed using Microsoft Excel (Microsoft, Redmond, WA) and MATLAB software (MATLAB 7.12, The MathWorks Inc., Natick, MA, 2011). P values < 0.05 were considered statistically significant. Pearson's correlation coefficients were calculated to investigate the correlation between the PFT parameters and the optimal CT based features. Spearman correlation coefficient was calculated to investigate the correlation between SGRQ scores and CT based features.

First experiment is to classify a given subject into either COPD or non COPD class using the three feature sets. Nonsmoker and GOLD0 subjects were considered as non COPD group in this experiment. Feature selection is carried out on 90 subjects (30 non COPD/ 60 COPD) out of 162 subjects used in the experiment. Second experiment is to classify a given subject into their corresponding severity stage. Feature selection is carried out on 75 subjects (15/severity stage) out of 135 subjects ranging from GOLD0 to GOLD4 stage.

For both training and test subjects, the optimal features from the feature selection process were used in further classification experiments. Feature selection and classification experiments were implemented using WEKA machine learning tool (33). For training purposes, dataset was divided into training and testing sets and repeated ten times, with each split randomly selected each time. For each split, area under receiver operator characteristic curve (AUC) is reported. The best k (number of neighbors) value in the kNN algorithm is selected by cross validation. Predictions of test data are ranked by the probability of the class label and AUC for each class is separately calculated using one versus all approach. By considering the number of instances of a particular class label as

the weight, average AUC of the ten splits is computed. Multiple regression analysis was performed using EXCEL software (Microsoft, Redmond, WA) to find the correlation between optimal features from each feature set and PFT measurements. Adjusted R squared correlation coefficient is reported for each combination of optimal features which takes the sample size and number of predictor variables into account.

Table 2.1: Demographic information and PFT measures of the subjects in this study. The numbers reported are mean values with standard deviation in parentheses

Parameters	**Non-COPD**	**COPD**
Age	67.4 (6.79)	67.6 (5.87)
Gender (M/F)	34/23	57/39
Height (cm)	168.5 (8.66)	168.2 (9.02)
Weight (kg)	81 (11.80)	79.9 (21.30)
BMI	28.5 (4.08)	28.01 (6.26)
Pack years	16 (8.30)	39.05 (12.21)
FEV_1% predicted	0.9 (0.13)	0.55 (0.27)
FEV_1/FVC	0.7 (0.05)	0.46 (0.15)
GOLD STAGE (N/0/1/2/3/4)	27/30/0/0/0/0	0/0/29/29/28/19

2.3. Results

2.3.1. Correlation Results

Pearson's linear correlation coefficient, r, and corresponding P values were calculated between the PFT measurements and the optimal set of features from each feature set which were selected in the feature selection process. Spearman's correlation coefficient was reported to find the correlation between SGRQ total score and CT based features. The results are shown in table 2.2 and all the correlations have shown statistical significance of $P < 0.001$. Air trapping measure in the density based feature set showed strong negative correlation with FEV1/FVC ($r = -0.84$) and also showed higher correlations than the emphysema extent measure. Texture based features have also shown strong correlations with FEV1/FVC measure. A strong positive correlation is seen between the mean Jacobian and PFT parameters (FEV1%, $r = 0.80$; FEV1/FVC, $r = 0.76$). Similarly, of all the features, mean Jacobian ($r = -0.63$) and median Jacobian ($r = -0.63$) features showed strong negative correlations with the SGRQ total scores. Median feature of Laplacian of Gaussian at 4.8mm ($rho = -0.61$) in the texture based feature set showed good negative correlations with the SGRQ total score whereas emphysema ($rho = 0.46$) and air trapping ($rho = 0.56$) scores were poorly correlated.

2.3.2. COPD vs. Non COPD Classification

As an initial experiment, the performance of biomechanical and the combination feature set in detecting the presence and absence of COPD was evaluated. The dataset is divided into two classes: COPD and non COPD. Classifier is asked to classify a given subject into either of these classes using the four feature sets. The results of this experiment are shown in table 2.3. Biomechanical feature set (AUC = 0.85) performed equally well

with the density (AUC = 0.83) and texture (AUC = 0.89) based feature sets. Texture (R2= 0.72) based features showed higher correlations with FEV1/FVC measures whereas the biomechanical feature set (R2 = 0.71) showed higher correlations with FEV1% measure. All these correlations have shown a statistical significance of $P < 0.001$.

2.3.3. COPD Severity Classification

In the second experiment, COPD severity classification was performed using the four feature sets. The subjects used in this experiment ranges from GOLD0 to GOLD4 stages of COPD. Classifier is asked to classify a given subject into their corresponding GOLD stage. The results of this experiment are shown in table 2.4. Biomechanical features were more effective in recognizing COPD severity than the density and texture feature sets by achieving an AUC of 0.81 and also correlated well with the FEV1% predicted measure ($r = 0.71$), which is a COPD severity measure from PFT diagnosis. The combination feature set (ALL) achieved an AUC of 0.80 by showing higher correlations with all the diagnostic measurements. All these correlations have shown a statistical significance of $P < 0.001$.

Table 2.2: Relationship between CT derived features and clinical diagnostic measures of COPD. Pearson linear correlation coefficient is represented with r and Spearman correlation coefficient is represented with $\boldsymbol{\rho}$. All the correlations have shown statistical significance of $P < 0.0001$

Features	r **FEV$_1$%**	r **FEV$_1$/FVC**	ρ **SGRQ**
Mean Jacobian	0.80	0.76	-0.63
Median Jacobian	0.76	0.75	-0.63
Skewness Jacobian	-0.42	-0.52	0.35
Standard deviation of Jacobian	0.74	0.64	-0.59
Standard deviation of Strain	0.70	0.59	-0.53
Median Gaussian at 1.2mm	0.67	0.76	-0.52
Kurtosis Gaussian at 2.4mm	-0.59	-0.60	-0.39
Mean Gaussian at 2.4mm	0.68	0.77	-0.51
Median Gaussian at 2.4mm	0.69	0.78	-0.51
Skewness Gaussian at 4.8mm	-0.57	0.60	0.41
Skewness gradient magnitude at 1.2mm	-0.55	-0.61	0.47
Skewness gradient magnitude at 4.8mm	-0.61	-0.66	0.55
Median Laplacian of Gaussian at 4.8mm	0.70	0.72	-0.61
Kurtosis Laplacian of Gaussian at 4.8mm	0.24	0.26	-0.2
Emphysema (voxels below -950HU)	-0.65	-0.73	0.46
Air trapping (below -856HU)	-0.78	-0.84	0.56

Table 2.3: Classification results of COPD/non COPD classification. AUC values reported from the ROC analysis with standard deviation in the parenthesis. Correlation results from multiple regression analysis between optimal features of density, texture, lung biomechanical features with PFT parameters and SGRQ scores. All the correlations have shown statistical significance of $P < 0.001$

Feature Sets	**AUC**	**FEV_1%predicted (R^2)**	**FEV_1/FVC (R^2)**	**SGRQ Total score (R^2)**
Density	0.83 (0.04)	0.57	0.68	0.30
Texture	0.89 (0.04)	0.58	0.72	0.37
Biomechanical	0.85 (0.05)	0.71	0.68	0.41
ALL	0.87 (0.05)	0.73	0.77	0.47

Table 2.4: COPD severity classification results. AUC values reported from the ROC analysis with standard deviation in the parenthesis. Correlation results from multiple regression analysis between optimal features of density, texture, lung biomechanical features with PFT parameters and SGRQ scores. All the correlations have shown statistical significance of $P < 0.001$

Feature Sets	**AUC**	**FEV_1%predicted (R^2)**	**FEV_1/FVC (R^2)**	**SGRQ Total score (R^2)**
Density	0.76 (0.04)	0.57	0.69	0.26
Texture	0.73 (0.03)	0.57	0.70	0.30
Biomechanical	0.81 (0.03)	0.71	0.63	0.35
ALL	0.80 (0.03)	0.72	0.73	0.35

Table 2.5: AUC values at each GOLD stage of COPD from COPD severity classification experiment. The standard deviation values are represented in parenthesis

Feature Sets	**GOLD0**	**GOLD1**	**GOLD2**	**GOLD3**	**GOLD4**
Density	0.86 (0.05)	0.74 (0.05)	0.58 (0.09)	0.79 (0.04)	0.88 (0.06)
Texture	0.80 (0.04)	0.77 (0.04)	0.57 (0.08)	0.69 (0.06)	0.85 (0.09)
Biomechanical	0.82 (0.05)	0.74 (0.08)	0.78 (0.07)	0.84 (0.07)	0.96 (0.04)

2.4. Discussion

The two classification experiments conducted in this study show that the estimates of regional lung tissue expansion and contraction can serve as a useful parameter to describe COPD in pulmonary CT scans. Such COPD quantification, based on regional lung mechanics, is a step forward in understanding the disease impact on the lung function. The relationship between the CT derived biomechanical features and clinical diagnostic measures (PFT measurements, SGRQ scores) were estimated by correlation, as shown in table 2. The jacobian features, which capture local volume changes, have shown strong correlations with FEV1% predicted ($r = 0.80$), FEV1/FVC measures ($r = 0.76$). It has also shown strong negative correlations ($\rho=-0.63$) with the SGRQ scores, which depicts the disease impact on patient's quality of life. Overall, the biomechanical measures have shown strong correlations with the severity diagnostic measure, FEV1% predicted. This suggests a strong relation between estimates of lung mechanics and severity level of COPD. On the other hand, density and texture based features have shown higher sensitivity towards diagnostic measure, FEV1/FVC with strong correlations.

Density based features have been previously shown to be effective in COPD diagnosis [18, 28, 30, 81]. Earlier studies using CT textural patterns have also been shown to be successful in judging the presence of COPD [35-37, 44, 50]. The proposed lung biomechanical features were tested against these existing CT derived features. Moreover, in our study, all these three feature sets were combined to form a single feature set (ALL) and the combined performance was thereby evaluated. As a first classification experiment, a two-class problem was defined by dividing the dataset into two groups; COPD (GOLD1-4) and non COPD (nonsmokers and GOLD0). The biomechanical features showed similar performance with the existing density and texture features in discriminating subjects with and without COPD, with an AUC of 0.85, as shown in table 3. Also, a good correlation with the PFT measurements and SGRQ scores was shown. However, it should be noted that texture based features performed reasonably better than the biomechanical features. Since, the subject range in this classification is from nonsmokers to GOLD4 (very severe); there is a possibility of minimal lung functional changes happening at the initial stages. As a consequence, this may lead to a higher number of misclassifications between nonsmokers, GOLD0 and GOLD1 groups, resulting in overall reduction of the classifier performance with biomechanical features. In this study, density and texture based features proved their sensitivity in recognizing COPD presence or absence by achieving an AUC of 0.83 and 0.89. The optimal features from these two feature sets showed strong correlations (R2=0.68, 0.72) with the diagnostic measure, FEV1/FVC.

In the second experiment, a five class problem was then defined to categorize COPD subjects into their corresponding GOLD stage. Biomechanical features are more effective in COPD severity classification (AUC = 0.81) than the density (AUC = 0.76) and

texture (AUC = 0.73) feature sets, as shown in table 4. The strong correlations with FEV1% predicted show the sensitivity of biomechanical features to the level of COPD severity. Another interesting observation that can be made from this experiment is the performance of these features at different stages of the disease. In table 5, the AUC values of the feature sets in classifying each severity stage of COPD is shown. It shows that the biomechanical feature set performance is improved at the later stage of the disease than at the initial stages. All the feature sets were less effective in classifying GOLD1 and GOLD2 stage subjects. Especially, in classifying GOLD2 subjects, lung biomechanical features are more sensitive than the density and texture based features. This suggests the possibility of major lung functional changes at GOLD2 stage, which were captured by lung biomechanical features. This shows that the lung mechanics provide valuable information at later stages of the disease which was not possible to capture using the density and textural features.

In both the experiments, another feature set (ALL) is evaluated, which is formed by combining all the three feature sets together. While recognizing COPD presence or absence in the first experiment, ALL achieved similar AUC (0.87, table 3) but it has shown better correlations with the PFT measurements and SGRQ total scores. Similarly, in the second experiment (table 1.4), adding biomechanical features to the density (AUC = 0.76) and textural features (AUC = 0.73), further showed an improvement in the classifier performance (AUC = 0.80). Also, there is a strong correlation with the clinical diagnostic measures of the disease. This shows biomechanical features add useful measures to the density and texture based features for more accurate diagnosis of COPD severity from CT images. The proposed features performed comparatively well with the previous methods of COPD diagnosis and severity classifications. The adaptive multiple feature method

(AMFM), proposed by Uppaluri et al., based on textural patterns of 2D CT images achieved an accuracy of 100% in classifying normal and severe emphysema subjects but with no significant correlation with PFT measures of emphysema [35-37]. The extension of 2D AMFM to 3D AMFM proposed by Xu et al. showed better results in discriminating normal smoker and nonsmoker lung parenchyma [38]. Another texture based approach proposed by Sorensen et al. based on Gaussian filter versions of CT, achieved an AUC of 0.713 in classifying COPD and Non-COPD subjects (18). In COPD severity classification, registration based ventilation measures proposed by Murphy et al. achieved 67% classification accuracy [70]. In COPD diagnosis and severity experiments, the biomechanical feature set achieved an AUC of 0.85 and 0.81, as shown in table 2.3 and 2.4, and also correlated well with the PFT measures and SGRQ scores. However, in addition to the density and texture based features that were used in this study, there are several other CT derived features providing robust quantification of COPD [45, 49, 82]. The texture based feature set consists of only three basic Gaussian filtered versions of the image at multiple scales. The number of features used in this study was less which gives a definite scope in testing the effectiveness of several other features either individually or in combination with the proposed biomechanical features. A complete system consisting of all the CT derived features related to both emphysema and small airway disease may result in more accurate diagnosis of COPD.

2.5. Summary

This study demonstrates the effectiveness of the registration based estimates of lung tissue expansion and contraction in COPD diagnosis. Three measures were extracted from the registered scans and the features based on these three measures showed good correlations with the pulmonary function. The classification experiments illustrated that the proposed measurements perform equally well or better than the density and texture feature sets in assessing COPD presence and severity. Also, the inclusion of biomechanical features to the density and texture improved the classifier performance with higher correlation to pulmonary function indices. With further testing on larger databases, the proposed approach may be used for accurate measure of the pulmonary function and disease.

CHAPTER 3

RELATIONSHIP BETWEEN CT REGISTRATION-BASED LUNG MECHANICS AND PATIENT OUTCOMES IN COPD

3.1. Introduction

Airflow obstruction is the hallmark of chronic obstructive pulmonary disease (COPD); however, computed tomography (CT) is increasingly used to characterize and phenotype subtypes of COPD [83]. The major subtypes of structural lung disease visualized on CT, emphysema and thickened airway walls, are both independently associated with airflow obstruction [84, 85]. These metrics of disease on CT have also been shown to be associated with important patient reported and objective outcomes such as dyspnea,[86] quality of life, [87, 88] exercise capacity, [89, 90] the BODE (Body-Mass Index, Airflow Obstruction, Dyspnea, and Exercise Capacity) index,[87] and mortality [91]. A substantial number of patients with COPD, however, have significant discordance between spirometry and CT findings. We recently demonstrated that a biomechanical measure of structural lung disease (the Jacobian determinant, an elasticity measure of local lung volume change assessed through matching images acquired at multiple lung volumes) substantially explains the differences between static CT images and airflow obstruction on spirometry.[92, 93] However, it remains important to determine if the Jacobian determinant is associated with standard clinical measures of patient outcomes. Such determination will enhance its use in better phenotyping patients. We analyzed data from a large subset of a well characterized cohort of participants with COPD who underwent clinical, physiological and radiographic assessments. We hypothesized that the mean Jacobian determinant, an

indirect measure of lung elasticity, would provide additional explanation for the variations in clinically relevant outcomes including dyspnea, quality of life, functional capacity, and the BODE index, as well as mortality.

3.2. Methods

3.2.1. Patient Selection

We analyzed participants enrolled in the Genetic Epidemiology of COPD (COPDGene) study, a large, ongoing, multicenter cohort study that includes current and former smokers aged 45 to 80 years, and without other chronic lung diseases except COPD and asthma. Demographics were collected as per the COPDGene protocol via self-administered questionnaires. Details of the study protocol have been previously published.[51] Post-bronchodilator spirometry was performed using the ndd EasyOne spirometer to assess airflow obstruction. COPD was diagnosed using the ratio of forced expiratory volume in the first second (FEV_1) to the forced vital capacity (FVC) of < 0.70, and severity categorized according to Global initiative for Chronic obstructive Lung Disease (GOLD) guidelines.[94] All participants provided written informed consent and the research protocol was approved by the institutional review board at each participating center. The first 1000 participants to enroll, and with complete image registration CT data, were included in the study reported here.

3.2.2. Morbidity Data

Respiratory-related quality of life was assessed using the St. George's Respiratory Questionnaire (SGRQ).[95] Scores were calculated for the three main subdomains of the SGRQ: symptoms, activities and impact. Total score ranges from 0 to 100, with higher scores indicating worse quality of life. The minimum clinically important difference

(MCID) for SGRQ is 4 units. Dyspnea was quantified using the modified Medical Research Council dyspnea score; the score ranges from 0 to 4, with greater score indicating worse dyspnea.[96] Exercise tolerance was assessed using the six minute walk distance (6MWD); MCID for the 6MWD is 26 m.[97] The multidimensional BODE index was finally calculated using body mass index, FEV_1 %predicted, mMRC and 6MWD; the scale ranges from 0 to 10, with greater scores indicating a higher risk of mortality.[98] We also obtained data on mortality on longitudinal follow-up.

3.2.3. CT Image Acquisition

Volumetric CT scans were acquired with the subject in the supine position during a carefully coached breath-hold to either full inspiration (total lung capacity; TLC) or end expiration (functional residual capacity; FRC). The scanning protocol included a collimation, 0-5mm; tube voltage, 120kV; tube current, 200mAs; gantry rotation time, 0.5s; and a pitch, 1.1. The images were reconstructed with a standard kernel (dependent upon the make and model of the scanner) and a slice thickness of 0.75mm and an interval of 0.5mm.

3.2.4. CT Image-based Measures

Densitometry: Using 3D Slicer software, we measured emphysema and gas trapping based on density mask analyses.[51] Emphysema was quantified by using the percentage of voxels at TLC with attenuation < -950 Hounsfield units (HU) and gas trapping was quantified as the low attenuation areas on FRC scan that are < -856 HU. We used Pulmonary Workstation 2 (VIDA Diagnostics, Coralville, IA, USA) to measure the wall area percentage of segmental airways (WA%) that represent airway remodeling.[51]

Image Registration: The full inspiration (TLC) and end expiration (FRC) scans were registered for each subject. A lung mass-preserving registration method was used to capture volume changes between the two phases of respiration.[99] A sum of squared tissue volume difference (SSTVD) method was used as a similarity metric. This method has been shown previously to be effective in lung image registration protocols.[92, 93] The transformation matrix from the registration process was used to derive regional tissue expansion and contraction measures between TLC and FRC volumes. In this study, we used the Jacobian determinant metric to represent regional deformation patterns in COPD patients. The Jacobian determinant measures the local volume change and estimates the pointwise expansion and contraction during deformation of the lung from TLC to FRC. This results in a deformation map that has values ranging from 0 to infinity. A Jacobian determinant value greater than 1 indicates local expansion whereas less than 1 indicates local contraction. A Jacobian determinant value equal to 1 indicates neither local expansion nor contraction. We used the mean of the Jacobian deformation map as a lung mechanical measure for each subject representing local deformation patterns between TLC and FRC volumes. **Figure 1** shows representative Jacobian deformation maps for participants with different disease severity and quality of life

3.2.5. Statistical Analyses

We expressed all values as mean (standard deviation, SD). Pearson and Spearman correlation analyses were performed to assess the pairwise relationship of Jacobian determinant with SGRQ scores, BODE index, mMRC, 6MWD and FEV_1. Association between Jacobian determinant and SGRQ was assessed using univariate and multivariable linear regression models after adjustment for age, sex, race, pack-years, BMI, FEV_1, CT

emphysema, CT gas trapping, WA%, and CT scanner type. As there was an overrepresentation of zero BODE scores, we used zero-inflated Poisson regression analyses to test the association between Jacobian determinant and the BODE index, after adjustment for the above mentioned variables, except for FEV_1 and BMI as they are part of the BODE index. Finally, to test the discriminatory accuracy of the Jacobian determinant in predicting the BODE score, we categorized the BODE score at its median (4 or less versus 5 to 10) and calculated the c-index for CT variables using receiver operating characteristics (ROC) analyses. The threshold of 4 was also based on the substantially worse survival for participants with BODE>4 in the original study.[98] We compared the c-index for the Jacobian determinant with that for percent emphysema in predicting BODE$\geq$4 scores. In addition, the capacity of the Jacobian measure to predict a categorized BODE (0 to 4 versus 5 to 10) was assessed using multivariable logistic regression classifier after adjustment for the above mentioned variables. The area under the curve and Akaike information criterion (AIC) were used to compare the capacity of models in predicting categorized BODE (0 to 4 versus 5 to 10). We used the DeLong comparison method to compare the c-indices of different models. To calculate prediction of mortality on follow-up, we performed Cox proportional hazards analysis. Variables significant on univariate analysis at $p<0.05$ were entered into a multivariable Cox proportional hazards model to calculate adjusted hazards ratio for mortality for the Jacobian determinant; we forced CT scanner type into the model as this is clinically important. All tests of significance were two-tailed, and we considered an alpha level of <0.05 as statistically significant. All analyses were performed using Statistical Package for the Social Sciences (SPSS 22.0, SPSS Inc., Chicago, IL, USA) and R statistical software (version 3.2).

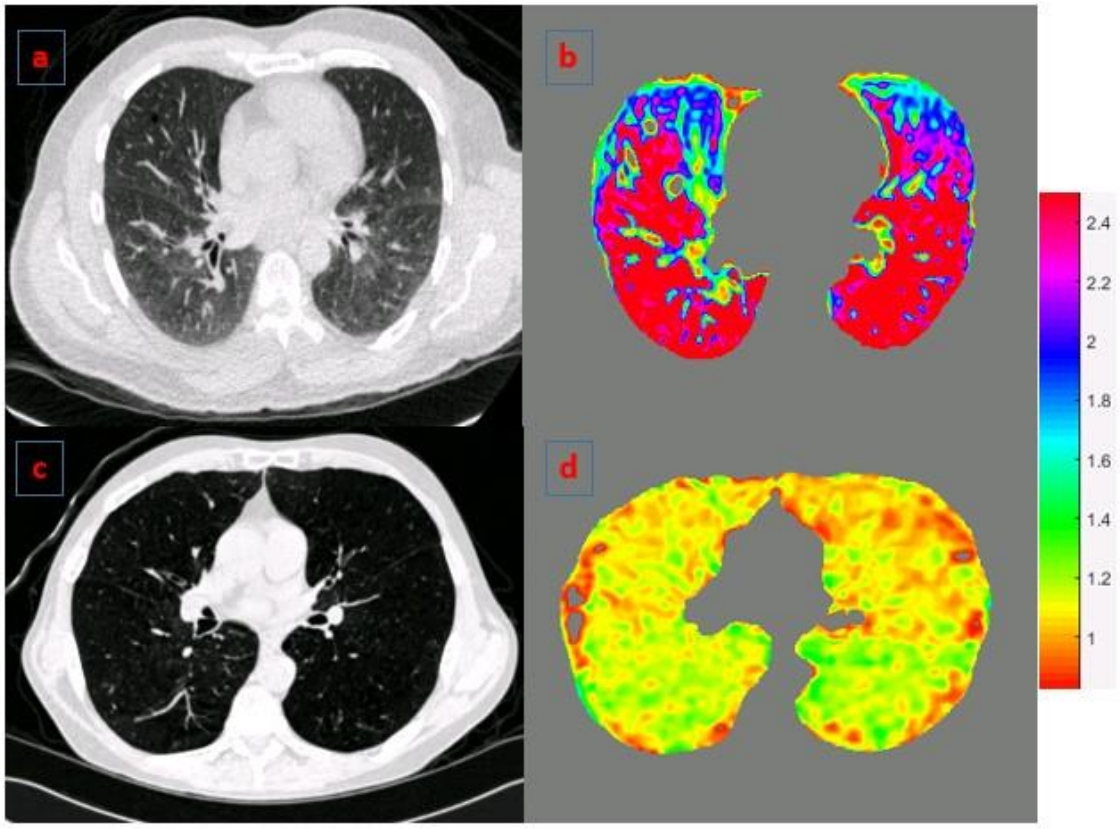

Figure 3.1: Panels a and b show axial CT section and the corresponding deformation map respectively for a representative participant with GOLD 1 with low BODE index. Panels c and d show similar images for a representative participant with GOLD 4 COPD and high BODE index. The colors depict the Jacobian deformation map from full inspiration to end expiration and show the variability in regional tissue expansion patterns across both subjects. Jacobian determinant = 1 represents no deformation; >1 = local expansion; and <1 = local contraction.

3.3. Results

Table 3.1: Baseline demographics, physiologic assessments, CT quantification of COPD and morbidity scores

Parameter	Mean (SD)
Age (years)	64.6 (8.2)
Female (%)	240 (49)
African American (%)	78 (16)
BMI (kg/m^2)	27.5 (5.8)
Smoking pack-years	52.9 (26.1)
Current Smokers (%)	333 (68)
FEV_1 (L)	1.49 (0.7)
FEV_1 % Predicted	53.2 (22.0)
FVC (L)	2.96 (1.0)
FVC % Predicted	80.0 (21.3)
FEV_1/FVC	0.49 (0.12)
CT Emphysema (%)	12.4 (12.1)
CT Gas Trapping (%)	37.9 (20.3)
Airway Wall Area (%), segmental airways	62.3 (3.1)
SGRQ (Total Score)	37.6 (22.4)
6MWD (m)	360 (145)
BODE index#	3 (1-5)
mMRC score#	2 (1-3)

Demographics: Of the first 1,000 participants to enroll, 562 participants had COPD GOLD stages 1 to 4. We excluded 72 participants due to image registration errors in boundary alignment. **Table 3.1** shows the baseline demographics, physiologic assessments, CT quantification of COPD and respiratory morbidity scores. The mean age of the participants was 64.6 (8.2) years. The cohort was comprised of 250 (51.1%) males and 240 (48.9%) non-Hispanic Whites. Participants had a substantial cigarette smoking burden with mean pack-years of 52.8 (26.1); 336 (68%) were active smokers at the time of enrollment. The participants encompassed the spectrum of disease severity, with 62 (12.7%), 204 (41.6%), 138 (28.2%) and 86 (17.6%) having GOLD severity stages 1 through 4 respectively.

Correlation between the Jacobian measure and respiratory morbidity: Pair-wise relationship analysis between the Jacobian determinant and patient outcomes was performed. There was an inverse and statistically significant association between the Jacobian determinant and total SGRQ scores ($r = -0.46$; $p<0.001$), the BODE index ($r = -0.60$; $p <0.001$), and mMRC scores ($r = -0.41$; $p <0.001$). There was a positive association between the Jacobian determinant and the six-minute walk distance ($r = 0.47$; $p <0.001$) and FEV_1 ($r = 0.60$; $p <0.001$).

CT measures and SGRQ: Table 3.2 shows univariate and multivariable associations between the CT metrics of emphysema, gas trapping, WA% and the Jacobian measure with SGRQ. On univariate regression, the Jacobian determinant was significantly associated with SGRQ (unadjusted regression co-efficient β=-38.1, 95%CI= -46.8 to -29.2; $p<0.001$); this relationship held true after adjustment for age, sex, race, BMI, FEV_1, smoking pack years, CT emphysema, CT gas trapping, airway wall area (WA%), and CT scanner type. (β=-11.75, 95%CI= -21.6 to -1.7; $p=0.020$).

Table 3.2: Univariate and multivariable associations of mean Jacobian determinant measure with SGRQ

Parameter	Univariate Regression		Multivariable Regression	
	β (95%CI)	P value	β (95%CI)	P value
Age (years)	-0.50 (-0.7, -0.2)	< 0.001	-0.68 (-0.9, -0.4)	< 0.001
African American race	12.22 (6.9, 17.5)	< 0.001	6.73 (1.6, 11.7)	0.009
Female sex	-0.91 (-4.9, 3.0)	0.652	-1.69 (-5.5, 2.1)	0.390
BMI (kg/m^2)	0.21 (-0.1, 0.5)	0.219	0.39 (0.0, 0.7)	0.013
FEV_1 (L)	-15.4 (-17.8, -13.2)	< 0.001	-10.65 (-14.2, -7.0)	< 0.001
Smoking pack-years	0.11 (0.03, 0.18)	0.003	0.16 (0.1, 0.2)	< 0.001
CT Emphysema (%)	0.57 (0.4, 0.7)	< 0.001	0.33 (0.0, 0.5)	0.002
CT Gas Trapping (%)	0.44 (0.3, 0.5)	< 0.001	-0.01 (-0.1, 0.1)	0.990
Airway Wall Area, (%)	2.51 (1.8, 3.1)	< 0.001	0.95 (0.3, 1.5)	0.002
Mean Jacobian determinant	-38.08 (-46.8, -29.2)	< 0.001	-11.75 (-21.6, -1.7)	0.020

CT measures and 6MWD: The relationship between CT metrics and the 6MWD is shown in Table 3.3. On univariate analysis, the Jacobian measure was significantly associated with distance walked (β=770.1, 95%CI= 600.0 to 940.1; p<0.001); this association was maintained after multivariable adjustment (β=321.15, 95%CI= 134.1 to 508.1; p<0.001)

CT measures and BODE index: Table 3.4 shows the relationships between CT metrics and BODE index. The Jacobian determinant was significantly associated with the BODE index on univariate analysis (β= -1.77, 95%CI= -2.04 to -1.51; p<0.001), and after adjustment for age, sex, race, BMI, FEV_1, smoking pack years, CT emphysema, CT gas

trapping, airway wall area percent, and CT scanner type (β= -0.4, 95%CI= -0.8 to -0.01; p = 0.039). We also compared the utility of the Jacobian determinant in predicting BODE index 5-10 with logistic regression analyses after adjustment for other CT variables, as well as age, race, sex, smoking pack years and CT scanner type.

Table 3.5 shows that when compared to a model with traditional CT indices of COPD (Model A), including the Jacobian determinant (Model B) improves the prediction of greater BODE score (AIC 328.7 vs. 323.1; $p < 0.001$). On comparing CT indices in isolation after adjustment for age, race, sex, pack-years and CT scanner variability in the prediction of high BODE score (5 to 10), the c-index for CT emphysema was 0.80 (95%CI 0.75 to 0.85; p=0.010) and 0.69 (95%CI 0.64 to 0.75; p=0.040) for WA%. The adjusted c-index for Jacobian alone was 0.77 (95%CI 0.72 to 0.82; p=0.024). Combining traditional CT measures with Jacobian determinant resulted in greater accuracy in predicting high BODE score (5 to 10) with c-index 0.86 (95%CI 0.82 to 0.90; p<0.001), p<0.001 for comparison with all other models based on individual imaging measures.

CT measures and mortality: We had follow-up data for 441 of the 490 participants for a median of 6.8 years (interquartile range 6.6 to 6.9). Of these, 99 (22.4%) died on follow-up. On univariate analyses, all CT measures were associated with mortality; unadjusted hazards ratio (HR) for CT emphysema 1.03 (95%CI 1.02 to 1.05; p<0.001), CT gas trapping 1.03 (95%CI 1.02 to 1.04; p<0.001), WA% 1.08 (95%CI 1.01 to 1.15; p<0.001) and Jacobian determinant 13.16 (95%CI 4.52 to 38.46; p<0.001). After adjustment for age, pack-years of smoking, FEV_1, CT emphysema, gas trapping, WA% and CT scanner type, the Jacobian determinant was associated with mortality (adjusted HR = 4.26, 95%CI = 0.93 to 19.23; p = 0.06).

Table 3.3: Univariate and multi-variate association of mean Jacobian determinant measure with six minute distance walked (6MWD)

Parameter	Univariate Regression		Multivariable Regression	
	β (95%CI)	**P value**	**β (95%CI)**	**P value**
Age (years)	-2.75 (-7.4, 1.9)	0.251	-3.52 (-7.7, 0.6)	0.097
African American	-331.10 (-431.6, -230.5)	< 0.001	-290.51 (-385.6, -195.3)	< 0.001
Female sex	-74.66 (-151.8, 2.49)	0.057	-31.00 (-103.6, 41.6)	0.402
BMI (kg/m^2)	-7.07 (-13.6, -0.5)	0.035	-10.79 (-16.6, 41.6)	< 0.001
FEV_1 (L)	315.72 (270.7, 360.6)	< 0.001	204.08 (136.2, 271.9)	< 0.001
Smoking pack-years	-1.18 (-2.6, 0.2)	0.115	-2.14 (-3.3, -0.9)	< 0.001
CT Emphysema (%)	-8.19 (-11.3, -5.0)	< 0.001	-7.26 (-11.8, -2.6)	0.001
CT Gas Trapping (%)	-7.10 (-9.0, -5.1)	< 0.001	2.95 (-0.3, 6.2)	0.081
Airway Wall Area (%)	-40.24 (-52.3, -28.2)	< 0.001	-12.03 (-23.5, -0.5)	0.040
Mean Jacobian determinant	770.10 (600.0, 940.1)	< 0.001	321.15 (134.1, 508.1)	< 0.001

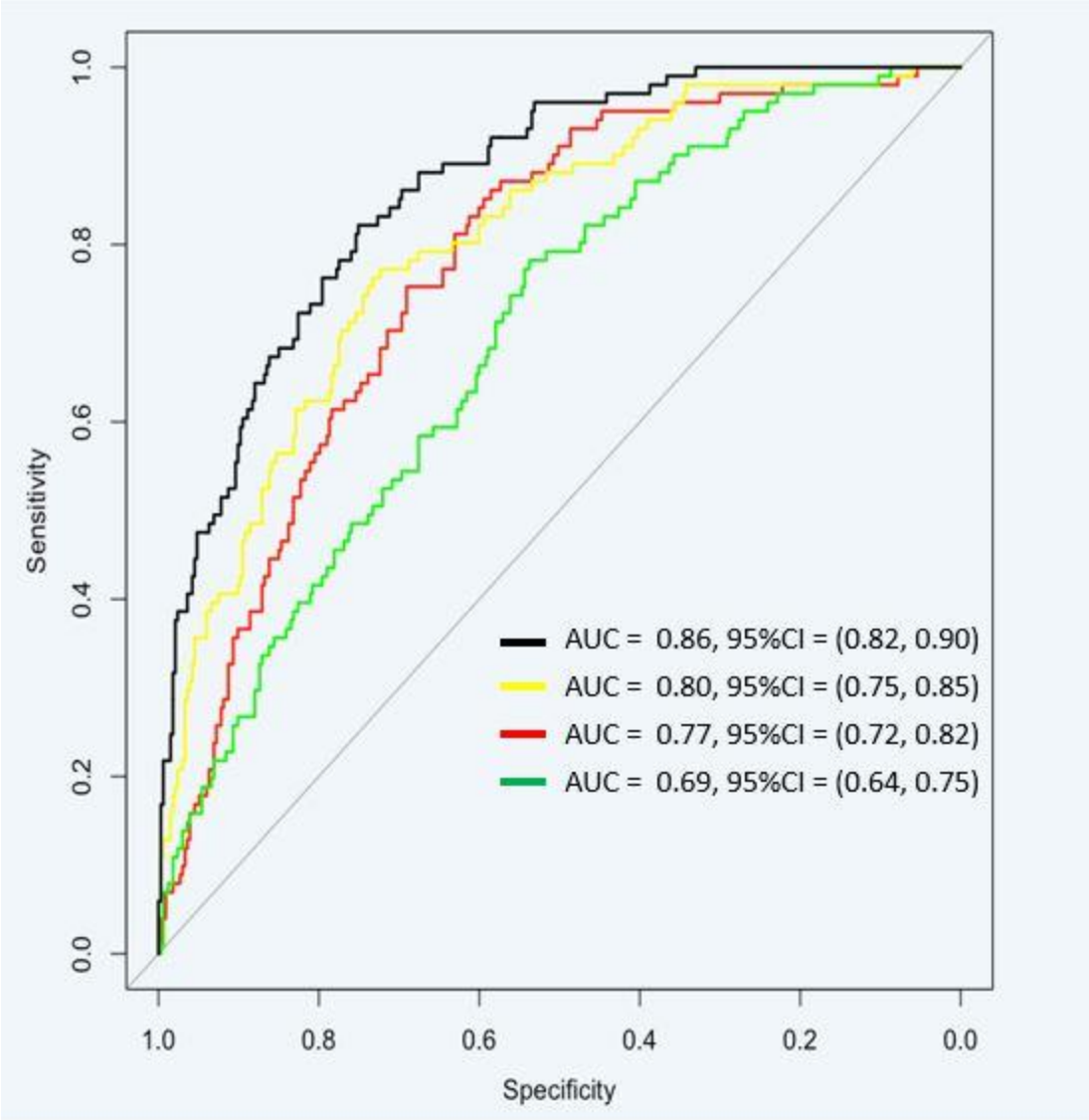

Figure 3.2. Receiver operator characteristic (ROC) curves in predicting BODE index (1-4) vs 5-10). All models are adjusted for age, race, sex, pack-years and CT scanner variability. Green represents c-index for Wall area% of segmental airways; Yellow = CT emphysema; Red: Jacobian determinant; Black = Combined CT model including CT emphysema, WA% and Jacobian determinant.

Table 3.4: Univariate and multivariable associations of mean Jacobian determinant measure with BODE index

Parameter	Univariate Regression		Multivariable Regression	
	β (95%CI)	P value	β (95%CI)	P value
Age (years)	-0.004 (-0.010, 0.002)	0.189	-0.04 (-0.014, 0.001)	0.054
African American	0.22 (0.083, 0.350)	0.001	0.16 (-0.008, 0.325)	0.059
Female sex	-0.01 (-0.112, 0.082)	0.783	0.15 (0.040, 0.275)	0.008
Smoking pack-years	0.002 (0.003, 0.004)	0.013	0.00 (0.001, 0.005)	0.001
CT Emphysema (%)	0.02 (0.021, 0.029)	< 0.001	0.01 (0.003, 0.018)	0.003
CT Gas Trapping (%)	0.02 (0.023, 0.028)	< 0.001	0.01 (0.009, 0.020)	< 0.001
Airway Wall Area (%)	0.08 (0.064, 0.102)	< 0.001	0.07 (0.050, 0.089)	< 0.001
Mean Jacobian determinant	-1.77 (-2.044, -1.507)	< 0.001	-0.41 (-0.803, -0.019)	0.039

3.4. Discussion

We demonstrated a strong relationship between the Jacobian determinant mean, a biomechanical elasticity measure of regional parenchymal volume change, and important patient outcomes including dyspnea, respiratory quality of life, functional capacity and the BODE index, a strong predictor of mortality. On multivariable analyses, we found that the effect size of a unit change in the Jacobian determinant is stronger than the effect sizes of static CT measures of COPD such as emphysema percentage, gas trapping and airway wall thickness, and also that adding the Jacobian determinant to traditional CT metrics improves the prediction of the BODE index, thus providing novel and independent information applicable to COPD phenotyping and prognosis.

It is well established that there is, at best, a modest correlation between FEV_1, the primary measure of disease severity in COPD, and clinical outcomes such as respiratory health related quality of life and dyspnea,[100, 101] and FEV_1 does not fully explain the morbidity associated with COPD. In this regard, our findings extend the results of other recent studies that demonstrated a relationship between CT metrics of COPD and clinically relevent outcomes. Although lung function impairment is correlated with poor functional outcomes, SGRQ is influenced by a number of factors that are not fully explained by FEV_1 such as cough and exacerbations. Grydeland and colleagues demonstrated that CT indices of emphysema and airway disease improved the prediction of respiratory symptoms over spirometry alone.[86] Gietema et al. showed that both airway wall thickness and emphysema are independently associated with respiratory-quality of life, [88] and Martinez et al. reported that there was a stronger association between SGRQ and airway wall thickness than between SGRQ and CT emphysema.[87] On the other hand, they also found that the BODE index was influenced more by emphysema than by airway wall thickness. Other studies have also found significant associations between measures of emphysema and airflow obstruction, exercise tolerance and dyspnea.[84, 85, 89, 90, 102]

The possible reasons for why the Jacobian determinant shows independent associations with outcomes merits discussion. FEV_1 is a global measure of lung function impairment and is influenced by both airway narrowing and decreased lung elastic recoil associated with emphysema. However, in a given patient, it is usual to see multiple subtypes of emphysema such as centrilobular and panlobular emphysema with differential impact on lung function.[103-105] The degree of CT emphysema does not translate linearly into airflow obstruction,[85, 92] and it is likely that different types and distribution

patterns of emphysema contribute differentially to airflow obstruction.[103-105] Although we did not study emphysema subtypes, the mean Jacobian determinant by offering a rough measure of lung elasticity likely reflects a more direct physiologic link between structural lung disease and the lung mechanics reflected by spirometry. Previous studies found that imaging metrics offered marginal incremental, albeit independent information, over that offered by spirometry in the prediction of respiratory quality of life. However, we showed that CT-based metrics derived from image-matching offer information that are not only independent and additive, but with effect sizes greater than FEV_1 for all the outcomes studied. In addition, dyspnea contributes significantly to respiratory quality of life as well as reduction in functional capacity, and even patients with relatively preserved FEV_1 can experience significant dyspnea and hence a poorer quality of life. This could be due to factors other than FEV_1 such as poorer diaphragmatic position due to resting as well as dynamic hyperinflation, both of which might be reflected better by changes in lung elasticity than by static CT measures of emphysema and airway disease. Our findings provide new insight into the complex pathophysiological basis and the heterogeneity of causes of changes in dyspnea and SGRQ. These findings are pertinent as dyspnea and SGRQ are frequently used as outcome measures in clinical trials of pharmacologic and non-pharmacologic therapies, once again highlighting the importance of phenotyping COPD patients.

Table 3.5: Logistic regression models for a BODE index (1-4) vs. (5-10)

Parameters	Odds Ratio (95% CI)	P-value	AIC
Adjusted multivariable model for CT measures			
CT Emphysema (%)	1.04 (1.00, 1.09)	0.034	328.71
CT Gas Trapping (%)	1.06 (1.03, 1.09)	< 0.001	
Airway Wall Area (%)	1.28 (1.15, 1.44)	0.288	
Adjusted multivariable model for CT measures with Jacobian determinant			
CT Emphysema (%)	1.06 (1.02, 1.11)	0.004	323.81
CT Gas Trapping (%)	1.03 (1.00, 1.07)	0.041	
Airway Wall Area (%)	1.24 (1.12 1.40)	< 0.001	
Mean Jacobian	1.78 (1.16, 2.76)	0.009	

We also showed that the Jacobian estimate of local lung volume change was significantly associated with the BODE index which predicts all-cause and respiratory-specific mortality in COPD.[98] This is a novel finding and adds to the findings of previous studies which demonstrated a relationship between CT emphysema and both the BODE index and mortality.[87, 91, 106] It is unclear whether the poorer mechanics are a more sensitive reflector of underlying emphysema that has been shown to be independently associated with poor outcomes, or if the affected lung mechanics have an independent role in disease progression and mortality. Of note, lung volume reduction surgery improves symptoms and mortality in a subset of patients,[107] and it is plausible that the benefits of lung volume reduction are largely due to improved lung elasticity in the ipsilateral preserved lobe [108].

One of the limitations of our study is that the CT scans were not spirometrically controlled.[109, 110] As varying respiratory effort can affect the reproducibility of image-

registration metrics, participants were coached to maximum inhalation and end expiration. As this was a multicenter trial, a number of different scanners were used for image acquisition; however, we adjusted for scanner variability. For calculating the Jacobian determinant, CT scans were obtained at only two volumes. Although this limited our ability to assess regional differences in lung mechanics along the entire spectrum of lung inflation and deflation, [111] our metrics are applicable to clinically obtained scans without the excessive radiation risks that would incurred in acquiring dynamic scans. Our study was strengthened by the inclusion of participants enrolled in a large well characterized cohort of current and former smokers that included a high proportion of African Americans.

3.5. Summary

In conclusion, biomechanical metrics of local lung expansion and contraction offer better prediction of respiratory quality of life and the BODE index and offer incremental information beyond traditional measures of lung function and static CT metrics. Thus, the Jacobian determinant mean can add to our ability to phenotype COPD patients based on the complex pathophysiological heterogeneity that extends beyond lung function measures alone.

CHAPTER 4

ROLE OF CT REGISTRATION-BASED LUNG MECHANICS IN COPD DIAGNOSIS

4.1. Introduction

The diagnosis of chronic obstructive pulmonary disease (COPD) is currently based on the detection of airflow obstruction by spirometry.[94] It is increasingly recognized that airflow obstruction as measured by impairment in the forced expiratory volume in 1 second (FEV_1) does not fully explain the morbidity associated with the disease, and this functional definition can be complemented by anatomic measures of disease using widely available imaging modalities.[112] Computed tomography (CT) has become the gold standard in the quantitative assessment of the presence and distribution of emphysema, a major component of COPD, and relies on using a fixed Hounsfield threshold value below which all lung areas are deemed emphysematous in a CT scan obtained at full inspiration.[37] CT measures of emphysema correlate well with pathology,[113] and numerous studies have shown a strong correlation between spirometry and CT emphysema. [114-121] The agreement between CT emphysema and spirometry is however not perfect, and in some cases, CT densitometry may be more sensitive in detecting emphysema than spirometry.[115, 122]

It is our observation that many COPD patients have marked discordance between FEV_1 and degree of emphysema on volumetric CT.[85, 123] Some subjects with severe airflow obstruction have mild emphysema on CT and conversely, some patients with severe emphysematous destruction of the lung have relatively mild spirometric impairment. While some of these differences, especially in the former group, are likely due to airway

narrowing, the reasons for this discrepancy between expected changes on spirometry and CT have not been systematically studied, particularly in the disproportionate emphysema group. Since airflow obstruction is due to a combination of airway narrowing and loss of elastic recoil due to emphysema, it is possible that static single-volume CT images do not capture lung mechanics sufficiently to explain lung function defects. We hypothesized that biomechanical measures of regional lung tissue expansion and contraction using image registration applied to paired inspiratory and expiratory CT scans will provide a link between CT-derived quantitative measures and spirometry. Through a demonstration of this link, we seek to provide an improved understanding of patient specific links between the presence and distribution of quantitative emphysema and airflow obstruction.

4.2. Materials and Methods

4.2.1. Data Collection

Data for this study was acquired from the Genetic Epidemiology of COPD (COPDGene) study; this is a large multicenter study of current and former smokers aged 45 to 80 years. Details of the study protocol have been previously published.[51] Post bronchodilator spirometry was performed using the ndd Easy-One spirometer to assess airflow obstruction.[124] COPD was diagnosed based on a fixed threshold for the ratio of FEV_1 to the forced vital capacity (FVC) of <0.70; disease severity was graded according to the Global initiative for chronic Obstructive Lung Disease (GOLD) guidelines.[94] Reference values for spirometry were drawn from the National Health and Nutrition Examination Survey (NHANES) III cohort.[125] Volumetric CT scans were acquired with the subject in supine position during a carefully coached breath hold to either full inspiration (total lung capacity, TLC) or end tidal expiration (functional residual capacity,

FRC); or at one center to full expiration (residual volume, RV).[51] The scans followed an imaging protocol with collimation, 0-5mm; tube voltage, 120kV; tube current 200mAs; gantry rotation time of 0.5s; and pitch, 1.1. The images were reconstructed with a standard kernel with a slice thickness of 0.75 mm and a reconstruction interval of 0.5 mm. 3D Slicer software (www.airwayinspector.org) was used to measure emphysema and gas trapping. Pulmonary Workstation 2 (VIDA Diagnostics, Coralville, IA, USA) was used to measure airway dimensions. [51]. Emphysema was quantified by using the percentage of voxels at TLC with attenuation less than -950 Hounsfield Units (HU) (low attenuation area, $\%LAA950_{insp}$), and also as the HU value at the 15th percentile (Perc15). [51, 126] Gas trapping was calculated as the percentage of voxels at FRC with attenuation less than -856 HU ($\%LAA856_{exp}$).[127] We used wall area percentage of segmental airways (WA%) and gas trapping to measure airway disease.[51] The COPDGene study was approved by the institutional review boards of all 21 participating centers, and written informed consent was obtained from each subject.

4.2.2. Case Selection

Subjects with GOLD stage I to IV disease, without physician-diagnosed bronchial asthma and with good quality expiratory images, were included. As there is no published data on the degree of emphysema to be expected for a given value of FEV_1, we used the percentile method to assess discrepancy between CT and spirometry to derive a sample size of convenience and also to create two widely disparate groups by spirometry and CT emphysema. We arranged all subjects (n=2982) in ascending order of severity of airflow obstruction as assessed by percent predicted FEV_1 to calculate the percentile values for spirometric abnormality; a second list was created by arranging all subjects in ascending

order of severity of CT emphysema as determined by the continuous measure Perc15 percentile. Concordance between spirometry and CT was assessed by subtracting percentile ranking for CT from percentile ranking for spirometry. Those with values closest to 0 (n=100) were considered "Matched" as they had expected ranking for spirometry compared to CT emphysema, and this group served as the reference group. Those with the greatest positive percentile ranking difference for spirometry compared to CT (n=100) were considered spirometry predominant, and those with the greatest positive percentile ranking difference for CT compared to spirometry (n=100) were considered CT predominant. 3 subjects in the CT predominant group were excluded due to failure of image registration matching.

4.2.3. Image Registration

The inspiratory and expiratory CT images were registered for each subject, and expiratory image matched to inspiratory image. A lung mass-preserving registration method was used to capture volume changes between these two targeted lung inflation levels.[61, 93] A sum of squared tissue volume difference was used as a similarity metric. This similarity criterion aims to find a registration transformation that minimizes the local difference of tissue volume inside the lungs scanned at different pressure levels. This method has been shown to be effective in lung image registration protocols.[61, 66, 93] The final transformation matrix from inspiration to expiration was derived from the registration protocol and in turn used to extract displacement field information.

Three measures were calculated from the registration process: Jacobian, strain information, and anisotropic deformation index (ADI). *Jacobian* measures the local volume change and estimates the pointwise volume expansion and contraction during the

deformation from inspiration to expiration. Jacobian has values from 0 to infinity. A Jacobian value of 1 indicates neither local expansion nor contraction. Values greater than or lesser than 1 represent local expansion and contraction respectively. Maximum principle *strain* was computed from the displacement field information to extract how much a given displacement differs locally from inspiration to expiration. Strain analysis expresses the geometric deformation caused by action of stress in the lung. *ADI* provides the orientation preference of lung deformation by calculating the ratio of length in the direction of maximal extension to the length in the direction of minimal extension within a unit volume of 1 mm.[66] The larger the ADI value, more the anisotropy is with deformation. The co-efficient of variation (CV) across the whole lung was calculated for each of these biomechanical measures to assess heterogeneity and dispersion.

4.2.4. Statistical Analyses

Univariate regression analyses were performed for CT variables with FEV_1 to assess association, and those with $p<0.05$ were included in multivariable models. Multivariable regression analyses were performed to assess associations between FEV_1 and CT metrics, after adjustment for age, race, sex, body mass index (BMI) and scanner type. Multicollinearity diagnostics were performed and variables with a variance inflation factor of greater than 10 (strain mean, ADI mean and ADI CV) were excluded from the model. Independent contribution of each covariate to the variance in FEV_1 was calculated using squared semi-partial correlation coefficient (r^2).

Further, to assess differences in the discordant groups of interest, three categories were created using differences in percentile rankings: Cat_{spir} with predominant airflow obstruction on spirometry and minimal CT emphysema; Cat_{CT} with predominant CT

emphysema and relatively minimal airflow obstruction on spirometry; and $Cat_{matched}$ with matched FEV_1 and CT emphysema. Two regression models were created with mentioned categories as outcome variables using multinomial logistic regression. CT variables significantly associated with FEV_1 were entered into the models and all models were adjusted for age, race, sex, BMI, and CT scanner type. At this stage, $\%LAA950_{insp}$ was substituted for Perc15 as a measure of emphysema as Perc15 was already used to derive the groups, and $\%LAA950_{insp}$ is more commonly used clinically to quantify CT emphysema. Model A comprised of $\%LAA950_{insp}$, $\%LAA856_{exp}$ and WA%. Biomechanical measures (mean Jacobian, CV of Jacobian, and CV of strain) were added to the predictors in Model A to create Model B. With $Cat_{matched}$ as reference category, multinomial logistic regression was used to predict Cat_{spir} and Cat_{CT}. Model fit statistics are shown in terms of Akaike Information Criterion (AIC) derived from information theory. AIC is used to estimate the quality and model comparisons and is defined as: AIC = -2Lm+ 2k, where Lm represents maximum log-likelihood and K is the number of variables in the model. AIC takes both goodness of fit and number of variables into account while penalizing the increase in number of variables and thus avoids over fitting scenarios. The smaller the AIC, the better is the model prediction. All analyses were performed using R statistical software (Version 3.0.1) and Statistical Package for the Social Sciences (SPSS 22.0, SPSS Inc., Chicago, IL, USA).

4.3. Results

The three categories were well separated by percentile differences for spirometry and CT emphysema (Supplemental Figure 1). The percentile difference in the Cat_{spir} category was -65.7 (SD8.2), range -93.5 to -53.2; difference in Cat_{CT} was 61.1 (7.8), range 51.6 to 79.1; and in $Cat_{matched}$ was -0.04 (0.63), range -1.03 to 1.06 ($p<0.001$ for all comparisons). Representative cases are depicted in Figure 4.1. Baseline demographics, spirometry and CT features for the three categories are described in Table 4.1. Compared to those in the $Cat_{matched}$, those with Cat_{spir} were younger and were more obese. There were significant differences in airway disease between the three categories, with the disproportionate spirometric category showing most airway disease.

A number of CT metrics of lung deformation were associated with airflow obstruction. On univariate analyses, there was a significant association between FEV_1 and Jacobian mean (regression co-efficient $\beta = 2.49$, 95%CI 2.17 to 2.81; $p<0.001$), Jacobian CV ($\beta = 3.90$, 95%CI 3.38 to 4.42; $p<0.001$), ADI mean ($\beta = 0.25$, 95%CI 0.20 to 0.30; $p<0.001$), ADI CV ($\beta = 0.69$, 95%CI 0.52 to 0.87; $p<0.001$), strain mean ($\beta = 3.55$, 95%CI 3.16 to 3.94; $p<0.001$) and strain CV ($\beta = -1.68$, 95%CI -3.06 to -0.30; $p = 0.02$). Of these, after assessment of multicollinearity, Jacobian mean, Jacobian CV and strain CV were selected for inclusion in the multivariable model to predict independent associations with FEV_1 (Table 4.2). We also assessed the relative independent contributions of the CT metrics and found that the Jacobian mean explained 7.6% of the variation in FEV_1 compared to CT emphysema which explained only 2.6%. Wall rea% and Jacobian CV were other strong predictors, explaining 4.3% and 2.3% of the variance in FEV_1, respectively.

Table 4.1: Demographic information, radiographic and spirometry measures

Variables	**Cat_{spir}** (n=100)	**Cat_{CT}** (n=97)	**$Cat_{matched}$** (n=100)
Age (years)	60.4 (7.8)**	65.0 (8.2)	64.5 (9.0)
Sex (%Males)	60 (60)	69 (71)	57 (57)
Race (% Non-Hispanic Whites)	74 (74)*	85 (88)	84 (84)
BMI (kg/m^2)	33 (7.3)***	26.6 (5.2)	26.4 (6.0)
Smoking pack years	57.3 (29.0)	51.4 (25.8)	50.4 (24.3)
FEV_1 (L)	1.15 (0.35)**	2.75 (0.68)¥	1.45 (0.82)
FEV_1 % predicted	38.0 (9.0)¥	92.6 (13.7)¥	50.8 (26.6)
FVC (L)	2.29 (0.63)¥	4.48 (0.94)¥	3.01 (0.94)
FEV_1/FVC	0.51 (0.10)*	0.61 (0.07)¥	0.46 (0.17)
%Emphysema (LAA_{insp}<-950 HU)	1.5 (1.2)¥	17.3 (8.9)	19.4 (18.0)
%Gas trapping (LAA_{exp}<-856 HU)	20.5 (12.6)¥	34.9 (11.8)**	44.5 (26.4)
Wall Area%	65.1 (2.7)¥	59.3 (2.4)¥	62.2 (2.8)

All values expressed as mean (standard deviation) unless other specified. *p<0.05 **p<0.01 ¥p<0.001. Cat_{spir} = category with disproportionate spirometric abnormality. Cat_{CT} = category with disproportionate CT abnormality. $Cat_{matched}$ = matched CT and spirometric abnormalities. BMI = Body mass index. FEV_1 = Forced expiratory volume in the first second. FVC = Forced vital capacity. LAA_{insp}<-950 HU = Low attenuation areas <-950 Hounsfield Units at end inspiration. LAA_{exp}<-856 HU = Low attenuation areas <-856 Hounsfield Units at end expiration. Wall Area% = (wall area/total bronchial area)×100, calculated as the average of six segmental bronchi in each subject.

Table 4.3 shows a comparison of measures of lung mechanics between the three categories. The same measures of lung mechanics that were significant on univariate regression with FEV_1, and after collinearity adjustments were included in the two multinomial logistic regression models shown in Table 4.4. Comparison of AIC between the two models shows that inclusion of biomechanical measures (Model 2) predicts the categories better than the model that contains only static single-volume based CT metrics of structural lung disease (Model 1), AIC 255.8 vs. 320.8. As worsening disease can result in increase in TLC, which in turn can compensate for increase in RV and tend to preserve FVC and thus FEV_1, we also performed sensitivity analyses with addition of CT measured TLC to the above model, with no change in prediction of FEV_1.

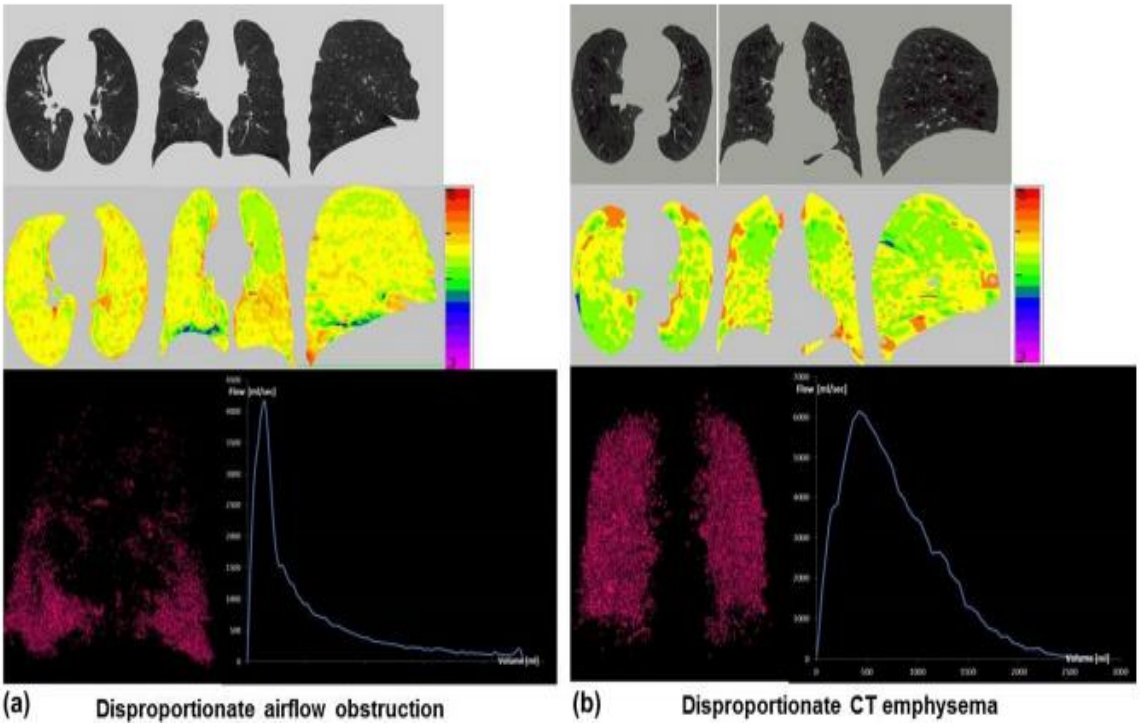

Figure 4.1: Panel A shows computed tomographic (CT) images for subject with severe airflow obstruction (FEV1 %predicted 32.6) but with relatively minimal emphysema (1.5% volume <-950HU on end inspiratory images). Panel B shows features for subject with severe emphysema on CT (20.8%) but with relatively minimal airflow obstruction (FEV1 %predicted 99.6). Top row represents the overlay of emphysema voxels on the CT images. Middle row represents the overlay of Jacobian color map on the CT images from each category. Jacobian value (=1) represents no deformation; >1 represents local expansion; <1 local contraction. Bottom row represents 3D visualization of emphysema voxels in each category with flow volume loop.

Table 4.2: Multivariable linear regression for prediction of FEV_1

Variable	β	95% CI	p value
Age (years)	-0.017	-0.024 to -0.010	<0.001
Male Sex	-0.51	-0.64 to -0.39	<0.001
LAA_{insp}<-950 HU	-0.025	-0.034 to -0.016	<0.001
LAA_{exp}<-856 HU	0.007	0.014 to 0.146	0.06
Wall Area%	-0.08	-0.10 to -0.05	<0.001
Jacobian Mean	1.72	1.33 to 2.10	<0.001
Jacobian CV	1.45	0.86 to 2.04	<0.001
Strain CV	1.90	0.77 to 3.03	0.001

FEV_1 = Forced expiratory volume in the first second. CI = Confidence intervals. LAA_{insp}<-950 HU = Low attenuation areas <-950 Hounsfield Units at end inspiration. LAA_{exp}<-856 HU = Low attenuation areas <-856 Hounsfield Units at end expiration. Wall Area% = (wall area/total bronchial area)×100, calculated as the average of six segmental bronchi in each subject. CV = Co-efficient of variation.

Table 4.3: Biomechanical CT measures for the three categories

	Cat_{spir} (n=100)	**Cat_{CT}** (n=97)	**$Cat_{matched}$** (n=100)
Jacobian Mean	1.38 (0.18)	1.73 (0.20)¥	1.44 (0.23)
Jacobian CV	0.21 (0.08)*	0.46 (0.16)¥	0.25 (0.10)
Strain Mean	0.36 (0.12)*	0.65 (0.15)¥	0.41 (0.16)
Strain CV	0.57 (0.07)¥	0.61 (0.06)	0.62 (0.09)
ADI Mean	1.03 (0.53)	3.20 (2.71)¥	1.34 (0.94)
ADI CV	1.06 (0.36)*	1.71 (0.69)¥	1.25 (0.36)

All values expressed as mean (standard deviation) unless other specified. *$p<0.05$ ¥$p<0.001$. CT = computed tomography. Cat_{spir} = category with disproportionate spirometric abnormality. Cat_{CT} = category with disproportionate CT abnormality. $Cat_{matched}$ = matched CT and spirometric abnormalities. CV = Co-efficient of variation. ADI = Anistropic deformation index.

4.4. Discussion

We show that using dual-volume based biomechanical measures of lung tissue deformation rather than static single-volume measures of CT emphysema considerably improves prediction of spirometric airflow obstruction and also concordance between CT and spirometry. This improved linkage between CT metrics and spirometry provides a validation of the mechanics-based measures derived from image matching, and offers the ability to link regional lung mechanics to spirometry which provides only a single metric reflecting a composite of regional lung differences. By providing a comprehensive map of regional lung mechanics coupled with regional maps of emphysema, patient selection for

therapies for severe emphysema can be better determined and outcomes can be evaluated in light of this new understanding of lung structure-function relationships.

A number of studies have analyzed the correlation between static single-volume CT measures of emphysema and spirometric airflow obstruction. One large study examining this showed a correlation between the two of -0.76 when emphysema was defined at <-950HU threshold.[84] While this degree of correlation is good, it leaves room for a significant amount of discrepancy. Emphysema is a heterogeneous disease and the distribution of lung disease affects spirometry. Studies that examined the relative distribution of emphysema by zone found that upper zone emphysema correlates better with the diffusing capacity of carbon monoxide whereas predominant lower zone emphysema correlates better with FEV_1. [128-131] We previously showed that emphysema like changes in the right middle lobe correlate the least with spirometry.[132] There is also a differential effect of central versus peripheral involvement of the lung, with a greater correlation of central involvement with FEV_1.[128] However, these studies do not provide a composite measure of emphysema that improves agreement with spirometry. While CT gas trapping as an indirect measure of small airway disease has a greater correlation with airflow obstruction,[85] this is likely significantly influenced by the degree of baseline emphysema in the preceding respiratory cycles.[83]

We add to the literature by showing three additional measures that improve agreement between CT and spirometry. Not surprisingly, the spirometry predominant group had significantly greater airway disease. Perhaps of more interest is the CT predominant group in which subjects had substantial degrees of emphysema with relatively minimal airflow obstruction. The divergence in emphysema measures and expected

spirometry impairment is likely partly due to the fact that single-volume-based CT measures are static whereas spirometry is a dynamic measure. By using image registration applied to matched pairs of inspiratory-expiratory CT scans, we show an improved agreement between dynamic spirometric measures and biomechanical CT measures. While measures of airways disease including differences in airway wall thickness and air trapping also account for some of the disagreement, we found that after adjustment for indices of airway disease, biomechanical measures account for considerable additional variability. Our findings suggest that the presence of CT emphysema may not always translate into airflow obstruction, and that not all emphysema translates into loss of elastic recoil equally. The image-matching-based metrics more directly link CT-based findings with the integrated mechanics associated with spirometry.

We found that a greater value for the Jacobian mean predicts a higher FEV_1. The Jacobian mean is reflective of the over-all volume change of the individual lung regions. Ju et al showed that greater degree of lobar heterogeneity of emphysema on single-volume CT images was associated with less airflow obstruction.[133]. We extend these findings by demonstrating that image-matching based measures of biomechanical heterogeneity (Jacobian and strain CVs) are predictive of lung function, and these biomechanical changes are provided on a lobar and sub-lobar basis. It is pertinent to note that the Jacobian CV and strain CV are more strongly associated with the prediction of the Cat_{CT} category, one in which there is significant CT emphysema but the spirometric abnormality remains relatively masked. Though we did not assess the type of emphysema qualitatively, panlobular emphysema tends to be more homogeneous, is associated with higher lung compliance, and is associated with a lower FEV_1 for the same level of quantitative

emphysema of centrilobular distribution.[103, 104] Centrilobular emphysema tends to be more heterogeneous and is associated with lesser FEV_1 reduction for a given degree of emphysema. This is especially relevant for subjects with very mild airflow obstruction who might harbor significant structural lung disease prior to development of spirometric abnormality. We speculate that more local heterogeneity indicates relative canceling effects of the pressure effects created by greater and lesser expansive lung regions, a form of local pseudo restriction. The Jacobian CV might be a novel measure of biomechanical lung heterogeneity that can explain a significant proportion of the discrepancy. Our findings have a number of potential clinical implications. The diagnosis of COPD has traditionally relied on demonstrating airflow obstruction on spirometry. CT emphysema has been proposed as a new metric of disease that provides complementary information but it has been observed that the amount of CT-based emphysema does not directly translate to the degree of airflow obstruction.[134] By providing CT-derived measures of regional lung mechanics to the more commonly used quantitative CT metrics derived from a single lung volume, we now provide a closer link between quantitative CT and spirometry. As CT emphysema is being increasingly used for assessment of structural lung disease for interventions such as bronchoscopic lung volume reduction, patient selection might be better served by the inclusion of regional measures of lung mechanics to the list of measures assessed by quantitative CT. Addition of biomechanical measures prior to lung resection surgeries may also improve prediction of postoperative lung function.

Our study has some limitations. First, CT scans were not spirometrically gated; however, patients were coached to maximum inspiration and end exhalation. Second, this was a multicenter study and hence a number of scanners were used to acquire the CT scans.

However, we did adjust for scanner variability in our analyses, and emphysema and air trapping were assessed from the same lung volumes as those used for the biomechanical measures, thus linking these measures to each other, accounting, in part, for protocol differences and subject variability. Third, although we adjusted for airway disease by use of WA%, the current resolution of CT limits visualization of airways beyond the segmental level. There is also a growing understanding that WA% is a composite of changes in airway wall thickness and luminal dimensions and may not fully reflect peripheral airway disease.[135] To address these issues, we also used gas trapping as a surrogate of small airways disease. Fourth, CT scans were obtained at only two volumes, thus limiting our ability to account for regional differences in lung mechanics reflected in the non-linearity of the pressure volume curve either on a global or regional basis.[111] With the considerable reduction in radiation doses afforded by evolving CT detector and x-ray gun technologies coupled with improved iterative reconstruction methods,[136, 137] improved details of mechanical characteristics of the lung, by utilizing dynamic imaging or greater numbers of lung volumes, may become more practical while limiting radiation exposure. Finally, even though we reduced the sample size to 300, this was intentionally done to examine the cases with the most discordance. This was necessary as there is no previous literature to guide us as to how much abnormality on CT predicts the abnormality on spirometry and vice versa. Our study also has a number of strengths. Sites were continuously coached in regards to the proper performance of lung volume coaching and CT protocol adherence. Study subjects were drawn from a cohort that is well characterized phenotypically, and hence included a large sample size and included a high proportion of African Americans

4.5. Summary

In conclusion, compared to single-volume CT assessment of emphysema, biomechanical measures derived from dual-volume CT show improved agreement with airflow obstruction on spirometry. This has implications for disease detection, for the understanding of links between regional lung disease and spirometrically derived lung function, as well as therapy planning.

CHAPTER 5

PREDICTION OF COPD PROGRESSION USING CT REGISTRATION-BASED LUNG MECHANICS

5.1. Introduction

Chronic obstructive pulmonary disease (COPD) is characterized by airflow obstruction, and the rate of decline of lung function is greater than age related changes in a substantial proportion of patients, even after smoking cessation [94]. COPD is the third leading cause of death in the United States and airflow obstruction is associated with significant morbidity and healthcare costs. Progression of disease in COPD is variable, and although some patients have a relatively slow rate of lung function deterioration, others suffer an inexorable decline resulting in significant symptoms, respiratory failure, and mortality [138]. Despite significant advances in phenotyping COPD and the development of markers to predict exacerbations and mortality [138, 139], there is unfortunately a distinct lack of biomarkers that can help identify early disease as well as predict disease progression [140].

The dominant pathogenetic mechanisms for COPD have involved proteinase-antiproteinase imbalance, oxidative stress and inflammation; however, biomarkers related to these pathways have not been shown to be useful. Recently, a computed tomographic (CT) metric of functional small airways disease has been shown to be associated with progressive lung function decline, and data suggests small airways disease may precede the development of emphysema [71, 141]. The forced expiratory volume in the first second (FEV_1) is affected by both resistance to airflow in the small airways as well as the elastic recoil of the lung parenchyma. A less explored mechanism for emphysema initiation and

progression is mechanical forces and stress fatigue [142]. It is plausible that emphysema begets more emphysema, and hence regions of the lung adjacent to emphysematous regions are subject to abnormal forces of stretch during tidal respiration [142-147]. At end expiration, the alveolar walls are under significant mechanical stress, and cyclical breathing imposes additional mechanical forces on already weakened elastin and collagen fibers, which over a longtime can result in rupture of the alveolar wall in surrounding susceptible regions, effectively creating a penumbra [144, 147]. While, CT-based quantification of COPD has seen significant advances, the contribution of mechanical forces in the progression of emphysematous tissue destruction and subsequent quantification using CT images is needed. This can be achieved by CT image registration techniques.

Using image registration on paired inspiratory-expiratory images, voxels on inspiratory images can be matched with corresponding voxels on expiratory images, and a biomechanical metric called Jacobian measure, an estimate of local lung expansion and contraction with respiration, can be calculated [59, 93]. We hypothesized that the Jacobian measure is associated with lung function decline, and that regions of the lung in the penumbra around the regions of emphysematous lung would have abnormal mechanics. Using this metric for estimating lung mechanics, we can assess the normal appearing area surrounding emphysematous regions but with abnormal mechanics, the mechanically affected lung (MAL). We also hypothesized that by enabling estimation of the regions subject to abnormal stretch, percentage MAL would predict lung function decline.

5.2. Methods

5.2.1. Dataset

We included the subjects with confirmed COPD (GOLD 1-4) from the initial 2000 subjects who had completed a 5-year follow up from the Genetic Epidemiology of COPD (COPDGene) study [51]; a large multicenter study of current and former smokers aged 45 to 80 years. Post-bronchodilator spirometry was performed to assess airflow obstruction. COPD was diagnosed based on fixed threshold for the ratio of forced expiratory volume in one second (FEV_1) to the forced vital capacity (FVC) less than 0.7; severity of the disease was graded based on Global Initiative for Chronic obstructive Lung Disease (GOLD) guidelines. Demographic variables such as age, gender, race, body mass index (BMI), and St. George's respiratory questionnaire (SGRQ) scores were collected. A written informed consent was obtained from each subject and the study was approved by the institutional review boards of all 21 participating centers. Baseline demographics and CT density metrics were shown in Table 5.1. The change in FEV_1 between baseline and 5-year follow up for each subject was used as representative of disease progression. Volumetric CT scans were obtained at full inspiration (total lung capacity, TLC) and end-tidal expiration (functional residual capacity, FRC). Subjects with CT images acquired at residual volume (RV) instead of functional residual capacity (FRC) were excluded. The scans followed an imaging protocol with collimation, 0-5mm; tube voltage, 120kV; tube current 200mAs; gantry rotation time of 0.5s; and pitch, 1.1. The images were reconstructed at standard kernel with a slice thickness of 0.75 mm and a reconstruction interval of 0.5 mm. 3D Slicer software was used to measure emphysema and gas trapping. Airway dimensions were measured from Pulmonary Workstation 2 (VIDA Diagnostics, Coralville, IA, USA).

5.2.2. CT Image Registration

The main task of image registration is to find the spatial relationship between two images. A moving image and a fixed image is defined prior, where the moving image represents the image being transformed into the same coordinate system as the fixed image. In this study, the inspiration image taken at TLC is the moving image and the expiration image taken at FRC is the fixed image. The points in the deformation matrix from the registration represents the amount of deformation occurred between inspiration and expiration at each point in the lung. A lung mass-preserving registration method was used to capture local volume changes between the two phases. A sum-of-squared tissue volume difference (SSTVD) measure is used as the similarity metric in the registration process. The SSTVD has previously shown to be effective in lung image registration protocols [58, 59]. The Jacobian determinant of the deformation matrix provides point-wise tissue expansion and contraction measures between the two respiratory cycles. A Jacobian value greater than 1 at a lung voxel represents tissue expansion whereas the value at a voxel is less than 1, it represents tissue contraction.

5.2.3. CT Measures

Emphysema was quantified by using the percentage of voxels at TLC with attenuation less than -950 Hounsfield Units (HU) (low attenuation area, %LAA950insp), Gas trapping was calculated as the percentage of voxels at FRC with attenuation less than -856 HU (%LAA856exp). We also used wall area percentage of segmental airways (WA %) representing airway disease due to remodeling of the airways.

5.2.4. Emphysema and Normal Lung Tissue - Definition

The deformed TLC image from the registration process is now matched with the FRC image, and is used to label the emphysema and normal lung tissue in each subject. Emphysema regions were defined as the voxels that are less than -950 Hounsfield Units (HU), the most commonly used threshold to define emphysema in CT scans [13]. The regions that are not part of emphysema tissue are defined as normal regions (Voxels greater than -950 HU). The sum of emphysema and normal regions constitute the entire lung mask. Tissue labeling is shown in Figure 5.1.

5.2.5. Emphysema and Normal Lung Tissue - Spatial Relationship

A distance map is created based on diseased regions in the lung for each subject. The regions that are labeled as emphysema were assigned a value of 1 while the rest of the voxels were assigned a value of 0. Euclidean distance analysis was used to compute the distance between every normal voxel to the nearest emphysema voxel. The closer the normal voxel to an emphysema voxel, the smaller the assigned distance to that particular voxel. We categorized the voxels that are in the range of 1 mm to 5 mm to the emphysema regions and further explored the influence of emphysema on the surrounding normal tissue at each step of distance using this analysis (shown in Figure 5.2).

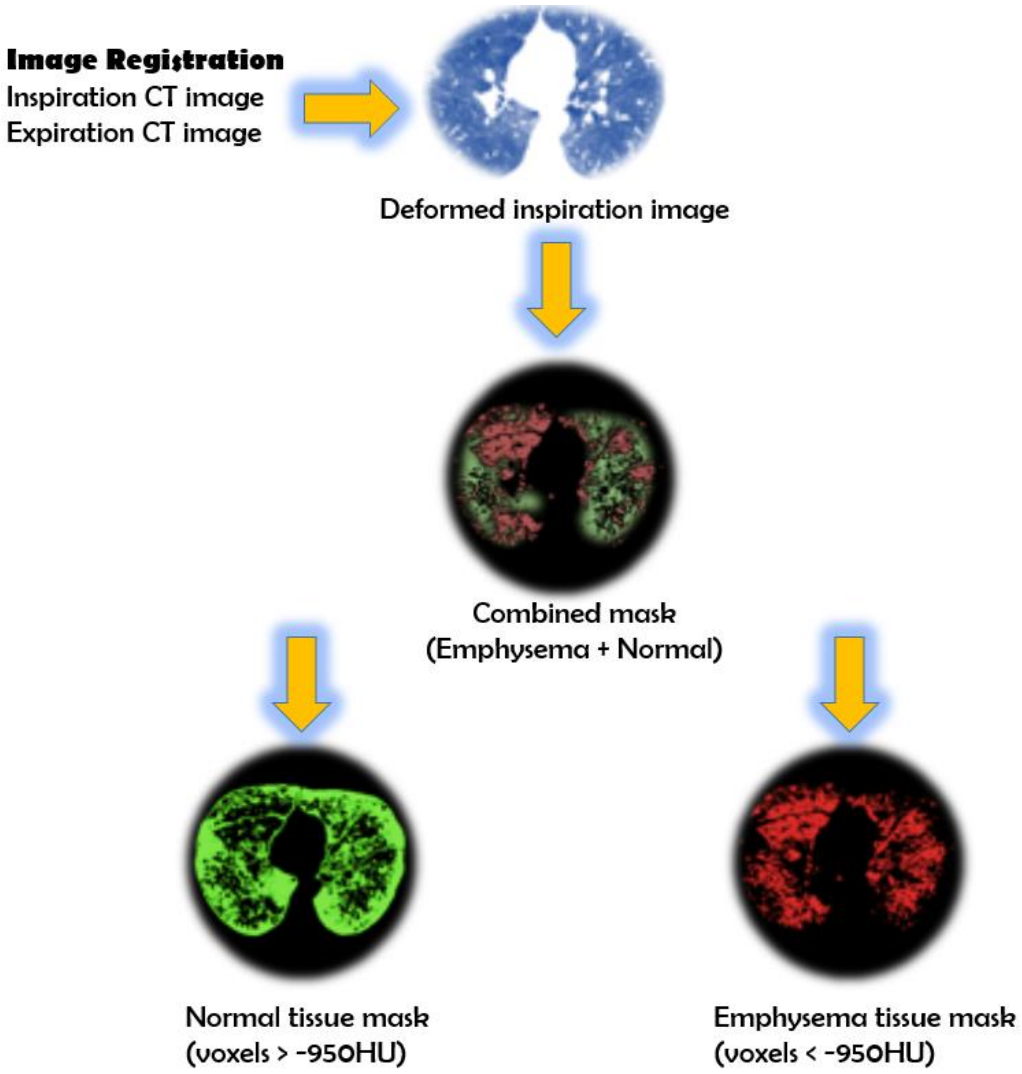

Figure 5.1 Mask extraction framework. Red color represents emphysema voxels and green color represents normal voxels in the lung.

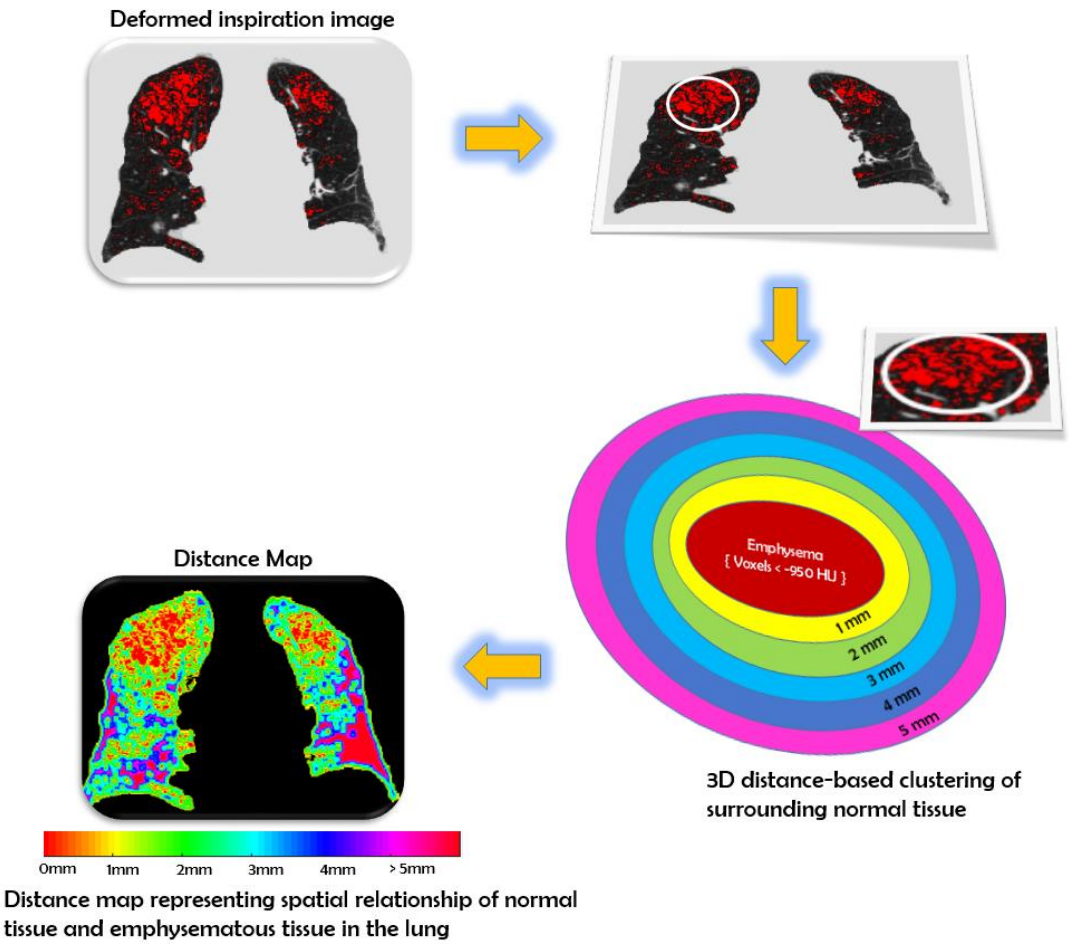

Figure 5.2. 3D distance map extraction framework.

5.2.6. Statistical Analyses

The baseline demographics are expressed as mean (standard deviation, SD). The trend of mean Jacobian measure in the normal regions across GOLD stages of COPD were shown using boxplots. ANOVA (analysis of variance) was performed to compare the normal tissue mean Jacobian values across GOLD stages. Tukey honest significant difference test was performed to compare the individual groups. Association between normal mean Jacobian in each subject with FEV_1 was assessed using univariate and multivariate linear regression models after adjustment for age, sex, race, pack-years, body mass index (BMI), pack years, current smoking status, and CT scanning protocol. CT-

based measures of emphysema, gas trapping, and segmental airway wall area thickness (WA %) were also included in the regression model. A similar univariate and multivariate regression analysis was performed to find the association between change in FEV_1 after a 5 year follow up and mean Jacobian of normal regions in the whole lung, normal regions with in 1 mm, 2 mm, and 3 mm of emphysematous tissue.

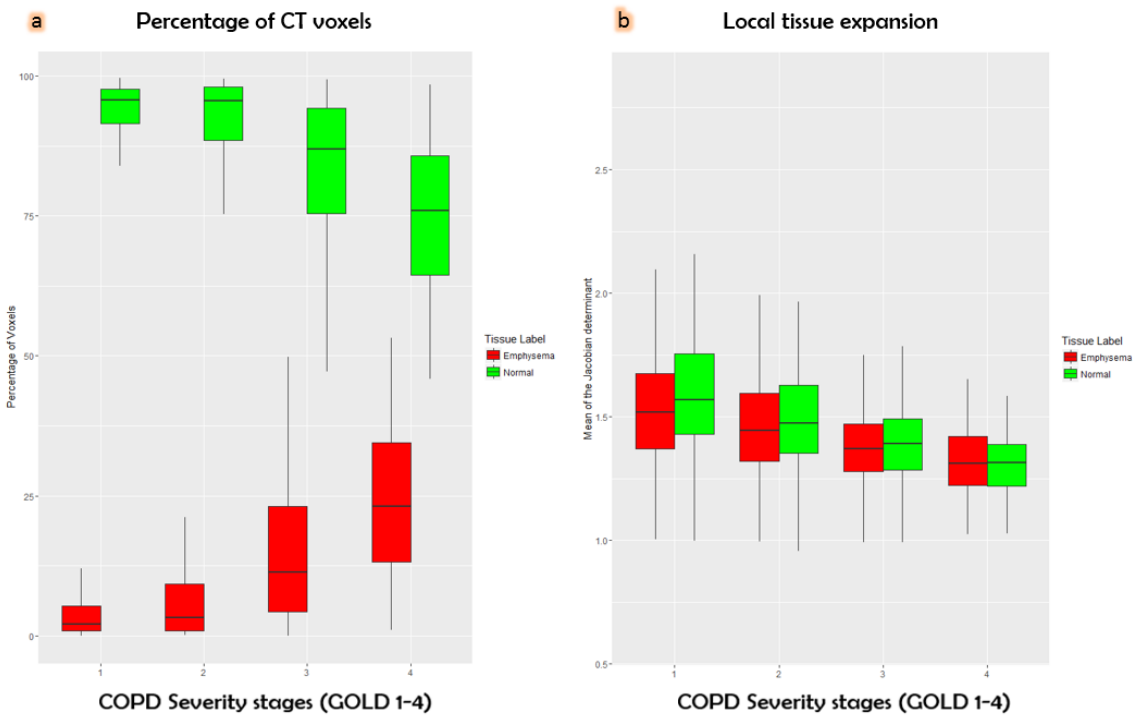

Figure 5.3. (a) The percentage of CT voxels classified as emphysema and normal tissue based on CT density-based thresholds. (b) The mean Jacobian of the normal and emphysematous lung tissue in COPD subjects across GOLD severity stages. The groups are significantly different ($p< 0.0001$) based on the Tukey honest significant difference test and ANOVA analysis.

5.3. Results

5.3.1. Demographics

Of the first 2,000 participants who had completed a follow up study, 680 subjects were used in this study who had COPD GOLD stages 1 to 4. Table 5.1 shows the baseline demographics, physiologic assessments and CT measures of emphysema, gas trapping, and segmental airway wall thickness. The mean age of the subjects is 62.95 (σ = 8.38) where 44 percent of subjects are female. The average pack years is 49.81 (σ = 23.89) where 37 percent of subjects are current smokers.

Table 5.1. Baseline demographics

Parameters	**Mean (SD)**
Age	62.95 (8.38)
Female (%)	44.00
African-American (%)	24.55
BMI	27.83 (5.67)
Pack Years	49.81 (23.89)
Current Smokers (%)	37.00
FEV_1 % predicted	58.81 (21.62)
FEV_1/FVC	0.52 (0.12)
CT Emphysema (%)	12.42 (12.04)
CT Gas Trapping (%)	36.55 (19.42)
CT airway wall area thickness (WA %)	62.20 (3.05)

Table 5.2. Univariate and multivariable associations of normal mean Jacobian determinant measure with absolute FEV1 (n=680)

Parameter	**Univariate Regression**		**Multivariable Regression**	
	β (95%CI)	**P value**	**β (95%CI)**	**P value**
Age (years)	-0.017 (-0.024, -0.010)	< 0.001	-0.017 (-0.022, -0.012)	< 0.001
African American race	-0.100 (-0.230, 0.030)	0.132	-0.209 (-0.299, -0.120)	< 0.001
Female sex	-0.597 (-0.700, -0.493)	< 0.001	-0.567 (-0.641, -0.493)	< 0.001
BMI (kg/m^2)	-0.007 (-0.010, 0.009)	0.888	-0.016 (-0.023, -0.009)	< 0.001
Smoking pack-years	-0.001 (-0.003, 0.008)	0.201	-0.003 (-0.001, 0.001)	0.705
Scanner	-0.144 (-0.305, 0.017)	0.079	0.119 (0.014, 0.224)	0.026
Smoking Status	0.276 (0.162 0.390)	< 0.001	-0.033 (-0.124, 0.057)	0.176
CT Emphysema (%)	-0.026 (-0.031, -0.022)	< 0.001	-0.015 (-0.021, -0.010)	< 0.001
CT Gas Trapping (%)	-0.019 (-0.021, -0.017)	< 0.001	-0.011 (-0.015, -0.001)	< 0.001
Airway Wall Area, (%)	-0.081 (-0.098, -0.063)	< 0.001	-0.064 (-0.077, -0.050)	< 0.001
Coefficient of variation of the Jacobian determinant	0.030 (0.025, 0.035)	< 0.001	0.099 (0.052, 0.146)	< 0.001

Table 5.3. Univariate and multivariable associations of normal mean Jacobian determinant measure at baseline with absolute change in FEV1 values after a 5 year follow up (n=680)

Parameter	Univariate Regression		Multivariable Regression	
	β (95%CI)	P value	β (95%CI)	P value
Age (years)	0.754 (0.230, 1.279)	0.004	0.268 (-0.320, 0.858)	0.370
African American race	-0.770 (-11.034, 9.494)	0.883	-6.080 (-16.662, 4.501)	0.259
Female sex	18.601 (9.828, 27.373)	< 0.001	-7.852 (-17.722, 2.017)	0.118
BMI (kg/m^2)	0.831 (0.053, 1.608)	0.036	-0.333 (-1.181, 0.513)	0.439
Smoking pack-years	-0.088 (-0.273, 0.096)	0.351	-0.111 (-0.292, 0.070)	0.229
Scanner	1.751 (-10.992, 14.495)	0.787	3.610 (-8.617, 15.838)	0.562
Absolute FEV_1	-22.722 (-28.40,17.039)	< 0.001	-40.416 (-49.11, -31.720)	< 0.001
Smoking Status	-11.026 (-20.107, -1.944)	0.017	-10.088 (-20.709, 0.532)	0.062
CT Emphysema (%)	-0.046 (-0.421, 0.328)	0.808	0.217 (-0.383, 0.818)	0.477
CT Gas Trapping (%)	-0.138 (-0.352, 0.076)	0.207	-1.249 (-1.669, -0.830)	< 0.001
Airway Wall Area, (%)	1.316 (-0.121, 2.759)	0.073	-1.443 (-3.054, 0.168)	0.070
Normal Mean Jacobian determinant	-3.251 (-22.097, 15.595)	0.735	-4.122 (-9.284, 1.039)	0.117

Table 5.4. Multivariable associations between absolute change in FEV_1 in mL per year and mean Jacobian of normal voxels at baseline with in 1mm, 2mm, and 3mm distant to the emphysematous tissue.

	Parameters	β (95%CI)	p-value
MODEL A	CT Emphysema (%)	0.267 (-0.337, 0.872)	0.385
	CT Gas Trapping (%)	-1.277 (-1.688, -0.866)	< 0.001
	Airway Wall Area, (%)	-1.488 (-3.097, 0.121)	0.069
	Mean Jacobian determinant of normal tissue with in **1mm**	-5.022 (-10.003, -0.040)	0.048
MODEL B	CT Emphysema (%)	0.266 (-0.338, 0.870)	0.388
	CT Gas Trapping (%)	-1.283 (-1.697, -0.869)	< 0.001
	Airway Wall Area, (%)	-1.500 (-3.111, 0.110)	0.067
	Mean Jacobian determinant of normal tissue with in **2mm**	-5.084 (-10.130, -0.038)	0.048
MODEL C	CT Emphysema (%)	0.266 (-0.345, 0.862)	0.401
	CT Gas Trapping (%)	-1.283 (-1.698, -0.866)	< 0.001
	Airway Wall Area, (%)	-1.500 (-3.115, 0.110)	0.067
	Mean Jacobian determinant of normal tissue with in **3mm**	-5.084 (-10.108, 0.087)	0.054

*All models were adjusted for age, race, gender, pack years, smoking status, scanner protocol, BMI, and FEV_1 at baseline

5.3.2. Mechanics of Normal Lung Tissue – Across GOLD Stages

Figure 5.2 shows the distribution of mean Jacobian in the normal regions of the lung across COPD severity stages. Tukey comparison tests were performed and the mean Jacobian of normal lung tissue is significantly different between GOLD stages with a decreasing trend along the severity scale. Analysis of variance was performed and the differences between group means were significant ($p< 0.001$)

5.3.3. Association with Baseline FEV_1

Table 5.2 shows univariate and multivariate association between the standard deviation of the Jacobian of the normal voxels in the whole lung and absolute FEV_1 values. The heterogeneity of local tissue expansion is significantly associated with FEV_1 in both univariate (β=0.030, 95%CI= 0.204 to 0.307; $p<0.001$) and multivariate (β=0.099, 95%CI= 0.052 to 0.146; $p<0.001$) regression analysis. Multivariate model was adjusted for age, race, gender, BMI, pack years, smoking status, CT scanner protocol, CT emphysema, CT gas trapping, and airway wall thickness.

5.3.4. Association with FEV_1 Change Over Time

Table 5.3 shows univariate and multivariate association between the mean Jacobian of the normal voxels in the whole lung at baseline and change in FEV_1 values after a 5 year follow up. The normal mean Jacobian is not significantly associated with FEV_1 change in the univariate analysis (β=-3.251, 95%CI= -22.097 to 15.595; p=0.735). While adjusted for age, race, gender, BMI, pack years, smoking status, CT scanner protocol, CT emphysema, CT gas trapping, and airway wall thickness: the normal tissue mean Jacobian approached near statistical significance (β=-4.122, 95%CI= -9.284 to 1.039; p=0.117). Table 5.4 shows the multivariate associations between absolute change in FEV_1 and mean Jacobian of

normal voxels with in 1mm, 2mm, and 3mm distant to the emphysematous tissue. The mean Jacobian of voxels with in 1mm (β=-5.022, 95%CI=-10.003 to -0.040; p=0.048), 2mm (β=-5.084, 95%CI=-10.130 to -0.038; p=0.048), and 5mm (β=-5.084, 95%CI=-10.108 to -0.087; p=0.054) range is statistically significant with FEV_1 change.

5.4. Discussion

We demonstrated that the mechanics of normal regions in the lung as derived from CT image registration techniques are significantly associated with FEV_1 decline. The traditional labeling of normal lung tissue based on CT density thresholding technique might not depict a complete picture on functional aspects of these regions. We showed that the "normal-looking" regions with abnormal mechanics which are closer to emphysema regions, experiences significant deterioration in its functional ability with increasing severity of the disease. We refer to these regions as the mechanically affected lung (MAL). It is clear that the extent of diseased tissue increases with disease severity in turn decreasing the percentage of normal tissue in the lung. However, the influence of pathological tissue on the nearby normal tissue and its elasticity in COPD patients has not been studied before. Suki et al. proposed an emphysema progression mechanism stating that the collagen fibers in the emphysematous tissue becomes weaker over time and may lead to mechanical stress variations in the nearby alveolar walls [148, 149]. The authors have used a computer model of the lung tissue consisting a network of linearly elastic springs to compare the effects of mechanical force-based tissue destruction. The authors have showed there are clear structural differences between chemical-based breakdown of the tissue and force-based breakdown. Further, the heterogeneity and the size of emphysema clusters might play a role in the mechanical properties of the lung tissue. We examined this influence of

emphysematous tissue on the normal regions of the lung using CT image registration-based lung mechanics. The measure representing local tissue expansion or contraction ability, Jacobian determinant, has been previously shown to be effective in COPD diagnosis and also improved agreement between spirometry-based airflow obstruction and CT-based emphysema [92, 93]. We initially labelled the lung regions into either emphysema or normal tissue based on the CT densitometry techniques (emphysema represented by voxels <-950HU). We calculated the mean Jacobian of the normal regions in COPD subjects and grouped them according to their disease severity, as shown in Figure 5.3. Although the voxels are "normal-looking" on CT images based on the traditional densitometry techniques, the mechanical properties of the normal regions significantly diminishes with increasing severity. The extent of mechanically affected lung (MAL) increases with GOLD severity in COPD patients.

We have shown previously that the CT derived lung mechanics were strongly correlated with patient outcomes in COPD and spirometry-based airflow obstruction measures [92], especially FEV_1. In our first step towards understanding the normal tissue mechanical properties, we estimated the relationship between the normal tissue mechanics and absolute FEV_1 values. The results are shown in Table 5.2. The standard deviation of the Jacobian of the normal tissue representing the heterogeneity of local tissue expansion is significantly associated with FEV_1 in both univariate and multivariate regression analysis where the multivariate model is adjusted for demographics and CT measures of emphysema, gas trapping, and airway wall thickness. Along with the mechanical measures, CT derived measures were also shown significant association with FEV_1. To our knowledge, the strong associations between CT-derived mechanical properties of normal

lung tissue and FEV_1 has not been reported before. There is a clear need for further exploration on what makes the normal regions to transform into diseased regions over a period of time. To achieve this partly, we performed similar regression analyses but this time predicting the rate of FEV_1 decline instead of baseline FEV_1. The results are shown in Table 5.3. Although, there is no significant association between normal tissue mechanics and FEV_1 change in univariate analyses ($p=0.735$) and multivariate analyses ($p=0.117$). We believe this might due to the fact that the overall percentage of mechanically affected lung (MAL) tissue is smaller when estimated in the entire lung.

We further investigated the hypothesis that the emphysematous tissue would have greater effect on mechanical properties of nearby normal lung tissue than the regions that are located far from the diseased tissue. We tested this hypothesis by creating a distance map representing every normal voxel in terms of how far the voxel lies from the emphysematous voxel. We categorized the normal voxels into three categories: voxels that lie within 1mm, 2mm, and 3mm distant to the emphysematous tissue. We calculated the mean Jacobian of the voxels in each category representing their tissue expansion or contraction ability from inspiration to the expiration, and then performed regression analyses with FEV_1 change values. The results are shown in Table 5.4. Unlike the overall normal mean Jacobian association, the voxels that are closer to emphysematous tissue are significantly associated with the rate of decline in FEV_1. The strong associations with FEV_1 decline and mechanical properties of normal tissue that is closer to emphysematous tissue is worthy of discussion. This might add to our current understanding of COPD progression especially how emphysema regions transform from mosaic pattern to large clusters. If we are able to provide a quantitative metric of tissue expansion capability of the normal regions

of the lung, this might lead to early detection of disease and categorize early, mild, and rapid progression in COPD population.

Although it can be reasonably argued that the labelling of normal tissue is solely based on emphysema component (voxels > -950HU) ignoring the contribution of airway disease and remodeling effects to the tissue, we adjusted for the CT-based gas trapping and airway wall thickness in all the multivariate regression analyses performed. Galban et al. proposed the parametric response mapping (PRM) technique to differentiate functional small airway diseased tissue from the emphysematous tissue in COPD patients [67] and a recent study have shown that the percentage of functional small airway disease in the lung is strongly associated with rate of decline in FEV_1 using the same cohort we used in this study [71]. We plan to further explore the proposed spatial relationship analysis in regards to PRM based labeling of emphysema and airway disease. The main goal of our current study is to examine the effects of emphysematous regions on the surrounding lung parenchyma and how the mechanical properties of the normal tissue alter based on spatial location from the diseased regions. One of the limitation of our study is that the patients were not spirometrically gated during CT image acquisition, which might influence the density measures and registration-based lung mechanical measures. The participants in this study were coached to full inspiration and end expiration. Another limitation is the use of -950 HU as the density threshold to define emphysema, it is possible that the use of -910 HU as the threshold might affect the current findings. We have chosen -950 HU since it is the most commonly used threshold [24].

5.5. Summary

In conclusion, the mechanical properties of lung tissue gets altered in the presence of disease, although it is considered as normal based on the traditional CT density-based techniques. We introduced a new distance analysis and created spatial distance maps to evaluate the relative influence of emphysematous tissue on the mechanical properties of surrounding normal lung parenchyma. We showed that the tissue expansion ability of the surrounding lung parenchyma of the emphysema regions in the lung is significantly associated with baseline FEV_1 and rate of decline in FEV_1. The clinical applicability and the role of normal lung parenchyma in phenotyping COPD population and predicting the progression at early stages is yet to be explored.

CHAPTER 6

DISCUSSION AND FUTURE WORK

In this thesis, we evaluated the role of CT image registration-based lung mechanics in COPD in the following general areas: the identification of COPD presence and severity, the relationship with patient outcomes in COPD, the role of CT lung mechanics in COPD diagnosis, and the use of lung mechanics in predicting disease progression in COPD patients. Although the CT density-based and texture-based measures provide useful information on COPD related parenchymal destruction and airway remodeling, these measures do not provide insights into patient-specific alterations in lung mechanics and regional parenchymal stresses. Using the CT image registration-based lung mechanical measures, we evaluated their role in COPD presence, severity and progression.

Chronic obstructive pulmonary disease (COPD) is currently the third-ranked cause of death in the United States and is associated with high morbidity and mortality [150]. It is estimated that 4.7 million deaths will be caused by COPD alone out of 68 million deaths worldwide by 2020 [78]. Although tobacco smoking is the most important risk factor of COPD, occupational exposure to dust, environmental air pollution, and genetic factors are also known risk factors. COPD is a progressive airflow limitation disorder and occurs due to a complex interplay between emphysema (tissue destruction), functional small airway disease (fSAD), and chronic bronchitis. Due to this heterogeneity nature of COPD, quantifying relative contribution of individual disease components and phenotyping accordingly is extremely challenging. In a recent study, it has been shown that there is a significant increase in the number of individuals who are diagnosed with COPD but never smoked [150], contradicting our traditional belief of COPD in non-smokers. According to

Global initiative for Obstructive Lung Disease (GOLD) guidelines, COPD diagnosis is considered in any individual with symptoms of dyspnea, chronic cough, and a history of risk factors for COPD. The presence of airflow obstruction assessed by post-bronchodilator spirometry is currently the gold standard for COPD diagnosis. If the post-bronchodilator ratio of forced expiratory volume in 1 second (FEV_1) to forced vital capacity (FVC) is less than 0.7, then COPD presence is confirmed. However, there is a widespread criticism on the use of this fixed ratio and several studies showed that the FEV_1/FVC ratio underestimates the presence of COPD in younger patients and overestimate the presence of COPD in older patients [151, 152]. The American Thoracic Society (ATS) and the European Respiratory Society (ERS) proposed a new threshold, the lower limit of normal (LLN) which is adjusted for age related lung functional changes [153]. However, Bhatt et al. recently showed that the LLN method underestimated the disease presence in a group of elderly patients, in whom there is significantly more emphysema and gas trapping as seen on CT, and further showed that there is a high discordance between the two diagnostic thresholds [154]. The controversy regarding the appropriate cutoff and what defines "normal" in COPD diagnosis is ongoing and a major source of interest. However, the simplicity and non-invasive ability made spirometry use the current gold standard in COPD diagnosis. CT has been increasingly being used as an additional tool to quantify the relative contribution of emphysema and airway disease in COPD patients which are missing from the spirometry measurements. CT-based quantification of low attenuation areas (% LAA) in the inspiration and expiration scans provides regional characterization of the COPD components. There have been a significant number of studies validating CT-based density measures and are pushed towards determining the targeted therapeutic strategies for COPD

patients [13, 20, 155]. However, the CT density-based quantification of emphysema and airway disease is known to be influenced by scanner miscalibration, image reconstruction algorithm, and poor coaching of the patient to the desirable lung volume. While CT density measures provides reasonable estimations of regional disease distribution and structural changes in lung parenchyma, these measures do not provide any insights on functional changes in COPD patients at various stages of disease. As spirometry estimates the lung function decline based on a global measure of lung volumes, CT image registration techniques can be used to capture the local volume changes in the lung parenchyma under disease conditions.

In our work presented in this thesis, we used image registration as a method by which inspiratory and expiratory images were mapped voxel-to-voxel to capture lung mechanical changes in COPD patients. The deformation of points from the inspiration image to the corresponding biological points in the expiration image can be estimated using image registration. In all the studies presented in this thesis, the full inspiration (TLC) and end expiration (FRC) CT scans were registered for each subject. A lung mass-preserving registration method, sum of squared tissue volume difference (SSTVD), was used as a similarity criterion to match the two images. The SSTVD method has been previously shown to be effective in lung image registration protocols [58, 59]. The deformation or transformation matrix from the image registration was used to derive three measures capturing the mechanical changes in the lung tissue from inspiration to the expiration. The more commonly used CT-based lung mechanical measure in this thesis is the mean of the Jacobian determinant, representing local volume change between inspiration and expiration images, as shown in Figure 6.1. The Jacobian deformation map ranges from 0 to infinity

where the value greater than 1 indicates local expansion and the values less than 1 indicates local contraction. The value equal to one represents neither expansion nor contraction. The other CT-based lung mechanical measures are derived based on strain analysis and orientation preference of the deformation. While strain components of lung deformation field represents the geometrical deformation caused by the action of stress in the lung, anisotropic deformation index (ADI) captures information on preferential directionalities involved in the volume change. Amelon et al. showed elevated ADI in the inferior regions of the lung and along the fissures representing lobar sliding [66]. The proposed indices: Jacobian, strain, and ADI allows for better understanding of the lung deformation under disease condition in turn helps us to establish a relationship between structural and functional changes in COPD patients. **In Chapter 2**, we **hypothesized** that the regional tissue mechanics from the image registration will provide valuable information on lung functional changes in COPD subjects and help identify COPD presence and severity. We also tested the role of commonly used CT density and texture measures in addition to the lung mechanical measures. We proposed three new measures of lung mechanics for COPD identification: Jacobian, strain, and anisotropic deformation index (ADI). We have used a supervised machine learning framework to evaluate the performance of CT-based lung mechanics, density, and texture measures individually and combined in classifying COPD patients. We performed two classification experiments: COPD versus non-COPD and COPD severity classification. In the first experiment, COPD versus non-COPD classification, the lung mechanical measures showed similar performance in comparison with the density measures. The texture feature set which comprised of global texture measures based on Gaussian filter bank as proposed in [44, 50], performed reasonably

better than the density and mechanical feature sets. In the second experiment, a five-class COPD severity classification, the mechanical features derived from the CT image registration performed significantly better than the density and texture measures. A stage-by-stage classification performance was also reported, showing the superior performance of the mechanical measures at the later stages of the diseases. This suggests the possibility of major lung functional changes at later stages that are being captured by the lung mechanical measures. We also combined density, texture, and mechanical measures and repeated the same experiments. While the combined feature subset performed no different than the individual subsets in COPD versus non-COPD classification, there is a significant improvement in COPD severity classification when mechanical measures were added to the current state of the art density and texture measures. This study demonstrates the effectiveness of CT derived lung mechanics in estimating functional changes in COPD patients at different stages of the disease. However, this evaluation is solely based on GOLD severity classification of COPD patients, which relies on spirometry diagnosis. Although, GOLD severity classification has gone through several iterations [12, 94], we have used an up-to-date severity categorization available. Another limitation of our study is the number of features used in the classification study, there were several other density and texture based measures which have been proven to be effective in COPD quantification [35-37, 40, 42-45, 48, 50]. We believe that a complete feature set related to both emphysema and airway disease components in COPD may help better phenotype the population.

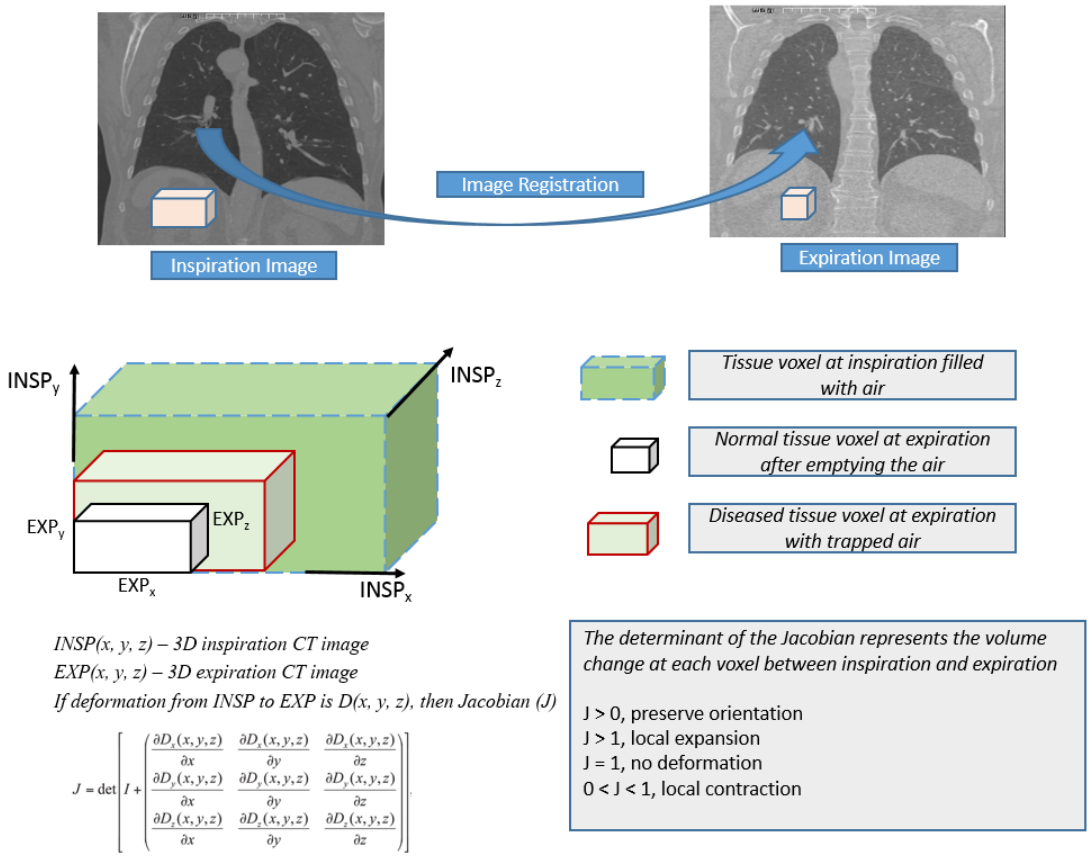

Figure 6.1. Explanation of the Jacobian measure

We demonstrated that the use of CT derived mechanical measures in addition to the density and texture measures, significantly improves the ability to classify COPD patients according to their severity. **In chapter 3**, we determined whether the CT derived lung mechanical measures are associated with patient outcomes in COPD to establish the role of mechanics further in clinical settings. In this study, we have used the mean of the Jacobian determinant as the sole measure of mechanics and used a statistical analyses to determine its association with various patient outcomes in COPD diagnosis. We **hypothesized** that the CT derived local tissue expansion and contraction measures would provide valuable information on functional changes related to patient outcomes in COPD.

The CT derived metrics representing emphysema and airway disease have previously been shown to be independently associated with spirometry diagnosis and objective outcomes such as dyspnea, quality of life, exercise capacity, the BODE (body mass index, airflow obstruction, dyspnea, exercise capacity) index, St. George's respiratory questionnaire (SGRQ), and mortality [81]. We have showed that the CT derived mean Jacobian measure offer information that are not only independent and additive, but with effect sizes greater than FEV_1 for all the patient outcomes. The Jacobian measure is significantly associated with SGRQ scores, exercise capacity index, and the BODE index. On multivariable regression analyses, the effect size of the Jacobian measures is stronger than the effect sizes of CT-based emphysema, gas trapping, and airway wall thickness measurements. In addition, when Jacobian measure is included to the traditional CT measures of disease, this improves the prediction of the BODE index. The association with the BODE index provides valuable information applicable to COPD prognosis. Although, we still do not know the reason behind the strong associations of the Jacobian measure with the clinical outcomes when compared with other CT-based measures, it is plausible that the Jacobian measure representing local tissue elasticity is providing a collective information on the emphysema and airway disease related manifestations in COPD. This also could be due to dynamic hyperinflation and poor diaphragmatic motion in COPD patients which might be reflected better by the Jacobian measures than the traditional CT measures of emphysema and airway disease. Our findings in this study are adjusted for age, gender, ethnicity, BMI, number of smoking years, and CT scanning protocol. The better prediction of respiratory quality of life, the BODE index, and the mortality by the Jacobian measure shows the

importance of regional tissue expansion and parenchymal stress-related functional changes in COPD patients.

The diagnosis of COPD is largely based on the detection of airflow obstruction by spirometry. However, it is increasingly clear that the spirometry based diagnosis does not fully explain the morbidity associated with the disease [12]. CT-based measures of emphysema and airway disease relies on fixed density threshold (-956HU or -856HU) to estimate the extent of the disease. However, it is our observation that many COPD patients have marked discordance between spirometry diagnosis and CT-based diagnosis. Some subjects with severe airflow obstruction on spirometry have mild emphysema on CT and conversely, patients with severe emphysema on CT has relatively mild spirometric airflow obstruction. While these differences in diagnosis might be contributed from extent of airway narrowing, the discordance between spirometry and CT diagnosis have not been systematically studied. **In Chapter 4**, we used such discordant dataset and CT derived lung mechanics to improve agreement between spirometry and CT-based diagnosis. We **hypothesized** that the lung mechanical measures will provide a link between CT-based diagnosis and spirometry diagnosis of COPD. We have created three subsets of patients: spirometry predominant, CT predominant, and matched diagnosis. We have shown that the CT-derived lung mechanical measures improved the concordance between traditional CT and spirometry diagnosis. The discordance in emphysema extent and spirometry is likely due to the fact that the CT measures are mostly static measures from a single volume, whereas spirometry related airflow obstruction measures are mostly dynamic. The improved agreement by using CT image registration-based lung mechanics might be due to the mechanical measures ability to capture the functional changes between volumes.

Especially, the Jacobian measure is reflective of the over-all volume change. We also showed the heterogeneity of Jacobian measure (as calculated by coefficient of variation) are more strongly associated with CT predominant group, showing the inability of spirometry to represent the changes related to disease heterogeneity. As CT measures are increasingly being used for assessment of structural lung disease for interventions such as bronchoscopic lung volume reduction, patient selection might be better performed by the inclusion of regional measures of lung mechanics to the current traditional CT measures. All the analyses performed in this study were adjusted for age, gender, race, BMI, number of smoking years, and CT scanning protocol. The major limitation of the study is not having a measure that clearly represents the airway disease in COPD patients. It is possible that the group with mild emphysema on CT and severe airflow obstruction on spirometry diagnosis is due to the extent of airway disease in these subjects. Although it is not an accurate representation, we did adjust for airway disease using CT-based airway wall area thickness (WA %) and gas trapping measures.

We established the importance of lung mechanics derived from the CT image registration methods in COPD diagnosis and phenotyping in Chapters 2, 3, and 4. **In chapter 5**, we tackle a much challenging and most important problem in the current COPD research, which is predicting disease progression in COPD patients. We examined the role of lung mechanics in identifying patients who progress relatively faster than the others. The traditional analyses of CT related measures of COPD heavily revolves around in labeling regions in the lung that are either emphysema or airway disease. The prediction of disease progression in COPD patients based on CT-based measures has been done previously [67, 156-159]. However, while there is much discussion on the extent of diseased tissue in the

lung, there is limited focus on what makes the normal lung tissue turn into disease tissue over a period of time. In this study, we **hypothesized** that the mechanical properties of the normal lung tissue at baseline provides valuable information on regions that are prone to convert from normal to diseased over a period of time. To our knowledge, the use of normal lung tissue mechanics in predicting COPD progression is novel to the field. In this study, we have shown that the normal lung tissue as labelled by traditional methods, are in fact exhibits poor mechanical properties with the increase in disease severity. The mean of the Jacobian determinant measure representing the local tissue expansion, specifically in the normal regions of the lung is significantly associated with both FEV_1 and FEV_1 change in the patients after a 5-year follow up. We also tested the concept of spatial relationship between diseased and normal lung regions in COPD patients. We **hypothesized** that the "normal looking" regions closer to either emphysema or airway disease regions will show poor mechanical properties than the farther regions, thus providing valuable information of regions that are prone to disease progression. We evaluated the mechanical properties of the normal lung tissue up to 5 mm from the diseased regions and found the regions that are closer to the diseased regions alone can contribute to change in FEV_1. The reason behind the strong associations between normal voxel mechanics that are closer to disease regions with FEV_1 change can be explained in relation to the studies done by Suki et al evaluating the structural damage of the nearby tissue in the presence of emphysema [142, 143, 148, 149]. It has been proposed that mechanical failure of the alveolar walls plays a vital role in emphysema progression and subsequent structural damage [160, 161], Suki et al. was the first to quantify the mechanical stress related changes in the lung parenchymal strips taken from emphysematous lungs [145]. The authors showed that the emphysematous lung tissue

breaks at 40% smaller stress than the normal lung tissue. The authors also identified greater dynamic nonlinearities in the tissue responsible for elastic recoil in the emphysematous lungs suggesting a significant collagen remodeling with in the alveolar wall hence overstretching the alveoli beyond its capability. In another study performed by the same group, a model representing emphysematous lung tissue comprised of linear elastic spring network was used to evaluate the damage to the nearby lung tissue in the process of emphysema progression. The authors showed that mechanical forces led to a varied tissue destruction pattern and emphysema cluster formations. To our knowledge, the use of CT image registration techniques to mimic and quantify the "normal" tissue destruction in relation to the nearby emphysematous tissue is first in the field. The conventional labeling of normal and diseased tissue based on CT density thresholds might not depict an accurate picture of underlying pathophysiology of COPD. The use of lung mechanical measures to the current mix of CT-based measures is more relevant now in accurately phenotyping COPD population.

It is known that in patients with emphysema, the tissue destruction results in reduced elastic recoil in turn increasing the total lung capacity (TLC), the volume at which CT images were acquired and useful in quantifying emphysema regions in the lung [162]. The distribution of Hounsfield Units (HU) were influenced by the both tissue destruction and hyperinflation at TLC. Madani et al. showed that the lung volume at the time of scanning has a significant effect on the CT density-based measures of emphysema and showed an underestimation of emphysema extent on TLC image by density thresholds [162]. Soejima et al. showed that the percentage of low attenuation areas in the lung increased with age and Gevenois et al. showed significant correlations of CT density

measures with age [163, 164]. The biomechanical measures proposed in this study are based on the regional deformation of lung parenchyma between end inspiration (TLC) and end expiration (FRC) and it is important to establish the variability introduced by factors such as lung volumes, breathing effort, CT image acquisition protocols, and age that influences CT density values. Du et al. tested the reproducibility of CT derived lung mechanical measures using 4D CT images and the influence of patient's respiratory effort on these measures [165-167]. The standardization of CT image acquisition protocol and minimal variations in patient's breathing effort is vital for reproducibility of any CT-based measures of disease including lung mechanical measures. It is important to establish and validate a robust lung mechanical feature set that are more physiologically meaningful and tolerant to external variations, specifically in relation to COPD diagnosis and phenotyping. There have been significant advancements in COPD research to phenotype airway predominant disease and emphysema predominant patients using CT images. Galban et al. proposed the parametric response mapping (PRM) method as an imaging biomarker that can differentiate airway disease from emphysema [67]. The PRM-based labeling of functional small airway disease (fSAD) and emphysema depends on the matching or registration of the inspiration image to the expiration image. This technique led to interesting developments in using CT images to phenotype lung tissue in COPD patients. It has been shown to be significantly associated with FEV_1 change in a study conducted on 2000 subjects after a 5-year follow up [71]. However, the major drawback of PRM is its reliance on traditional density thresholds (-950HU for emphysema and -856HU for airway disease), which has been shown to be influenced by patient's lung volume and CT reconstruction algorithm [80, 162, 168-170]. Boes et al. recently evaluated the impact of

sources of variability on PRM measurements and showed significant effects due to inadequate lung volumes during image acquisitions [171]. Similar factors affecting the CT density-based measurements of emphysema and airway disease will be applicable to PRM-based analysis, as PRM is dependent on the commonly used density-based thresholds. In the case of longitudinal studies, CT density-based thresholds are also influenced by lack of consensus and ongoing updates to the required CT acquisition protocol and reconstruction kernels. Apart from these limitations, the PRM method is novel and useful in differentiating airway disease tissue from the normal tissue. We believe the study of mechanics in PRM labeled normal, emphysema, and functional small airway disease regions would provide valuable information on how tissue expansion capability varies across disease components in COPD and with progression. The studies related to PRM technique were focused on analyzing disease regions, we think the normal lung tissue can be further categorized using CT-based mechanics, similar to the study mentioned in Chapter 5. Although, CT derived lung mechanics are shown to be effective in this thesis in regards to diagnosing COPD, it is still unknown how the mechanical properties of the lung tissue changes can be used to detect early progression. The work presented in this thesis is largely based on functional measures representing local volume change (mean of the Jacobian determinant); the influence of tissue mechanics in the presence of airway disease and emphysema separately needs further exploration. The elastic ability of the lung tissue at different severity stages of the disease might provide useful information on structural manifestations associated with COPD. It has been shown previously that the airflow obstruction identified by spirometry varies with the heterogeneity of disease [120, 172, 173]. The size of emphysema clusters and location of airway narrowing might play a role in the extent of airflow obstruction in

the patient, the study of lung mechanical measures under these circumstances demands further research. The identification of phenotypes in COPD requires longitudinal characterization of the disease progression. Major studies in COPD research: Evaluation of COPD Longitudinally to Identify Predictive Surrogate Endpoints (ECLIPSE), COPDGene, and Subpopulations and intermediate outcome measures in COPD (SPIROMICS) are currently gathering longitudinal data which helps further exploration of role of mechanics in phenotyping and disease progression. In the recent times, cluster analysis techniques have been used to group COPD patients based on radiographic features, demographics, and patient's health status [174-177]. The dimensionality of feature space in COPD research is ever increasing with the advances in imaging capabilities. These advancements are worthy of establishing robust computer aided diagnostic frameworks and reducing the high dimensional feature space. There is a great interest in using machine learning frameworks either supervised or unsupervised to create a robust feature space which is more relevant to COPD phenotyping and progression. The research related to CT texture-based quantification of COPD relies on such machine learning framework [38, 40-45]. Supervised learning usually requires a training set with annotated data from the clinicians and those are further used in training a machine to automatically classify new data. In chapter 1, we used a supervised machine learning classifier trained on CT-derived lung mechanical measures to confirm the presence and severity of COPD. While such supervised learning frameworks showed promise in COPD research, but are constrained by relatively constrained sample size affecting the reproducibility and clinical use of such techniques [178]. It is also important to mention to the effort and burden to gather huge database of manually labelled data as required for better results. There has been

considerable interest to use unsupervised learning, especially cluster analysis and deep learning techniques in COPD research [82, 178-180]. However, unsupervised learning frameworks require a large amount of training data to derive any relevant features, those representing underlying patterns in the data. It would be interesting to explore the CT-derived biomechanical feature maps using such unsupervised learning framework to extract underlying functional patterns of disease progression.

In conclusion, the work presented in this thesis introduced the use of CT image registration-based lung mechanical measures in identifying COPD presence, severity, and in predicting disease progression. We have shown the effectiveness of lung mechanical measures in capturing functional changes and demonstrated how these measures are highly relevant to the current state of the art research in COPD. The clinical applicability of the CT derived lung mechanics in COPD diagnosis demands discussion and worthy of further exploration.

APPENDIX

A.1. CT-based Lung Mechanics in COPD Phenotyping

Chronic obstructive pulmonary disease (COPD) is characterized by irreversible airflow limitation with progressive decline in lung function. COPD is a highly heterogeneous disease with multiple underlying phenotypes including emphysema and airway disease. Emphysema is characterized by parenchymal destruction and loss of elasticity. Airway disease results in airway wall remodeling and narrowing. Spirometry is used to diagnose COPD and evaluate severity on a global level. However, spirometry does not provide phenotypes or regional characteristics of the disease. Recently, pulmonary CT imaging has been used to characterize the heterogeneous nature of COPD by defining CT density-based measures of disease. This allows us to differentiate the COPD population into emphysema and airway predominant groups. Furthermore, we have used image registration to derive lung mechanical measures for regional lung function estimation. We have used these regional lung function measurements to estimate COPD severity.

The morphological manifestations of COPD patients as seen on CT images vary widely and not entirely in accordance with the spirometry diagnosis. This heterogeneous nature of COPD has led to several studies in understanding individual phenotypes in COPD. Phenotyping COPD population based on CT-based airway and emphysema measures has been shown previously. In this study, we investigate the differences in lung mechanics among the COPD phenotypes. We used a dataset of 415 subjects from the COPDGene trial. First, we divided the subjects into different phenotype groups: normal (NOR), airway disease predominant (AD), emphysema predominant (ED), and mixed phenotypes (MIX). To assign each subject to a phenotype group, we used CT-based

measures of airway wall percent (%AW) and emphysema percent (%EMPH). The mean %AW and mean %EMPH of asymptomatic smokers were used as thresholds, T1 (64%) and T2 (9%), respectively, to define the phenotype groups. The groups were defined as follows: NOR: %AW< T1 and %EMPH < T2; AD: %AW> T1 and %EMPH < T2; ED: %AW < T1 and %EMPH > T2; MIX: %AW > T1 and %EMPH > T2. Image registration was used to obtain a pixel wise transformation between inspiration and expiration images. The mean and standard deviation of the Jacobian of the transformation is used to estimate tissue expansion and heterogeneity of tissue expansion. Tukey's significance test is used to compare the local tissue expansion between groups. Table A1.1 shows the CT-based measures for each phenotype. We have shown that lung mechanical measures derived from CT image registration are significantly different between normal, emphysema, and airway predominant groups. The mean Jacobian and heterogeneity of local tissue expansion as represented by the standard deviation of Jacobian measure is significantly different between emphysema and airway predominant groups. This might be due to the loss of elasticity in emphysema regions of the lung. The mixed phenotype showed similar lung mechanics as airway predominant group. The tissue heterogeneity of normal patients is significantly different from the other three phenotypes.

Table A1.1. CT measures by phenotype. NOR: normal, AD: airway disease predominant, ED: emphysema predominant, MIXED: mixed phenotype. All values reported as mean

(standard deviation). Symbols *, ^, and º represent significant difference compared to NOR, AD, and ED respectively (Tukey significance test with P value < 0.05)

Parameters	NOR	AD	ED	MIXED
CT Emphysema	1.7 (1.6)	1.6 (1.3)	22.4 (12.9)*^	27.9 (10.9)*^º
CT Air Trapping	15.3 (12.1)	22.0 (12.5)*	44.1 (18.9)*^	60.4 (13.5)*^º
Airway Wall Area	60.5 (2.3)	66.9 (1.9)*	59.8 (2.3)*^	65.8 (1.1)*º
Jacobian Mean	1.6 (0.2)	1.3 (0.1)*	1.6 (0.2)^	1.3 (0.1)*º
Jacobian Std. Dev	0.5 (0.2)	0.3 (0.1)*	0.6 (0.3)*^	0.3 (0.1)*º

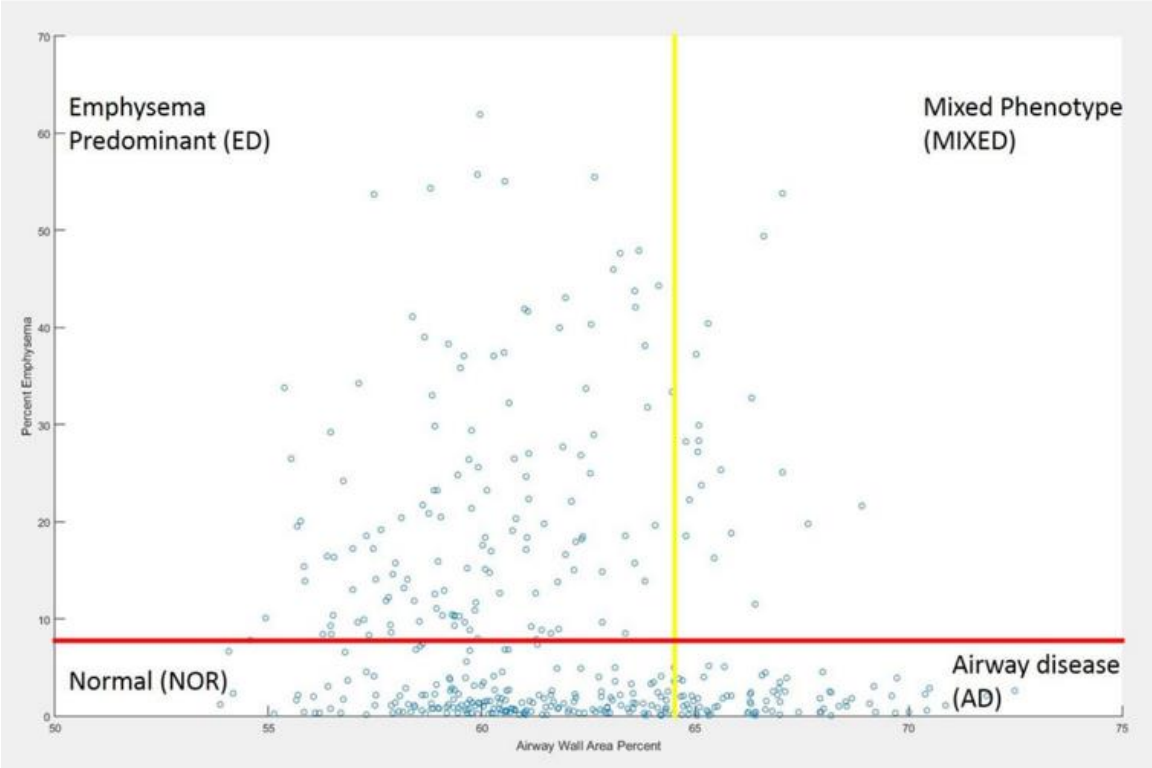

Figure A1.1. Phenotype division based on CT emphysema (%) on y-axis and airway wall area percent (WA %) on x-axis. Red line represents mean±2sd of CT emphysema (%) whereas yellow line represents mean±2sd of WA % in asymptomatic smokers.

A.2. CT-based Lung Mechanics in SPIROMICS

Subpopulations and Intermediate Outcomes in COPD Study (SPIROMICS) is a multicenter study designed to determine intermediate outcomes and endpoints in the population with COPD in order for better phenotyping of the patient populations. The study includes current and former smokers (> 20 pack years) with and without COPD and non-smokers without COPD aged 40-80 years. SPIROMICS participants provided demographic information, smoking history, and other related clinical outcomes. CT images were acquired at full inspiration (TLC) and residual volume (RV). Previously, in COPDGene study, CT scans were acquired at full inspiration (TLC) and functional residual capacity (FRC). We estimated CT image registration-based regional lung mechanics from SPIROMICS and evaluated the mechanistic differences across GOLD stages.

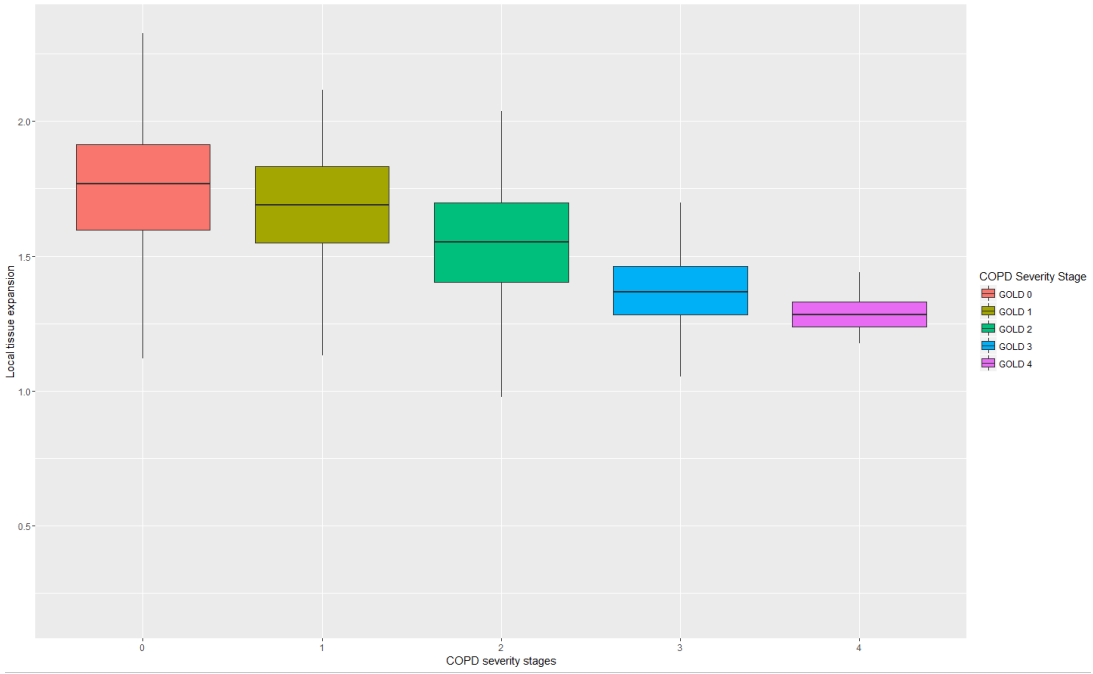

Figure A2.1. Mean of the Jacobian determinant across GOLD stages representing local volume change in SPIROMICS subjects (n=750)

Table A2.1. Pairwise comparison of mean of Jacobian determinant between COPD severity stages. Results are based on Tukey honest significant difference (HSD) test post ANOVA analysis.

1. Severity Stage Comparison	2. P value
3. GOLD 0 – GOLD 1	4. 0.305
5. GOLD 1 – GOLD 2	6. < 0.001
7. GOLD 2 – GOLD 3	8. < 0.001
9. GOLD 3 – GOLD 4	10. 0.535

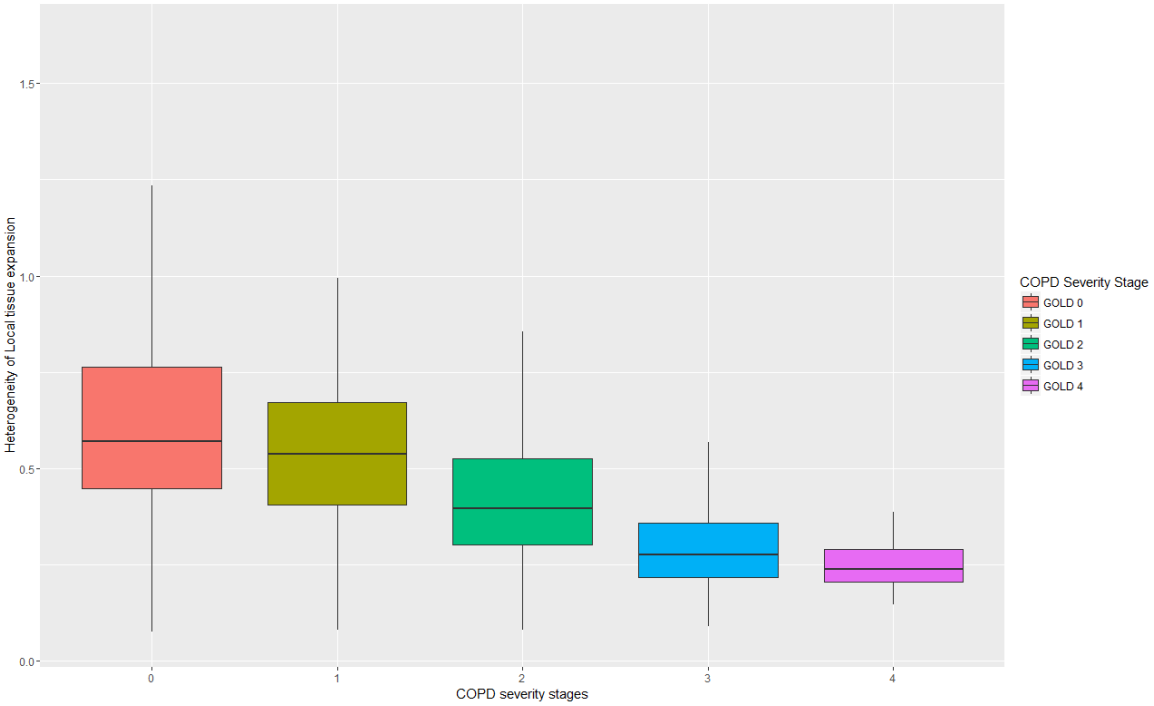

Figure A2.2. Heterogeneity of local tissue expansion across GOLD stages in SPIROMICS (n=750).

Table A2.2. Pairwise comparison of heterogeneity of local tissue expansion (Standard deviation of Jacobian determinant) between COPD severity stages. Results are based on Tukey honest significant difference (HSD) test post ANOVA analysis.

11. Severity Stage Comparison	12. P value
13. GOLD 0 – GOLD 1	14. 0.065
15. GOLD 1 – GOLD 2	16. < 0.001
17. GOLD 2 – GOLD 3	18. < 0.001
19. GOLD 3 – GOLD 4	20. 0.867

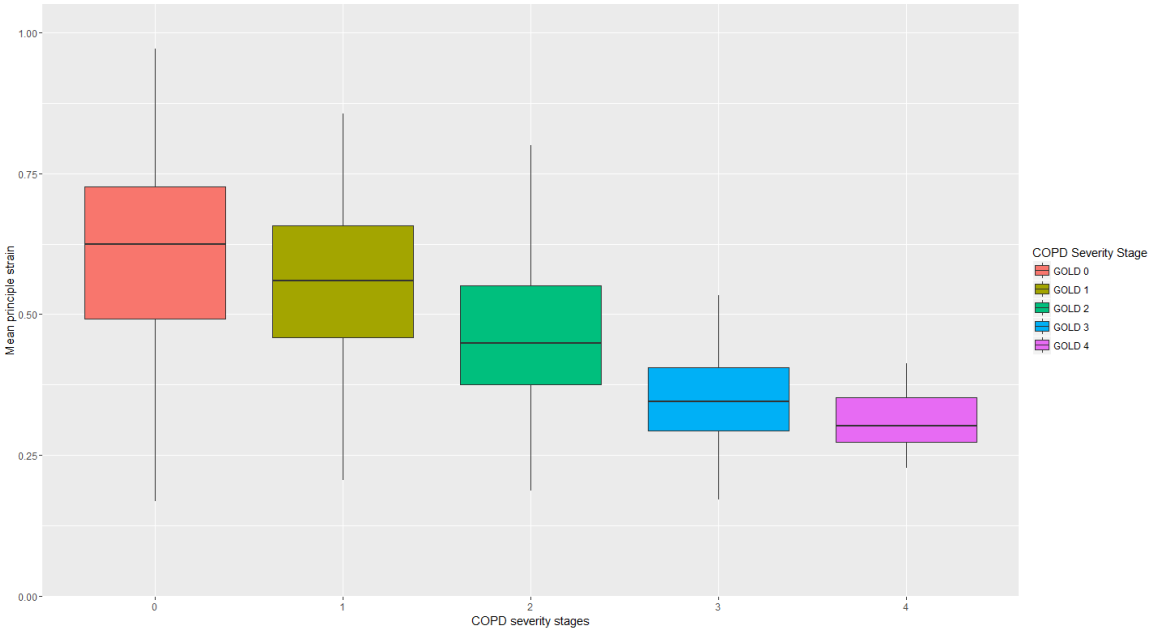

Figure A2.3. Mean of the principle strain across GOLD stages in SPIROMICS subjects (n=750).

Table A2.3. Pairwise comparison of mean principle strain between COPD severity stages. Results are based on Tukey honest significant difference (HSD) test post ANOVA analysis.

21. Severity Stage Comparison	22. P value
23. GOLD 0 – GOLD 1	24. 0.012
25. GOLD 1 – GOLD 2	26. < 0.001
27. GOLD 2 – GOLD 3	28. < 0.001
29. GOLD 3 – GOLD 4	30. 0.612

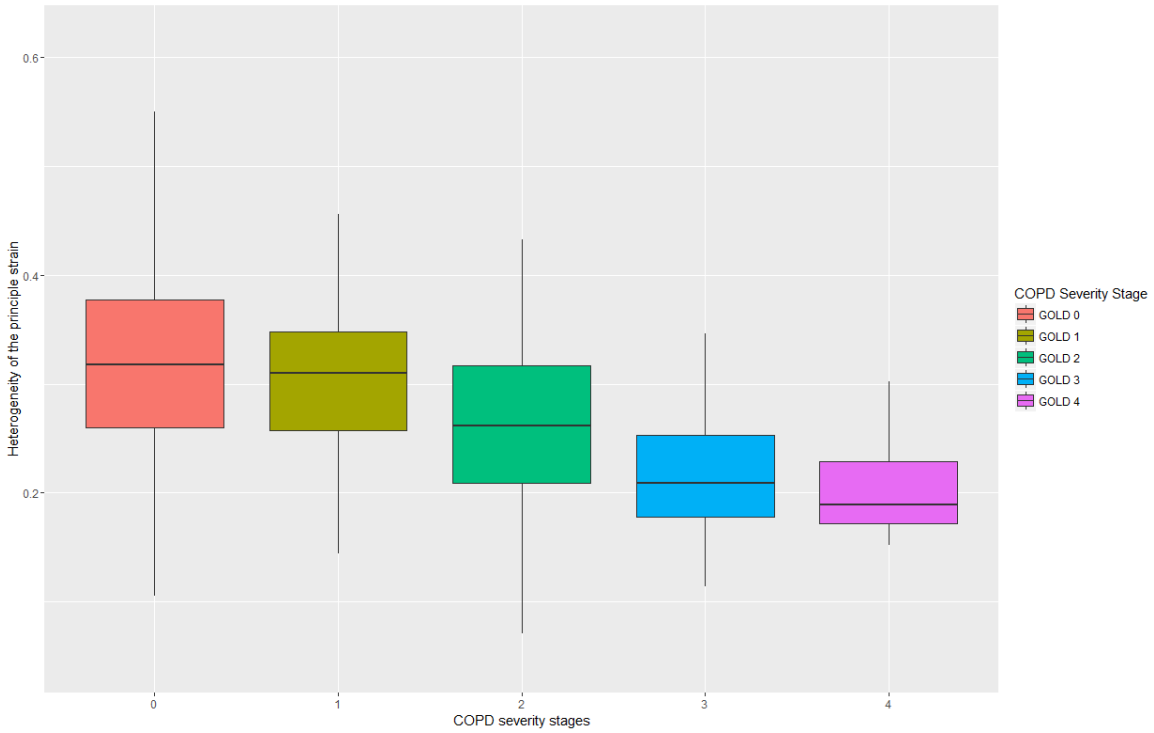

Figure A2.4. Heterogeneity of the principle strain (standard deviation of the strain map) across GOLD stages in SPIROMICS subjects (n=750).

Table A2.4. Pairwise comparison of mean principle strain between COPD severity stages. Results are based on Tukey honest significant difference (HSD) test post ANOVA analysis.

31. Severity Stage Comparison	**32. P value**
33. GOLD 0 – GOLD 1	34. 0.462
35. GOLD 1 – GOLD 2	36. < 0.001
37. GOLD 2 – GOLD 3	38. < 0.001
39. GOLD 3 – GOLD 4	40. 0.962

REFERENCES

1. Breatnach, E., G.C. Abbott, and R.G. Fraser, *Dimensions of the normal human trachea.* AJR Am J Roentgenol, 1984. **142**(5): p. 903-6.

2. Farkas, A., I. Balashazy, and K. Szocs, *Characterization of regional and local deposition of inhaled aerosol drugs in the respiratory system by computational fluid and particle dynamics methods.* J Aerosol Med, 2006. **19**(3): p. 329-43.

3. Tu, J., *Computational Fluid and Particle Dynamics in the Human Respiratory System*. 2013: Springer.

4. Kitaoka, H., P.H. Burri, and E.R. Weibel, *Development of the human fetal airway tree: analysis of the numerical density of airway endtips.* Anat Rec, 1996. **244**(2): p. 207-13.

5. Rodriguez, M., et al., *Pulmonary acinus: geometry and morphometry of the peripheral airway system in rat and rabbit.* Am J Anat, 1987. **180**(2): p. 143-55.

6. AnaesthesiaUK. *Tests of Pulmonary Function*. 2004; Available from: http://www.frca.co.uk/article.aspx?articleid=100023.

7. Seaman, J., A.C. Leonard, and R.J. Panos, *Health care utilization history, GOLD guidelines, and respiratory medication prescriptions in patients with COPD.* Int J Chron Obstruct Pulmon Dis, 2010. **5**: p. 89-97.

8. Rabe, K.F., et al., *Global strategy for the diagnosis, management, and prevention of chronic obstructive pulmonary disease: GOLD executive summary.* Am J Respir Crit Care Med, 2007. **176**(6): p. 532-55.

9. Dal Negro, R.W., L. Bonadiman, and P. Turco, *Prevalence of different comorbidities in COPD patients by gender and GOLD stage.* Multidiscip Respir Med, 2015. **10**(1): p. 24.

10. COPD, L.W.w. *What is COPD*. Available from: http://www.livingwellwithcopd.com/en/what-is-copd.html.

11. Fabbri, L., et al., *Global Strategy for the Diagnosis, Management, and Prevention of Chronic Obstructive Pulmonary Disease: GOLD Executive Summary updated 2003.* COPD, 2004. **1**(1): p. 105-41; discussion 103-4.

12. Wilke S, S.D., Spruit MA, et al. , *The 2014 updated GOLD strategy: A comparison of the various scenarios.* J COPD F, 2014.

13. Newell, J.D., Jr., J.C. Hogg, and G.L. Snider, *Report of a workshop: quantitative computed tomography scanning in longitudinal studies of emphysema.* Eur Respir J, 2004. **23**(5): p. 769-75.

14. Greene, R., *Fleischner Lecture. Imaging the respiratory system in the first few years after discovery of the X-ray: contributions of Francis H. Williams, M.D.* AJR Am J Roentgenol, 1992. **159**(1): p. 1-7.

15. Hounsfield, G.N., *Computerized transverse axial scanning (tomography): Part I. Description of system. 1973.* Br J Radiol, 1995. **68**(815): p. H166-72.

16. Ritenour, W.R.H.a.E.R., *Medical Imaging Physics*. 2002: WILEY.

17. Key, R. *Computed Tomography*. Available from: http://radiologykey.com/computed-tomography-4/.

18. Bafadhel, M., et al., *The role of CT scanning in multidimensional phenotyping of COPD.* Chest, 2011. **140**(3): p. 634-42.

19. Coxson, H.O. and P.D. Pare, *Phenotyping COPD using high resolution CT. Is it time to leave it for Watson?* COPD, 2012. **9**(2): p. 87-9.

20. Mishima, M., *[CT imaging of COPD--importance of phenotyping (emphysema dominant and airway disorder dominant)].* Nihon Rinsho, 2007. **65**(4): p. 648-54.

21. *Introduction to CT Physics*. 2007; Available from: http://www.odec.ca/projects/2007/kimj7j2/index_files/Page1674.htm.

22. *The definition of emphysema. Report of a National Heart, Lung, and Blood Institute, Division of Lung Diseases workshop.* Am Rev Respir Dis, 1985. **132**(1): p. 182-5.

23. Hayhurst, M.D., et al., *Diagnosis of pulmonary emphysema by computerised tomography.* Lancet, 1984. **2**(8398): p. 320-2.

24. Muller, N.L., et al., *"Density mask". An objective method to quantitate emphysema using computed tomography.* Chest, 1988. **94**(4): p. 782-7.

25. Coxson, H.O. and R.M. Rogers, *Quantitative computed tomography of chronic obstructive pulmonary disease.* Acad Radiol, 2005. **12**(11): p. 1457-63.

26. Gevenois, P.A., et al., *Comparison of computed density and microscopic morphometry in pulmonary emphysema.* Am J Respir Crit Care Med, 1996. **154**(1): p. 187-92.

27. Mishima, M., et al., *Standardization of low attenuation area versus total lung area in chest X-ray CT as an indicator of chronic pulmonary emphysema.* Front Med Biol Eng, 1997. **8**(2): p. 79-86.

28. Kauczor, H.U., et al., *CT attenuation of paired HRCT scans obtained at full inspiratory/expiratory position: comparison with pulmonary function tests.* Eur Radiol, 2002. **12**(11): p. 2757-63.

29. Kubo, K., et al., *Expiratory and inspiratory chest computed tomography and pulmonary function tests in cigarette smokers.* Eur Respir J, 1999. **13**(2): p. 252-6.

30. Lucidarme, O., et al., *Expiratory CT scans for chronic airway disease: correlation with pulmonary function test results.* AJR Am J Roentgenol, 1998. **170**(2): p. 301-7.

31. Knudson, R.J., et al., *Expiratory computed tomography for assessment of suspected pulmonary emphysema.* Chest, 1991. **99**(6): p. 1357-66.

32. Newman, K.B., et al., *Quantitative computed tomography detects air trapping due to asthma.* Chest, 1994. **106**(1): p. 105-9.

33. Matsuoka, S., et al., *Quantitative assessment of air trapping in chronic obstructive pulmonary disease using inspiratory and expiratory volumetric MDCT.* AJR Am J Roentgenol, 2008. **190**(3): p. 762-9.

34. Lab, A.P.P.I. *CT density-based emphysema and air trapping visualization*. Available from: https://www.i-clic.uihc.uiowa.edu/pics.html.

35. Uppaluri, R., et al., *Computer recognition of regional lung disease patterns.* Am J Respir Crit Care Med, 1999. **160**(2): p. 648-54.

36. Uppaluri, R., et al., *Interstitial lung disease: A quantitative study using the adaptive multiple feature method.* Am J Respir Crit Care Med, 1999. **159**(2): p. 519-25.

37. Uppaluri, R., et al., *Quantification of pulmonary emphysema from lung computed tomography images.* Am J Respir Crit Care Med, 1997. **156**(1): p. 248-54.

38. Xu, Y., et al., *MDCT-based 3-D texture classification of emphysema and early smoking related lung pathologies.* IEEE Trans Med Imaging, 2006. **25**(4): p. 464-75.

39. Madsen, M.T., et al., *Pulmonary CT image classification with evolutionary programming.* Acad Radiol, 1999. **6**(12): p. 736-41.

40. Park, Y.S., et al., *Texture-based quantification of pulmonary emphysema on high-resolution computed tomography: comparison with density-based quantification and correlation with pulmonary function test.* Invest Radiol, 2008. **43**(6): p. 395-402.

41. Hoffman, E.A., et al., *Characterization of the interstitial lung diseases via density-based and texture-based analysis of computed tomography images of lung structure and function.* Acad Radiol, 2003. **10**(10): p. 1104-18.

42. Ginsburg, S.B., et al., *Automated texture-based quantification of centrilobular nodularity and centrilobular emphysema in chest CT images.* Acad Radiol, 2012. **19**(10): p. 1241-51.

43. Ojala, T., and Matti Pietikäinen, *Unsupervised texture segmentation using feature distributions.* Pattern Recognition, 1999.

44. Sorensen, L., et al., *Texture-based analysis of COPD: a data-driven approach.* IEEE Trans Med Imaging, 2012. **31**(1): p. 70-8.

45. Nishio, M., Hisanobu Koyama, Yoshiharu Ohno, and Kazuro Sugimura, *Classification of Emphysema Subtypes: Comparative Assessment of Local Binary Patterns and Related Texture Features.* Advances in Computed Tomography, 2015. **4**.

46. Zulueta-Coarasa, T., Sila Kurugol, James C. Ross, George G. Washko, and Raúl San José Estépar, *Emphysema classification based on embedded probabilistic PCA.* 35th Annual International Conference of the IEEE Engineering in Medicine and Biology Society (EMBC), 2013.

47. Shin, H.-C., Holger R. Roth, Mingchen Gao, Le Lu, Ziyue Xu, Isabella Nogues, Jianhua Yao, Daniel Mollura, and Ronald M. Summers, *Deep convolutional neural networks for computer-aided detection: CNN architectures, dataset characteristics and transfer learning.* IEEE transactions on medical imaging, 2016.

48. Li, Q., Weidong Cai, and David Dagan Feng, *Lung image patch classification with automatic feature learning.* International Conference of the IEEE Engineering in Medicine and Biology Society (EMBC), 2013.

49. Anthimopoulos, M., Stergios Christodoulidis, Lukas Ebner, Andreas Christe, and Stavroula Mougiakakou, *Lung Pattern Classification for Interstitial Lung Diseases Using a Deep Convolutional Neural Network.* IEEE transactions on medical imaging, 2016.

50. Sorensen, L., *Pattern Recognition-Based Analysis of COPD in CT*, in *Faculty of Science*. 2010, University of Copenhagen.

51. Regan, E.A., et al., *Genetic epidemiology of COPD (COPDGene) study design.* COPD, 2010. **7**(1): p. 32-43.

52. Vestbo, J., et al., *Evaluation of COPD Longitudinally to Identify Predictive Surrogate End-points (ECLIPSE).* Eur Respir J, 2008. **31**(4): p. 869-73.

53. Sieren, J.P., et al., *SPIROMICS Protocol for Multicenter Quantitative CT to Phenotype the Lungs.* Am J Respir Crit Care Med, 2016.

54. Ibanez, L., Schroeder, W., Ng, L., Cates, J., *The ITK Software Guide*. 2005: Kitware Inc.

55. Ourselin, S., Alexis Roche, Gérard Subsol, Xavier Pennec, and Nicholas Ayache, *Reconstructing a 3D structure from serial histological sections,*. Image and vision computing, 2001.

56. Han, X., *Feature-constrained nonlinear registration of lung CT images.*, in *Medical image analysis for the clinic: a grand challenge*. 2010.

57. Gorbunova, V., et al., *Weight preserving image registration for monitoring disease progression in lung CT.* Med Image Comput Comput Assist Interv, 2008. **11**(Pt 2): p. 863-70.

58. Yin, Y., E.A. Hoffman, and C.L. Lin, *Mass preserving nonrigid registration of CT lung images using cubic B-spline.* Med Phys, 2009. **36**(9): p. 4213-22.

59. Reinhardt, J.M., et al., *Registration-derived estimates of local lung expansion as surrogates for regional ventilation.* Inf Process Med Imaging, 2007. **20**: p. 763-74.

60. Cao, K., *Local lung tissue expansion analysis based on inverse consistent image registration*, in *Electrical and Computer Engineering*. 2008, University of Iowa.

61. Reinhardt, J.M., et al., *Registration-based estimates of local lung tissue expansion compared to xenon CT measures of specific ventilation.* Med Image Anal, 2008. **12**(6): p. 752-63.

62. Christensen, G.E., Rabbitt, R.D., Miller, M.I., Joshi, S., Grenander, U., Coogan, T., Essen, D.V. *Topological properties of smooth anatomic maps.* in *Information Proceedings in Medical Imaging*. 1995. Boston: Kluwer Academic Publishers.

63. RC, B., *Advanced Calculus*. 1978, St. Louis: McGraw-Hill Book Company.

64. Lubliner, J., *Plasiticity Theory*. 2008, Mineola, NY: Dover Publication.

65. Pellegrino, R., et al., *Interpretative strategies for lung function tests.* Eur Respir J, 2005. **26**(5): p. 948-68.

66. Amelon, R., et al., *Three-dimensional characterization of regional lung deformation.* J Biomech, 2011. **44**(13): p. 2489-95.

67. Galban, C.J., et al., *Computed tomography-based biomarker provides unique signature for diagnosis of COPD phenotypes and disease progression.* Nat Med, 2012. **18**(11): p. 1711-5.

68. Gorbunova, V., et al., *Early detection of emphysema progression.* Med Image Comput Comput Assist Interv, 2010. **13**(Pt 2): p. 193-200.

69. Boes, J.L., et al., *Parametric response mapping monitors temporal changes on lung CT scans in the subpopulations and intermediate outcome measures in COPD Study (SPIROMICS).* Acad Radiol, 2015. **22**(2): p. 186-94.

70. Murphy, K., et al., *Toward automatic regional analysis of pulmonary function using inspiration and expiration thoracic CT.* Med Phys, 2012. **39**(3): p. 1650-62.

71. Bhatt, S.P., Xavier Soler, Xin Wang, Susan Murray, Antonio R. Anzueto, Terri H. Beaty, Aladin M. Boriek et al., *Association between functional small airways disease and FEV1 decline in COPD.* American Journal of Respiratory and Critical Care Medicine, 2016.

72. Choi, S., et al., *Registration-based assessment of regional lung function via volumetric CT images of normal subjects vs. severe asthmatics.* J Appl Physiol (1985), 2013. **115**(5): p. 730-42.

73. Petersen, J., Vladlena Gorbunova, Mads Nielsen, Asger Dirksen, Pechin Lo, and Marleen de Bruijne., *Longitudinal analysis of airways using registration.*, in *Fourth International Workshop on Pulmonary Image Analysis.* 2011.

74. Ederle, J.R., et al., *Evaluation of changes in central airway dimensions, lung area and mean lung density at paired inspiratory/expiratory high-resolution computed tomography.* Eur Radiol, 2003. **13**(11): p. 2454-61.

75. Kim, E.Y., et al., *Detailed analysis of the density change on chest CT of COPD using non-rigid registration of inspiration/expiration CT scans.* Eur Radiol, 2015. **25**(2): p. 541-9.

76. Matsuoka, S., et al., *Quantitative CT measurement of cross-sectional area of small pulmonary vessel in COPD: correlations with emphysema and airflow limitation.* Acad Radiol, 2010. **17**(1): p. 93-9.

77. Nishio, M., et al., *Paired inspiratory/expiratory volumetric CT and deformable image registration for quantitative and qualitative evaluation of airflow limitation in smokers with or without copd.* Acad Radiol, 2015. **22**(3): p. 330-6.

78. Lopez-Campos, J.L., W. Tan, and J.B. Soriano, *Global burden of COPD.* Respirology, 2016. **21**(1): p. 14-23.

79. Fromer, L. and C.B. Cooper, *A review of the GOLD guidelines for the diagnosis and treatment of patients with COPD.* Int J Clin Pract, 2008. **62**(8): p. 1219-36.

80. Hochhegger, B., et al., *Reconstruction algorithms influence the follow-up variability in the longitudinal CT emphysema index measurements.* Korean J Radiol, 2011. **12**(2): p. 169-75.

81. Martinez, C.H., Ya-Hong Chen, Phillip M. Westgate, Lyrica X. Liu, Susan Murray, Jeffrey L. Curtis, Barry J. Make et al., *Relationship between quantitative CT metrics and health status and BODE in chronic obstructive pulmonary disease.* Thorax, 2012.

82. Shin, H.C., et al., *Deep Convolutional Neural Networks for Computer-Aided Detection: CNN Architectures, Dataset Characteristics and Transfer Learning.* IEEE Trans Med Imaging, 2016. **35**(5): p. 1285-98.

83. Han, M.K., *Clinical correlations of computed tomography imaging in chronic obstructive pulmonary disease.* Ann Am Thorac Soc, 2013. **10 Suppl**: p. S131-7.

84. Schroeder, J.D., et al., *Relationships between airflow obstruction and quantitative CT measurements of emphysema, air trapping, and airways in subjects with and without chronic obstructive pulmonary disease.* AJR Am J Roentgenol, 2013. **201**(3): p. W460-70.

85. Bhatt, S.P., et al., *Comparison of spirometric thresholds in diagnosing smoking-related airflow obstruction.* Thorax, 2014. **69**(5): p. 409-14.

86. Grydeland, T.B., et al., *Quantitative computed tomography measures of emphysema and airway wall thickness are related to respiratory symptoms.* Am J Respir Crit Care Med, 2010. **181**(4): p. 353-9.

87. Martinez, C.H., et al., *Relationship between quantitative CT metrics and health status and BODE in chronic obstructive pulmonary disease.* Thorax, 2012. **67**(5): p. 399-406.

88. Gietema, H.A., et al., *Impact of emphysema and airway wall thickness on quality of life in smoking-related COPD.* Respir Med, 2013. **107**(8): p. 1201-9.

89. Diaz, A.A., et al., *Relationship of emphysema and airway disease assessed by CT to exercise capacity in COPD.* Respir Med, 2010. **104**(8): p. 1145-51.

90. Spruit, M.A., et al., *Determinants of poor 6-min walking distance in patients with COPD: the ECLIPSE cohort.* Respir Med, 2010. **104**(6): p. 849-57.

91. Johannessen, A., et al., *Mortality by level of emphysema and airway wall thickness.* Am J Respir Crit Care Med, 2013. **187**(6): p. 602-8.

92. Bhatt, S.P., et al., *CT-derived Biomechanical Metrics Improve Agreement Between Spirometry and Emphysema.* Acad Radiol, 2016.

93. Bodduluri, S., et al., *Registration-based lung mechanical analysis of chronic obstructive pulmonary disease (COPD) using a supervised machine learning framework.* Acad Radiol, 2013. **20**(5): p. 527-36.

94. Vestbo, J., et al., *Global strategy for the diagnosis, management, and prevention of chronic obstructive pulmonary disease: GOLD executive summary.* Am J Respir Crit Care Med, 2013. **187**(4): p. 347-65.

95. Jones, P.W., F.H. Quirk, and C.M. Baveystock, *The St George's Respiratory Questionnaire.* Respir Med, 1991. **85 Suppl B**: p. 25-31; discussion 33-7.

96. Mahler, D.A. and C.K. Wells, *Evaluation of clinical methods for rating dyspnea.* Chest, 1988. **93**(3): p. 580-6.

97. Polkey, M.I., et al., *Six-minute-walk test in chronic obstructive pulmonary disease: minimal clinically important difference for death or hospitalization.* Am J Respir Crit Care Med, 2013. **187**(4): p. 382-6.

98. Celli, B.R., et al., *The body-mass index, airflow obstruction, dyspnea, and exercise capacity index in chronic obstructive pulmonary disease.* N Engl J Med, 2004. **350**(10): p. 1005-12.

99. Ding, K., et al., *Comparison of image registration based measures of regional lung ventilation from dynamic spiral CT with Xe-CT.* Med Phys, 2012. **39**(8): p. 5084-98.

100. Westwood, M., et al., *Relationship between FEV1 change and patient-reported outcomes in randomised trials of inhaled bronchodilators for stable COPD: a systematic review.* Respir Res, 2011. **12**: p. 40.

101. Oga, T., et al., *Longitudinal deteriorations in patient reported outcomes in patients with COPD.* Respir Med, 2007. **101**(1): p. 146-53.

102. Castaldi, P.J., et al., *Distinct quantitative computed tomography emphysema patterns are associated with physiology and function in smokers.* Am J Respir Crit Care Med, 2013. **188**(9): p. 1083-90.

103. Kim, W.D., et al., *Centrilobular and panlobular emphysema in smokers. Two distinct morphologic and functional entities.* Am Rev Respir Dis, 1991. **144**(6): p. 1385-90.

104. Saetta, M., et al., *Extent of centrilobular and panacinar emphysema in smokers' lungs: pathological and mechanical implications.* Eur Respir J, 1994. **7**(4): p. 664-71.

105. Sverzellati, N., et al., *Physiologic and Quantitative Computed Tomography Differences between Centrilobular and Panlobular Emphysema in Copd.* Chronic Obstr Pulm Dis (Miami), 2014. **1**(1): p. 125-132.

106. Haruna, A., et al., *CT scan findings of emphysema predict mortality in COPD.* Chest, 2010. **138**(3): p. 635-40.

107. Fishman, A., et al., *A randomized trial comparing lung-volume-reduction surgery with medical therapy for severe emphysema.* N Engl J Med, 2003. **348**(21): p. 2059-73.

108. Scharf, S.M., et al., *Changes in pulmonary mechanics after lung volume reduction surgery.* Lung, 1998. **176**(3): p. 191-204.

109. Fuld, M.K., et al., *Systems for lung volume standardization during static and dynamic MDCT-based quantitative assessment of pulmonary structure and function.* Acad Radiol, 2012. **19**(8): p. 930-40.

110. Iyer, K.S., et al., *Repeatability and Sample Size Assessment Associated with Computed Tomography-Based Lung Density Metrics.* Chronic Obstr Pulm Dis (Miami), 2014. **1**(1): p. 97-104.

111. Jahani, N., et al., *Assessment of regional non-linear tissue deformation and air volume change of human lungs via image registration.* J Biomech, 2014. **47**(7): p. 1626-33.

112. Coxson, H.O., et al., *Using pulmonary imaging to move chronic obstructive pulmonary disease beyond FEV1.* Am J Respir Crit Care Med, 2014. **190**(2): p. 135-44.

113. Madani, A., et al., *Pulmonary emphysema: objective quantification at multi-detector row CT--comparison with macroscopic and microscopic morphometry.* Radiology, 2006. **238**(3): p. 1036-43.

114. Heremans, A., et al., *Measurement of lung density by means of quantitative CT scanning. A study of correlations with pulmonary function tests.* Chest, 1992. **102**(3): p. 805-11.

115. Hesselbacher, S.E., et al., *Cross-sectional analysis of the utility of pulmonary function tests in predicting emphysema in ever-smokers.* International journal of environmental research and public health, 2011. **8**(5): p. 1324-40.

116. Kinsella, M., et al., *Quantitation of emphysema by computed tomography using a "density mask" program and correlation with pulmonary function tests.* Chest, 1990. **97**(2): p. 315-21.

117. Haraguchi, M., et al., *Pulmonary function and regional distribution of emphysema as determined by high-resolution computed tomography.* Respiration; international review of thoracic diseases, 1998. **65**(2): p. 125-9.

118. Gould, G.A., et al., *Lung CT density correlates with measurements of airflow limitation and the diffusing capacity.* The European respiratory journal : official journal of the European Society for Clinical Respiratory Physiology, 1991. **4**(2): p. 141-6.

119. Washko, G.R., et al., *Computed tomographic-based quantification of emphysema and correlation to pulmonary function and mechanics.* COPD, 2008. **5**(3): p. 177-86.

120. Aziz, Z.A., et al., *Functional impairment in emphysema: contribution of airway abnormalities and distribution of parenchymal disease.* AJR Am J Roentgenol, 2005. **185**(6): p. 1509-15.

121. Pauls, S., et al., *Assessment of COPD severity by computed tomography: correlation with lung functional testing.* Clinical imaging, 2010. **34**(3): p. 172-8.

122. Spaggiari, E., et al., *Early smoking-induced lung lesions in asymptomatic subjects. Correlations between high resolution dynamic CT and pulmonary function testing.* La Radiologia medica, 2005. **109**(1-2): p. 27-39.

123. Lutchmedial, S.M., et al., *How Common is Airflow Limitation in Patients with Emphysema on Computerized Tomography of the Chest?* Chest, 2014.

124. Miller, M.R., et al., *Standardisation of spirometry.* Eur Respir J, 2005. **26**(2): p. 319-38.

125. Hankinson, J.L., J.R. Odencrantz, and K.B. Fedan, *Spirometric reference values from a sample of the general U.S. population.* American journal of respiratory and critical care medicine, 1999. **159**(1): p. 179-87.

126. Zach, J.A., et al., *Quantitative computed tomography of the lungs and airways in healthy nonsmoking adults.* Invest Radiol, 2012. **47**(10): p. 596-602.

127. Busacker, A., et al., *A multivariate analysis of risk factors for the air-trapping asthmatic phenotype as measured by quantitative CT analysis.* Chest, 2009. **135**(1): p. 48-56.

128. Nakano, Y., et al., *Comparison of low attenuation areas on computed tomographic scans between inner and outer segments of the lung in patients with chronic obstructive pulmonary disease: incidence and contribution to lung function.* Thorax, 1999. **54**(5): p. 384-9.

129. Gurney, J.W., et al., *Regional distribution of emphysema: correlation of high-resolution CT with pulmonary function tests in unselected smokers.* Radiology, 1992. **183**(2): p. 457-63.

130. Saitoh, T., et al., *Lobar distribution of emphysema in computed tomographic densitometric analysis.* Investigative radiology, 2000. **35**(4): p. 235-43.

131. Parr, D.G., et al., *Pattern of emphysema distribution in alpha1-antitrypsin deficiency influences lung function impairment.* American journal of respiratory and critical care medicine, 2004. **170**(11): p. 1172-8.

132. Bhatt, S.P., et al., *Disproportionate contribution of right middle lobe to emphysema and gas trapping on computed tomography.* PLoS One, 2014. **9**(7): p. e102807.

133. Ju, J., et al., *Impact of emphysema heterogeneity on pulmonary function.* PLoS One, 2014. **9**(11): p. e113320.

134. Enright, P., *HRCT-defined emphysema is not COPD to be treated with inhalers.* Thorax, 2014. **69**(5): p. 401-2.

135. Smith, B.M., et al., *Comparison of spatially matched airways reveals thinner airway walls in COPD. The Multi-Ethnic Study of Atherosclerosis (MESA) COPD Study and the Subpopulations and Intermediate Outcomes in COPD Study (SPIROMICS).* Thorax, 2014. **69**(11): p. 987-96.

136. Sieren, J.P., et al., *Sinogram Affirmed Iterative Reconstruction (SAFIRE) versus weighted filtered back projection (WFBP) effects on quantitative measure in the COPDGene 2 test object.* Med Phys, 2014. **41**(9): p. 091910.

137. Newell, J.D., Jr., et al., *Very low-dose (0.15 mGy) chest CT protocols using the COPDGene 2 test object and a third-generation dual-source CT scanner with corresponding third-generation iterative reconstruction software.* Invest Radiol, 2015. **50**(1): p. 40-5.

138. Nishimura, M., et al., *Annual change in pulmonary function and clinical phenotype in chronic obstructive pulmonary disease.* Am J Respir Crit Care Med, 2012. **185**(1): p. 44-52.

139. Duvoix, A., et al., *Blood fibrinogen as a biomarker of chronic obstructive pulmonary disease.* Thorax, 2013. **68**(7): p. 670-6.

140. Vestbo, J., et al., *Changes in forced expiratory volume in 1 second over time in COPD.* N Engl J Med, 2011. **365**(13): p. 1184-92.

141. McDonough, J.E., et al., *Small-airway obstruction and emphysema in chronic obstructive pulmonary disease.* N Engl J Med, 2011. **365**(17): p. 1567-75.

142. Suki, B., et al., *Biomechanics of the lung parenchyma: critical roles of collagen and mechanical forces.* J Appl Physiol (1985), 2005. **98**(5): p. 1892-9.

143. Suki, B., et al., *Mechanical failure, stress redistribution, elastase activity and binding site availability on elastin during the progression of emphysema.* Pulm Pharmacol Ther, 2012. **25**(4): p. 268-75.

144. Ritter, M.C., et al., *A zipper network model of the failure mechanics of extracellular matrices.* Proc Natl Acad Sci U S A, 2009. **106**(4): p. 1081-6.

145. Ito, S., et al., *Mechanics, nonlinearity, and failure strength of lung tissue in a mouse model of emphysema: possible role of collagen remodeling.* J Appl Physiol (1985), 2005. **98**(2): p. 503-11.

146. Maksym, G.N. and J.H. Bates, *A distributed nonlinear model of lung tissue elasticity.* J Appl Physiol (1985), 1997. **82**(1): p. 32-41.

147. Kononov, S., et al., *Roles of mechanical forces and collagen failure in the development of elastase-induced emphysema.* Am J Respir Crit Care Med, 2001. **164**(10 Pt 1): p. 1920-6.

148. Suki, B., et al., *Emphysema and mechanical stress-induced lung remodeling.* Physiology (Bethesda), 2013. **28**(6): p. 404-13.

149. Suki, B., K.R. Lutchen, and E.P. Ingenito, *On the progressive nature of emphysema: roles of proteases, inflammation, and mechanical forces.* Am J Respir Crit Care Med, 2003. **168**(5): p. 516-21.

150. Eisner, M.D., et al., *An official American Thoracic Society public policy statement: Novel risk factors and the global burden of chronic obstructive pulmonary disease.* Am J Respir Crit Care Med, 2010. **182**(5): p. 693-718.

151. Price, D.B., B.P. Yawn, and R.C. Jones, *Improving the differential diagnosis of chronic obstructive pulmonary disease in primary care.* Mayo Clin Proc, 2010. **85**(12): p. 1122-9.

152. Mannino, D.M., A. Sonia Buist, and W.M. Vollmer, *Chronic obstructive pulmonary disease in the older adult: what defines abnormal lung function?* Thorax, 2007. **62**(3): p. 237-41.

153. Brusasco, V. and R. Pellegrino, *Spirometry in Chronic Obstructive Pulmonary Disease. From Rule of Thumb to Science.* Am J Respir Crit Care Med, 2016. **193**(7): p. 704-6.

154. Bhatt, S.P., et al., *Comparison of spirometric thresholds in diagnosing smoking-related airflow obstruction: authors' response.* Thorax, 2014. **69**(12): p. 1147-8.

155. Nishimura, K., et al., *Comparison of different computed tomography scanning methods for quantifying emphysema.* J Thorac Imaging, 1998. **13**(3): p. 193-8.

156. Welte, T., C. Vogelmeier, and A. Papi, *COPD: early diagnosis and treatment to slow disease progression.* Int J Clin Pract, 2015. **69**(3): p. 336-49.

157. Vestbo, J., *Systemic inflammation and progression of COPD.* Thorax, 2007. **62**(6): p. 469-70.

158. van der Molen, T. and B.J. Kirenga, *COPD: early diagnosis and treatment to slow disease progression.* Int J Clin Pract, 2015. **69**(5): p. 513-4.

159. Harvey, B.G., et al., *Progression to COPD in smokers with normal spirometry/low DLCO using different methods to determine normal levels.* Eur Respir J, 2016. **47**(6): p. 1888-9.

160. West, J.B., *Distribution of mechanical stress in the lung, a possible factor in localisation of pulmonary disease.* Lancet, 1971. **1**(7704): p. 839-41.

161. Carloni, A., et al., *Heterogeneous distribution of mechanical stress in human lung: a mathematical approach to evaluate abnormal remodeling in IPF.* J Theor Biol, 2013. **332**: p. 136-40.

162. Madani, A., A. Van Muylem, and P.A. Gevenois, *Pulmonary emphysema: effect of lung volume on objective quantification at thin-section CT.* Radiology, 2010. **257**(1): p. 260-8.

163. Gevenois, P.A., et al., *The effects of age, sex, lung size, and hyperinflation on CT lung densitometry.* AJR Am J Roentgenol, 1996. **167**(5): p. 1169-73.

164. Soejima, K., et al., *Longitudinal follow-up study of smoking-induced lung density changes by high-resolution computed tomography.* Am J Respir Crit Care Med, 2000. **161**(4 Pt 1): p. 1264-73.

165. Du, K., et al., *Respiratory effort correction strategies to improve the reproducibility of lung expansion measurements.* Med Phys, 2013. **40**(12): p. 123504.

166. Du, K., et al., *Reproducibility of intensity-based estimates of lung ventilation.* Med Phys, 2013. **40**(6): p. 063504.

167. Du, K., et al., *Reproducibility of registration-based measures of lung tissue expansion.* Med Phys, 2012. **39**(3): p. 1595-608.

168. Stoel, B.C., et al., *Sources of error in lung densitometry with CT.* Invest Radiol, 1999. **34**(4): p. 303-9.

169. Yuan, R., et al., *The effects of radiation dose and CT manufacturer on measurements of lung densitometry.* Chest, 2007. **132**(2): p. 617-23.

170. Shaker, S.B., et al., *Volume adjustment of lung density by computed tomography scans in patients with emphysema.* Acta Radiol, 2004. **45**(4): p. 417-23.

171. Boes, J.L., et al., *The Impact of Sources of Variability on Parametric Response Mapping of Lung CT Scans.* Tomography, 2015. **1**(1): p. 69-77.

172. Russi, E.W., K.E. Bloch, and W. Weder, *Functional and morphological heterogeneity of emphysema and its implication for selection of patients for lung volume reduction surgery.* Eur Respir J, 1999. **14**(1): p. 230-6.

173. Tolnai, J., et al., *Functional and morphological assessment of early impairment of airway function in a rat model of emphysema.* J Appl Physiol (1985), 2012. **112**(11): p. 1932-9.

174. Weatherall, M., et al., *Distinct clinical phenotypes of airways disease defined by cluster analysis.* Eur Respir J, 2009. **34**(4): p. 812-8.

175. Miravitlles, M., M. Calle, and J.J. Soler-Cataluna, *Clinical phenotypes of COPD: identification, definition and implications for guidelines.* Arch Bronconeumol, 2012. **48**(3): p. 86-98.

176. Burgel, P.R., et al., *Clinical COPD phenotypes identified by cluster analysis: validation with mortality.* Eur Respir J, 2012. **40**(2): p. 495-6.

177. Burgel, P.R., et al., *Clinical COPD phenotypes: a novel approach using principal component and cluster analyses.* Eur Respir J, 2010. **36**(3): p. 531-9.

178. de Bruijne, M., *Machine learning approaches in medical image analysis: From detection to diagnosis.* Med Image Anal, 2016. **33**: p. 94-7.

179. van Tulder, G. and M. de Bruijne, *Combining Generative and Discriminative Representation Learning for Lung CT Analysis with Convolutional Restricted Boltzmann Machines.* IEEE Trans Med Imaging, 2016.

180. Anthimopoulos, M., et al., *Lung Pattern Classification for Interstitial Lung Diseases Using a Deep Convolutional Neural Network.* IEEE Trans Med Imaging, 2016.